UNIVERSITY OF CALIFORNIA,
IRVINE

Axial Load Capacities of Drilled Displacement Piles and the Impact of their Installation Technique on Surrounding Soils

THESIS

submitted in partial satisfaction of the requirements
for the degree of

MASTER OF SCIENCE

in Civil and Environmental Engineering

by

Genesis Figueroa Palacios

Thesis Committee:
Associate Professor Anne Lemnitzer, Chair
Associate Professor Mo Li, Member
Assistant Professor Joel Lanning, Member

2022

DEDICATION

To my family and friends.

TABLE OF CONTENTS

LIST OF FIGURES

Page

LIST OF TABLES

Page

ACKNOWLEDGEMENTS

My sincere gratitude to my advisor, Prof. Anne Lemnitzer for the all the support and guidance during my studies and research projects. I would also like to gratefully acknowledge the following professionals for their unconditional support of this project and their willingness to share data generously: Sam Warren (Farrell Design-Build, Inc.), Piyush Sharma and Danny Cohen (Morris-Shea Bridge Co., Inc.), Tim Siegel and Morgan NeSmith (Berkel and Company), Peter Faust (Malcolm Drilling), and Derek Deutscher (formerly Condon Johnson). Furthermore, I am grateful for all intellectual exchange and discussion during this study, specifically with: Dr. Antonio Marinucci (Google), Morgan NeSmith (Berkel), and the DFI ACIP&DD Committee under the leadership of Jonathan Hoff.

I would like to thank my committee members, Associate Professor Mo Li, and Associate Professor Joel Lanning for their time and support to finish my MS studies.

The text of Chapter 2 thesis is a reprint of the material as it appears in "Drilled Displacement Piles: Axial Load Capacity Prediction of with SPT and CPT Based Direct Methods, and Soil Improvement Assessment". (2022) DFI Journal - The Journal of the Deep Foundations Institute. Vol 16, Issue 2, used with permission from Deep Foundations Institute. The co-authors listed in this publication are Lemnitzer, A. and Marinucci, A.

With permission from Lemnitzer, A., Warren, S., and Marinucci, the research presented in this MS thesis is a reprint of the material previously published or currently under review as standalone publications in the following venues:

- Figueroa, G. Z., Lemnitzer, A., Marinucci, A., (2022). "Drilled Displacement Piles: Axial Load Capacity Prediction of with SPT and CPT Based Direct Methods, and Soil

Improvement Assessment". *DFI Journal - The Journal of the Deep Foundations Institute.* Vol 16, Issue 2; doi.org/10.37308/DFIJnl.20220512.262.

- Figueroa, G.Z., Lemnitzer, A., Warren, S., and Marinucci, A. (2022). "Axial capacities of drilled displacement piles predicted by SPT and CPT based methods". *International Conference on Deep Foundations and Ground Improvement*". Berlin, Germany, May 18th -20th, 2022.
- Figueroa, G.Z., Lemnitzer, A., Warren, S., and Marinucci, A. (2022). "Axial capacities of drilled displacement piles predicted by SPT and CPT based methods". *SuperPile 2022 Conference - Deep Foundations Institute*". St. Louis, Missouri, U.S., June 15th -17th, 2022.
- Figueroa, G.Z., and Lemnitzer, A. (2023). "Evaluation of soil improvement surrounding drilled displacement piles through pre- and post-installation CPT data". *Acta Geotechnica*. (Under review)

ABSTRACT OF THE THESIS

Axial Load Capacities of Drilled Displacement Piles and the Impact of their Installation Technique on Surrounding Soils.

by

Genesis Figueroa Palacios
Master of Science in Civil and Environmental Engineering
University of California, Irvine, 2022
Professor Anne Lemnitzer, Chair

Constructing DDPs involves a drilling process which combines the application of an axial force with the generation of a simultaneous torque to create a borehole in which the soil is first loosened (drilled) and then displaced towards the outside of the borehole using a drilling rod with integrated displacement body. This installation method has the potential to induce soil densification around the borehole vicinity, the magnitude of which depends on the soil type, pile installation procedure, and pile geometry/spacing. This thesis offers insights gathered from 55 construction projects in which more than 100 DDPs were installed and tested axially. High quality site exploration data (e.g., Cone Penetration Test (CPT) and Standard Penetration Test (SPT)) were evaluated to derive geotechnical analysis parameters. The test sites consisted of mostly mixed soil types with strongly stratified layers of sand, silt, and clay. Pile diameters ranged between 35 and 61 cm (14 to 24 inches). Prior to analyzing the axial performance of DDPs, a variety of failure interpretation methods were assessed to confidently extrapolate failure loads when field testing was terminated prior to pile failure. Results of this study suggested the Van der Veen's (1953) method to most closely estimate the load that triggers pile plunging

behavior specific to DDPs. Hereafter, in-situ axial load test results were compared with a wide range of analytical methods, including those developed specifically for DDPs. Predictive accuracy was assessed in terms of total pile capacity and pile settlement and separated based on pile diameter, stiffness, and soil type. Most examined analytical methods underpredict the in-situ pile capacities for both, CPT and SPT -based analysis. The use of SPT based predictions is recommended against.

An evaluation of pre- and post-installation soil properties surrounding newly installed DDPs have been carried out by interrogating a subset of data from 10 construction sites where Cone Penetration Tests (CPT) were performed before (CPT_{PRE}) and after (CPT_{POST}) pile construction. CPT key measurements, i.e., tip resistance (q_t) and sleeve friction (f_s), were corrected for overburden stress to obtain the normalized cone resistance (Q_t) and normalized friction ratio (F_r) and compared with pre-installation in-situ data to quantify the soil improvement ratio. Comparisons of pre and post installation measurements suggests the change in CPT-based soil resistances to be mostly associated with soil behavior type (Ic) and soil fines content (FC). Cohesive soils suggested substantially lower improvement potential than cohesionless soils. The spatial improvement was assessed by comparing pre-and post-installation soil measurements within 2-3 times of the pile diameter surrounding the DDP. Results show that there is no significant improvement is yielded at distances larger than 2D. Analytical comparisons between axial pile load capacities estimated with CPT_{PRE} and CPT_{POST} data does not differ considerably when using CPT_{POST} parameters for cohesive soils but showed a notable improvement (1.3-1.6 times) for mixed and cohesionless soils. However, when compared to in-situ failure loads observed from axial load tests, the use of post-installation CPT-based soil parameters for design was deemed too ambiguous.

INTRODUCTION

The use of Drilled Displacement Piles (DDP) is gaining increasing traction amongst the deep foundation industry. DDPs provide a fast and easy option to mitigate problematic in-situ conditions such as low bearing capacity, high settlements, and moderate liquefaction susceptibility. Particularly for sandy soils, DDP installation increases local soil resistance due to lateral displacement and compaction of adjacent soils (Siegel et al., 2007). DDPs are advocated as ideal construction technique for projects near vibration-sensitive sites and in zones with contaminated soils given the lack of spoils during construction (i.e., environmentally friendly construction). Additionally, financial and time efficiency have been identified as key advantages to DDP installation when placed in suitable soil types (Basu and Prezzi, 2009).

The construction of the DDP starts with the insertion of the displacement body into the ground by the rotation of the DDP construction tool and an axial force, without any soil removal. Hereafter, concrete grout is either placed with a tremie, or injected under pressure through the temporary casing, followed by the rebar cage placement. Most common DDP diameters range from 35.5 cm to 61 cm (~14 to 24 inches) with lengths up to 30m (~100 ft); however, the use of larger diameters and longer lengths have increased, allowing auger displacement piles to be considered in a broader range of project sites.

Unlike driven piles, which can be inspected and monitored before and during pile driving, DDPs are known for their blind nature. As-built DDPs require post installation non-destructive testing to verify concrete quality and to detect potential areas where soil inclusions might have occurred. Alternatively, axial, and lateral load tests can be conducted to evaluate the global pile performance, including load capacity, tolerable settlements, and tolerable lateral displacements. Static pile load testing commonly consists of applying sequentially increasing axial loads,

(typically in [2-5] % increments of the design load) and measuring the axial settlement at the top of the pile. This procedure provides load-settlement curves from which the failure load can be obtained experimentally or theoretically depending on whether the maximum load was reached during the test. To validate the design capacity, piles are commonly loaded to (1) their design loads times a safety factor or (2) a large enough load to reach geotechnical failure. A popular approach is to load pile specimens to at least 200% of their calculated design load to assure sufficient axial capacity. The Federal Highway Administration's (FHWA) report on 'Static Testing of Deep Foundations' (FHWA-SA-91-042, 1992), and the ASTM D1143M-20 (ASTM, 2020) highly recommends testing piles to failure whenever feasible, to "obtain the real safety factors intrinsic to the design". Within the database of DDPs collected by the authors, 33% of all piles were tested up to 2-2.5 times of their design load, 25% were tested up to 2.5-3 times of their design load, and 22% of piles were subjected to higher than 3 times their design load. The remaining 20% of all piles were subjected to an in-situ load less than two times the design load. A total of 30 out of the 129 piles reached complete geotechnical pile failure.

Different analytical methods to estimate the axial load capacity of piles have been developed for numerous types of pile installation techniques, soil conditions, loading protocols, among other variants. Most of the methods used for pile design were derived from driven pile or drilled shaft testing. This thesis will investigate the suitability of existing methods in predicting the axial pile capacity of Drilled Displacement Piles.

The change of radial stresses during DDP construction has been proven to be strongly dependent on the pile installation technique and to have a significant impact on the soil resistance. As stated previously, one of the primary benefits of the DDP installation technique is the densification of the soil surrounding the DDP, however, these effects are difficult to quantify and

challenging to take into consideration when designing the piling system. While a limited number of authors have developed methods to estimate the capacity specific to DDPs, the design methodologies are strongly linked to proprietary features of the respective DDP manufacturer. More specifically, the lateral soil displacement during pile installation strongly depends on the drilling tool, piling rig technology, and the installation parameters such as auger rotation, penetration rate, and installation torque during pile construction. Baxter *et al*., 2006, define three stress stages during the construction of a DDP. The first stage is related with the insertion of the drilling tool on the ground, in which the degree and extent of remolding is dependent on the geometry of the tool. The soil particles in the vicinity of the shaft are pushed into the adjacent soil which experiences an increase in lateral stresses. The second stage represents the stress relief after the passage of the displacement body of the drilling tool, with the soil particles in the vicinity of the shaft could potentially cave into the interior of the void created during the drilling process. The third stage is associated with the extraction of the drilling tool and the placement of concrete or grout inside the void. During this stage soil relaxation can occurred based on the type of soil surrounding the pile.

The soil improvement achieved by the construction of DDP has been studied by different authors by executing in-situ testing before and after the pile construction, conducting numerical modeling, and collecting experimental measurements through in-situ instrumentation. Comparisons of analytically estimated axial load capacities and actual in-situ failure loads of the DDP have also been documented in literature, suggesting an underestimation of the real capacity for most case studies. To experimentally measure the degree of change in the mechanical properties of the soil, pre and post CPT data have been commonly used. During the execution of the CPT, the cone resistance (q_t), and the sleeve friction resistance (f_s) are measured. Based on

CPT correlations proposed by Robertson and Cabal in 2014, different empirical relationships are employed to estimate soil properties and design parameters. The soil improvement is assessed based on the change of the normalized key parameters, cone resistance (Q_t) and friction ratio (F_r), as well as the change in soil behavior index (I_c).

This thesis presents data collected from 55 construction projects in which >100 DDPs were constructed and tested axially. For 10 of the construction projects, CPT testing was performed before and after pile construction to assess the soil improvement associated with the DDP installation technique. Moreover, the results of 129 axial load test are used to evaluate the ability of existing methods to accuracy estimate the axial load capacity of drilled displacement piles.

Chapter 1 presents a general overview of Drilled Displacement Piles including their construction procedures and advantages and disadvantages associated with this installation technique. Previous research on DDP such as the effect installation on the shaft resistance of the pile, comparison between the behavior of drilled shafts and DDPs, the relationship between the axial load capacity and the construction tool employed, among other topics, is also presented. Chapter 2 describes the collection, processing, and analysis of all case history data. The empirical relationships to estimate the soil properties are described and a review of analytical methods to estimate axial pile load capacities is provided. A series of different axial failure load interpretation methods is presented, and the most accurate methods to estimate the axial load failure is identified. The chapter closes with a comparison of CPT and SPT based prediction methods and evaluates their ability to predict pile failure loads. Chapter 3 studies the soil improvement due to DDP installation by comparing before and after CPT test results, hereafter labeled as CPT_{PRE}, and CPT_{POST} results, and the ratio obtained between the resistance before and after the pile installation. A spatial improvement is studied with CPT_{POST} data executed at different distances from the DDP.

The piles' axial load capacity was analytically compared by using pre- and post-installation soil properties and evaluated against field test data (when available). The summary and the conclusions derived from the study are presented in Chapter 4.

Chapter 1
Overview of Drilled Displacement Piles

1.1. Background

The main objective of employing deep foundations is to transfer heavy superstructure loading, from bridges or buildings into the ground; hereby passing weak or compressible soil layers and anchoring the foundation element into more competent strata to assure the stability and serviceability of a structure. Additionally, piles can help resist tensional or horizontal loads and accommodate the sensibility of a structure to differential settlement. Different types of materials such as reinforced concrete, timber, steel, or pre-cast concrete have been used for the construction of foundation elements. Different types of construction techniques include jacked, driven, drilled, or drilled displacement mechanisms.

Generally, piles are classified based on the construction procedure, and therefore distinguished by the amount of soil displaced during pile installation: (i) large displacement, (ii) small displacement, and (iii) non-displacement (or replacement). A large displacement pile is produced when a prefabricated pile is jacked or driven into the soil, for which the installation is performed by dropping a weight, vibration, or jacking. Small displacement piles occurred when a small cross section area, such as H section, or open-ended piles, are jacked or driven into the soil, this pile type can also be produced when the pile is placed into a pre-drilled hole. Non-displacement piles are built by excavating the soil before the pile is introduced into the ground or constructing it into the hole; the construction can be achieved by using a continuous flight auger or by underreaming. Drilled displacement piles combines the effects of a driven piles (axial load force applied to the drilling tool), and the torque applied by a continuous flight auger into the soil, without any soil removal.

1.2. Types of DDP construction tools

The amount of displacement of the soil during the construction of the piles have been proven to have a significant impact on the performance of the piles (i.e., displacement piles tend to improve the soil resistance, and the axial and lateral performance due to the densification achieved by introducing the pile into the ground, and therefore a stiffer load-displacement response.

The pile construction efficiency, and the lateral soil displacement during pile installation strongly depends on the drilling tool, piling rig technology, and the installation parameters such as auger rotation, penetration rate, and installation torque during pile construction. The surrounding soil, its composition, and mechanical properties, also play an important role on the construction of these elements. The Drilled Displacement (DD) construction tool has three essential elements per Basu and Prezzi, 2019, (i) the soil displacement body, (ii) a partial flight auger segment, and (iii) a sacrificial tip. There are different types of Drilled Displacement tools in the market, the most popular drilling tools are shown in Figure 1.1.

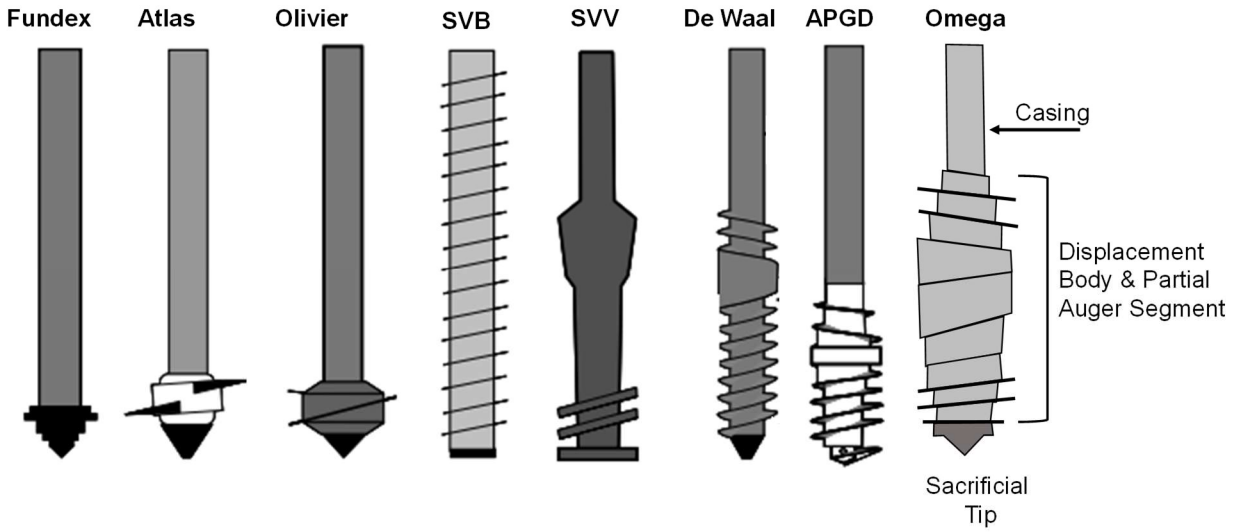

Figure 1.1. Drilled displacement tools for the construction of the piles. Adapted from Basu and Prezzi, 2019.

Per Paniagua, 2005, patented methods for the construction of DDP appeared since the early 20th century. The Atlas, Fundex, Olivier, and De Waal piles were part of the first generation of drilled displacement piles, they were formed by rotating the casing and the displacement body into the ground and leaving a large sacrificial tip. Such construction method resulted in a slower pile installation rate due to the penetration of the blunt part of the instrument. During the seventies, a second generation of DDP appeared, the new drilling tool was designed by adding flighting at the large stem or the lower end of the displacement body, such as the Schnecken-Verdrangungsbohrpfahl (SVB) and the STRABAG Vollverdrangungsbohrpfahl (SVV) piles. While this new design improved the penetration rate of the displacement body, the effects of the surrounding soil, and the final cross section of the pile where unknown and hard to define aspect of the piles. A larger displacement body was then promoted in the early nineties by Van Impe with the developed of the Omega pilling system (Paniagua, 2005). This last generation of DDP tools such as the Auger Pressure Grouted Displacement (APGD), and Omega piles are known for its drilling proficiency.

1.2.1. Fundex piles

The Fundex piles were created in the late sixties their home market comprised the Netherlands, and Belgium. The Middle and Far East along with other parts of Europe implemented this construction methodology for coastal and civil constructions as well. The diameter of the Fundex piles ranges between 0.38 to 0.45 m (15 to 18 inches), when the soil conditions are feasible, a diameter of 0.52 m (20.5 inches) could be implemented. The construction procedure of the Fundex piles is similar to the construction of the Atlas pile.

1.2.2. Atlas piles

The Atlas piles were developed around the 1960s in Belgium, this type of piles was employed all around Europe and Australia. In 1994 the construction rate achieved a production of about 100 to 150 meters of pile per day (Cock and Imbo, 1994). The pile assembly starts with the screwing into the ground the temporary casing, the displacement body, and the sacrificial tip with the rotation of the auger and a vertical force. Hereafter, the reinforcing cage is lowered followed by the extraction of the casing and the filling with concrete. After this procedure, a supplementary reinforcement could be placed inside the pile if needed. The final cross sectional of the pile would have a helical shape at all depth, and the diameter of the piles considered for the design is the diameter of the displacement body without considering the steel flanges length. The minimum and maximum pile diameter for Atlas piles range between 0.31 to 0.56 m (12 to 22 inches), and the length of the piles can be extended up to 25 m, or 28 m when the most powerful rig is used (Cock and Imbo, 1994).

1.2.3. Olivier piles

In 1996, the Belgian Gerdi Vankeirsbilck applied for the patent of the production of Olivier piles. During the installation of the Olivier pile, the casing, the partial auger, and the sacrificial auger are penetrated into the ground by a torque and axial force. Once the desired length of the pile is achieved, the sacrificial tip is released, and the reinforcement cage is placed into the temporary casing. The concrete is poured into the casing. Finally, the casing is extracted with an oscillating movement, forming a screw-shape shaft. The screw-shape pitch is around 0.25 m (~10 inches), and the external diameter is around 0.20 m (~8 inches) larger than the nominal diameter (partial auger diameter). The nominal diameter can vary between 0.36 and 0.56 m (14 and 22 inches).

1.2.4. Schnecken-Verdrangungsbohrpfahl (SVB) piles

The SVB pile was developed by the German company Jebens GmbH; this type of pile is a partial-displacement pile due to the lack of the displacement body. The piles are installed by the rotation of the helix-shaped steel casing into the ground through the application of torque and an axial force downwards. Once the pile toe depth is reached, the disposable plate used to seal the temporary casing is released, and the rebar cage and concrete are placed through the temporary casing. The extraction of the casing is then executed by a clockwise rotation of the auger casing and a vertical force upwards. While the partial-displacement pile is being installed, some of the soil particles could be transported by the helices to the surface (Paniagua, 2005).

1.2.5. STRABAG Vollverdrangungsbohrpfahl (SVV) piles

The SVV pile were also developed by the German company Jebens GmbH, contrary to the SVB pile, the SVV are a large-displacement type of pile. The patented drill head diameter is larger than the displacement body and casing diameter. The construction procedure is similar to the installation of the SVB piles. The maximum length of the SVV piles is 24 m, and the diameter could range between 0.40 and 0.67 m (16 and 26 inches) (Geoforum 2012).

1.2.6. De Waal piles

De Waal piles were invented in Europe in 1985 and has been installed in the U.S. since 1992 by the construction company Morris-Shea, the U.S. patent holder. Apart from the displacement body, the temporary casing, and the sacrificial tip, a partial auger is included on the drilling tool. The installation of this type starts by drilling clockwise the installation tool by rotation and an axial force, once the pile toe depth is reached, the sacrificial tip is detached due to the concrete injection. The extraction of the casing is made by a clockwise rotation and an axial force upwards. Once the

drilling tool is extracted, and the concrete have been poured into the hole, the rebar cage is lower into the pile.

1.2.7. Auger Pressure Grouted Displacement pile

In the earlies 2000s, the Auger Pressure Grouted Displacement (APGD) was invented by Ben Stroyer in New York (US), and patented by Berkel & Company Contractors, Inc. The novelty of this design of DDP consisted of the helical auger in an elongated displacement body with a central chamber. The filling of the created void was performed by pressure injecting the grout after extending up to the pile length. Moreover, the final cross-section of the pile is consistent and continuous. The pile diameter for this construction tool range between the 0.30 and 0.50 m (12 to 20 inches). Constructible could be up to 24 m length.

1.2.8. Omega piles

Omega piles were developed in Belgium in 1998, The pile diameter ranges between 0.40 to 0.61 m (16 to 24 inches), and the maximum pile length reached has been 29 m (96 ft). The installation of this type of piles is similar to the installation of the APGD piles with the difference that the concrete is pressure injected into the temporary casing even before the pile has not reached the desire length.

Figure 1.2 shows the general construction procedure of a DDP. It is important to note that the sequence and technique of placing the concrete- and rebar cage in the borehole as depicted in Figure 1.2 can vary depending on the DDP type and the proprietary methods developed within the industry.

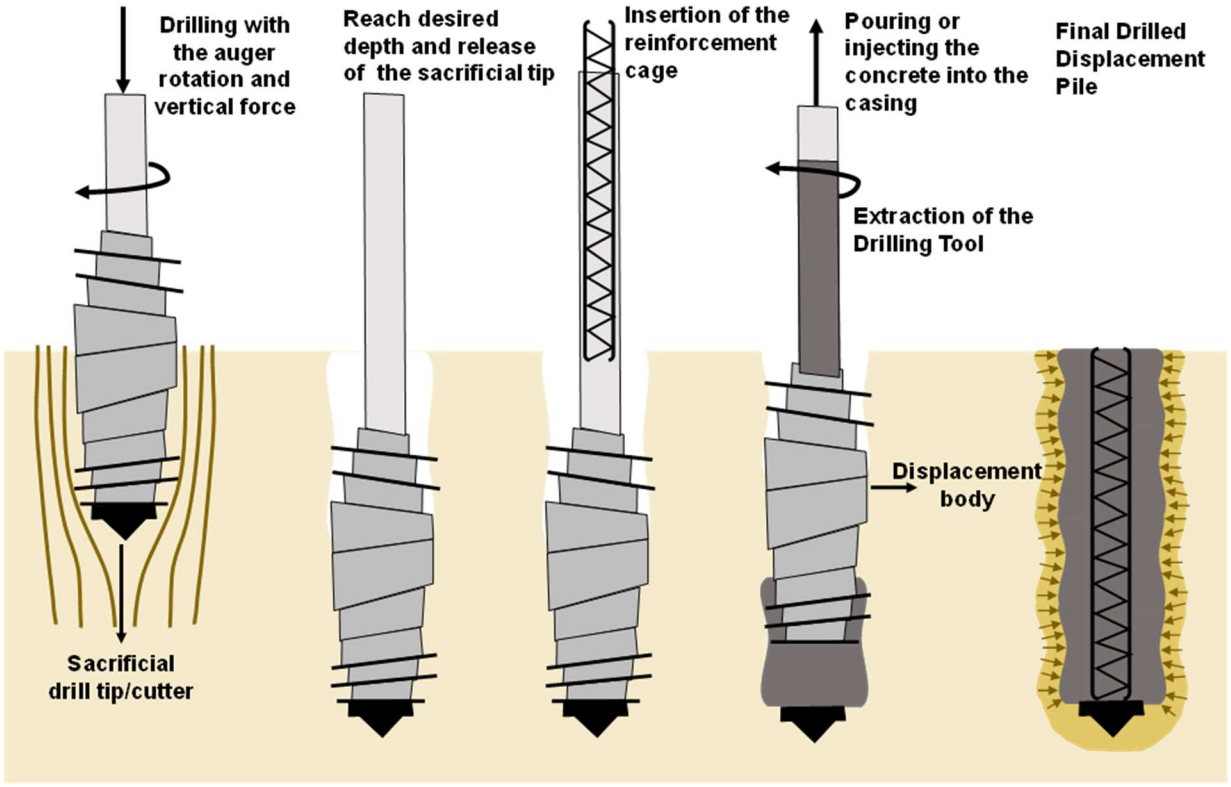

Figure 1.2. General construction procedure of a Drilled Displacement Pile (DDP). Adapted from Basu and Prezzi (2005).

1.3. Advantages and disadvantages of the use of DDP

As described above, the use of DDPs started in the 1960s in Europe, and has grown globally in the last decade. The main advantages of the DDPs are summarized below:

- Noise-free installation: Unlike pile driving, one of the noisiest construction activities (~120 dBA at 10 ft away), the DDP assembly is a silent operation throughout the entire process.
- Vibration-free installation: When the construction sites have vibration constraints in the proximity of vibration-sensitive structures such as hospitals, historic, or industrial buildings, the DDP technique offers a suitable pile construction methodology since there is no dynamic force applied to the ground and no vibration can be perceived.
- Minimal or no soil removal: During the construction of the DDP the soil removal is minimal and no soil is transported outside the borehole. This provides an environmentally friendly and cost-effective solution.
- Minimize the material waste: The mechanism employed for the pouring or injecting of the concrete (through the temporary casing) helps to minimize the concrete waste. Moreover, unlike prefabricated piles, where pile lengths are fixed prior to installation, the DDP length can vary according to the penetration of the drilling tool.
- Soil improvement: Due to the large horizontal displacements caused by the drilling tool for some soils (mainly cohesionless soils), the soil resistance can increase as a result of the densification of the soil surrounding the DDP. Therefore, the load-settlement or load-displacement curves can obtain a stiffer response. The soil improvement due to the construction of the DDP have also been used to mitigate liquefaction effects for some construction projects.

Although the construction of DDP offer many advantages for suitable projects, there are also some disadvantages that the designer and constructor need to consider.

- Based on NeSmith, 2002, the ideal soil type for the installation of DDP, to achieve the soil improvement, is a clean, well-graded sand with a loose density at a shallow depth, and a gradual increase of the density with depth.
- When the construction site soil profile present very dense soils, the drilling of the displacement body can be difficult to achieve, and therefore reduce the construction time-efficiency of the piles.
- For some of the DDPs, the cross section of the pile can be challenging to define, and therefore the analysis of the behavior of the piles can be misleading when using the common analytical methods.
- Since the use of DDPs is a relative new technique, there hasn't been many studies on the behavior of these elements. Only two authors have proposed methods to estimate the axial load capacity of these members. To date, no method to analyze the horizontal load response of this type of piles have been presented.
- Finally, unlike driven piles, which can be inspected and monitored before and during pile driving, DDPs are known for their blind nature. As-built DDPs require post installation non-destructive testing to verify concrete quality and to detect potential areas where soil inclusions might have occurred.

1.4. Previous research on DDPs related to this study

1.4.1. Research on axial load capacity of DDPs

Basu and Prezzi (2009) modeled the pile installation and axial loading via one-dimensional fine elements analysis. The authors proposed an analytical method to estimate shaft resistance of DDPs installed in sandy soils by considering the effects of the drilling tool on the soil's relative density and level of confinement. Basu and Prezzi proposed the inclusion of a lateral earth pressure coefficient into the analysis of shaft resistance at limit state for different installation velocity ratios. The "before - after" ratio of the lateral earth pressure coefficient following pile installation, was found to be 2.2 to 2.7 times larger than the respective ratio for drilled shafts, and only 0.4 – 0.47 the ratio of traditional displacement piles. Similarly, the finite element analysis suggested the limit unit shaft resistance for DDPs to be larger than for drilled shaft (non-displacement piles) but lower than for jacked piles (displacement piles). The influence of the velocity of penetration and rotation ratio, and the effects on the radial stress surrounding the pile were also assessed in every construction phase (i.e., during the penetration and extraction of the drilling tool, and the pile loading). Basu and Prezzi found the radial displacement of the soil during pile installation to reduce the radial stress around the pile shaft. Also, after the removal of the drilling tool, the torsional shear stress at the vicinity of the pile shaft becomes zero and the vertical shear stress reaches a negative limiting value. The installation effects, and therefore the relationship between the final and initial lateral earth pressure coefficient was proven to have a great impact on the shaft capacity of DDPs.

Shah and Deng (2016) studied the installation effects on the axial load response of four different piles installed in the same soil: drilled cast-in-place, continuous flight auger, drilled displacement, and drilled displacement steel piles. All piles had an identical length (12 m) and

nearly identical diameters. The piles were heavily instrumented and axially tested to failure. The shaft resistance along the pile length and the toe resistance were recorded. At shallow depths, all piles indicated lower shaft resistance than analytically predicted. This (rather expected result) can be attributed to the low confinement stress at shallow depths and limited soil densification near the ground surface. For deeper layers, the shaft and tip resistance measured for the piles was higher than what the analytical methods suggested. The total axial capacity of the DDP was found to be 1.5 times higher than the capacity of the drilled shaft.

Moshfeghi and Eslami (2018) studied the reliability of CPT based predictions for axially loaded DDPs by specifically focusing on the installation technique and drilling tool. The results of 65 static load tests on DDPs were used to find a correlation between the predictive performance and drilling tool employed during pile construction. Moshfeghi and Eslami found the accuracy of the predicted pile capacity to be dependent on the drilling tool; for instance, the capacity of Atlas piles, a DDP type originating from Europe, was best predicted by the Brettmann and NeSmith (2005) method. The study also showed that for some CPT direct methods, the axial load capacity results are highly conservative for clayey soils.

Rad et al. (2021) compared the torque applied during construction, and the axial load performance of three different piles. A drilled displacement pile (DeWaal), a helical pile, and a Tsubasa pile (a frequently used drilled displacement pile in Japan) were constructed and tested under compressive load. Two sets of experiments (large scale and model scale) were performed in the field, and in the laboratory, respectively; employing similar soil conditions: poorly graded sand (SP) with a friction angle between 32 - 34 degrees. The authors found that the DDP required a much higher torque compared to the other two piles, which was mainly attributed to the difference between the DDP diameter and the shaft diameter and geometry of the helical and Tsubasa pile.

For all piles, the amount of torque needed to penetrate the soil was found to be proportional with depth. Even though the need of a lower torque during construction of the helical and Tsubasa piles might be seen as an advantage, the axial load test results suggested the performance of the DDP to be superior compared to the other two pile types. During the compression load test, the DDP reached a higher ultimate load, around 1.4 times higher than the helical and Tsubasa pile, and a lower settlement (~10%D) at failure.

Siegel et al. (2019) studied the end resistance of continuous flight auger (CFA) piles and drilled displacement piles in clayey soil with interbedded sand seams. Experimental data from 15 compression load tests were compared with analytical predictions of pile tip resistance Q_{tip} (i.e., $Q_{tip} = 9*Cu$, where Cu is the clay's undrained shear strength). A higher tip resistance was measured for both pile types in comparison with the conventional analytical estimate of 9 times the shear strength for bored piles. The authors did not find significant differences between the tip resistance of the CFA and the DDP piles, the later was attributed to the type of soil in which both piles were installed and their amenability to improve the soil resistance due to the construction technique of the pile.

1.4.2. Research on soil improvement due to the construction of DDPs

Siegel *et al*. (2007) assessed the soil densification and lateral load increase due to the installation of DDPs in granular soils. Pre- and post-installation CPT data, referred to as CPT_{PRE} and CPT_{POST} results, were compared to obtain the ratio of tip resistance (q_t) before and after pile installation. The study showed a general increase in the tip resistance for all sites and suggests an inverse relationship between the level of improvement and the tip resistance measured before the construction of the pile (i.e., less improvement achieved at initially higher tip resistances).

Pucker and Grabe (2012) numerically studied the influence of different penetration (v_z) and rotation (v_r) velocity ratios (i.e., (v_z/v_r)) for two sandy soils with different relative densities (D_R = 20%, 50%, and 80%). Velocity ratios v_z/v_r of 5 (low) and 10 (high) were stablished to assess the effects of the drilling velocity on the level of ground densification. The results showed that the soil reaction force for a low velocity ratio, is higher than for a large velocity ratio. The rotational moment appears to be invariant regardless of the velocity ratio. The horizontal soil displacement for different velocity ratios and different D_R were assessed, showing that higher displacements were reached in sands with low relative density and at shallow depths. The spatial change in relative density was numerically evaluated for distances from 0 to 10D away from the pile (where D is the pile diameter), suggesting that sands tend to loosen up close to the installed pile [0-1D], be strongly densified from a distance between 1D-2D, and be moderately densified between 2D-7D for a particular drilling tool. For a sandy soil with low in-situ relative density (e.g., D_R = 20%), the increase of q_t, and therefore D_R, is significantly higher than for soils with higher D_R (e.g., 5 times increase of the tip resistance for a D_R equal to 20%, and 1.4 times higher for an initial D_R of 80%). The results were similar for the two types of sand, from which Pucker and Grabe (2012) concluded that the optimal drilling parameters are rather influenced by the geometry of the construction tool than by the soil parameters. However, given the limited ranges of soils included in this study, no further conclusions can be drawn pertaining to the improvement of sands with other properties or substantially different soil types.

Meng *et al.* (2015) studied the installation effects of DDPs in soft clay by measuring the horizontal displacement and pore water pressure dissipation during and after construction, and up to 15 days after pile installation. However, the piles installed by Meng *et al*. do not follow the traditional definition of a drilled displacement pile (i.e., no oversized displacement body was

included in the drilling rod). While it is assumed that no soil spill occurred, the piles assimilated a screw-type pile with a continuous inner core and a continuous outside blade arrangement, which created screw-like cut-ins inside the borehole, yielding two different diameters within the borehole: an internal diameter of 370 mm and external diameter of 500 mm. Two 20.4 m long piles were installed in clayey and silty soil layers with an average shear strength of 11.5 kPa. To measure the horizontal displacements induced by pile installation, inclinometers were placed at 0.6 (~1*D*), 2 (~4*D*), and 3 meters (~6*D*) away from the DDP, and at different depths. The maximum horizontal displacement was observed at the end of penetration or after concreting; displacements were observed to decrease with time as result of excess pore water pressure dissipation and subsequent radial consolidation. For instance, 15 days after concrete placement, the lateral displacement at pile mid-height (10m depth) decreased by 15%. A spatial improvement analysis at similar pile depths suggested the maximum horizontal displacement to occur at 1*D*. At a distance of 6*D* between the pile and the inclinometer, the maximum displacement was found to be seven times smaller than at 1*D*. The authors also recorded the change in the excess pore water pressure by installing piezometers at 2 and 4 meters (i.e., ~4*D* and 8*D*) away from the piles, and at different depths. The results suggested that maximum excess pore water pressures were generated at the end of penetration and during concrete placement and dissipated approximately after 3 days after.

Chapter 2

Axial Load Capacity Predictions of DDPs with SPT- and CPT-based Direct Methods

2.1. Database of static pile load tests

Data from more than 50 US-based, and 4 German construction projects was collected. The majority of data originated from the West and South-East of the United States, including California, Florida, and Louisiana as shown in Figure 2.1. All data was provided by members of the DFI technical committees. The authors performed a comprehensive review of the project information and filtered the projects based on the following:

- Availability of geotechnical site data obtained from high quality in-situ soil testing and sampling; information about the groundwater table location; proximity between in-situ soil test and the DDP location
- Description of the DDP design and construction, including pile diameter, pile length.
- Availability of axial load test data within a meaningful load-displacement range and suitable for failure interpretation.

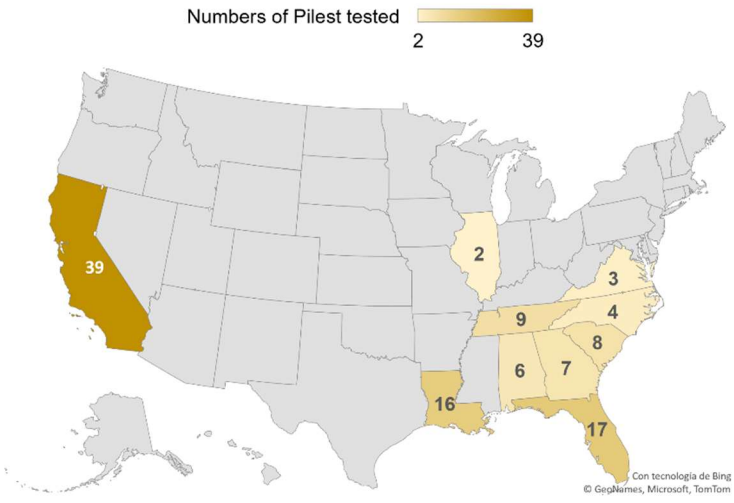

Figure 2.1. Location of the construction projects in The United States, and number of the piles tested by State.

The need for axial load tests to reach a substantial level of settlement to meaningfully interpret the pile axial failure load resulted in discarding several pile tests from this study. Only load test curves with visible onset of strength loss were kept. These remaining project data are summarized in Table 2, which shows the general site location, number of piles tested at each site, soil type, type of in-situ soil test (e.g. SPT/CPT), pile diameter (D), and pile length (L). The test sites consisted of mostly mixed types of soils with strongly stratified sand, silt, and clay layers. The nominal shaft diameters varied from 35 to 61 cm (14 to 24 inches). The embedment length of the piles ranged from 6 m to 29 m. A total of 129 static axial load test measurements were evaluated against CPT and SPT based predictions (i.e., direct methods). Potential effects of the various types of displacement drilling tools on the piles' axial capacity were not considered in this study, as this information was not consistently available for all projects. This restriction poses a limitation to the study, as the construction method (tool and grout placement) is known to affect the final performance behavior (see Moshfeghi and Eslami, 2018). Nevertheless, is also enabled the authors to conduct a more global performance evaluation without getting involved in proprietary and confidentiality related matters and obtain more data. The asterix (*) in Table 2.1 denotes sites where pre and post CPT tests were carried out. Post-CPT tests were conducted at a distance ranging from 0.75 to 1.2 m away from the installed pile to assess the potential spatial improvement of the surrounding soil.

2.2. Geotechnical data review

Cone Penetration Test (CPT) and Standard Penetration Test (SPT) data were subsequently processed to obtain geotechnical analysis/design parameters. CPT results were interpreted following Robertson and Cabal (2014). The SPT N-values (blow-counts/feet) reported in the boring logs were corrected to obtain N_{60} values, based on the sampler method, hammer type, and

Energy values reported by the respective testing company. SPT results were then further processed using empirical relationships from Hara *et al*. (1974) and Peck *et al.* (1974) to calculate the undrained shear strength and friction angle per Eqs. 2.1 and 2.2, respectively, i.e.,

$$S_u = 0.29 P_a (N_{60})^{0.72} \quad [2.1]$$

$$\phi' = 27.1 + 0.3\left(N_{1,60}\right) - 0.00054(N_{1,60})^2 \quad [2.2]$$

where S_u= undrained shear strength, P_a= atmospheric pressure (101.3 kPa), N_{60}= SPT blow count corresponding to 60% of the theoretical free-fall hammer energy, ϕ'= soil friction angle, and $N_{1,60}$ = energy and overburden pressure corrected SPT blow count.

Most CPT and SPT based design methods require the soil (layers) to be categorized into cohesionless or cohesive soils. Robertson and Cabal (2014) define the soil index behavior (I_c) as a function of the CPT based tip and side resistance. A value of I_c higher than 2.6 suggests the soil behavior to be silt like, clayey silt like to silty clay like, or clay-like in general. An I_c value lower than 2.6 suggests sand-like behavior, including silty sands to sandy silts and sands in general. The 2.6 value for the index behavior was employed as a threshold to categorize the soil layers. For the projects in which CPT data were not available, the Unified Soil Classification System (USCS) defined in the SPT logs was utilized for the same purpose. Table 2.1 categorizes each project location in sand-, clay-, and mixed sites using the I_c criteria described above. Sites with less than 20% of clayey-silt-like index behavior were classified as sandy soil sites. Sites with more than 70% of the clayey-silt behavior index were classified as clayey sites. All other sites were labeled as mixed soil sites. This classification resulted in 23 sandy soil sites; 11 clay sites; and 20 sites with highly stratified soil profiles (mixed soils). Figure 2.2 shows an example of the in-situ soil test data and an accompanying axial load-settlement curve Figure 2.3 for a project located near Redwood, CA. This site would be categorized as mixed site since 55% of the calculated soil

behavior indices (SBT) along the pile depth reach values higher than 2.6 (suggesting clayey soil), and 45% of the SBT indices are lower than 2.6 (suggesting sandy soil). Four piles were axially tested on this site, and Figure 2.3 shows the results for every pile (A, B, C, D). Pile A and C revealed clear plunging behavior (increase of settlement higher than 20% due to an 2% increase of axial load) at an axial load of 910 kN and 1230 kN, respectively. For piles B and C, the plunging behavior cannot be clearly observed. The maximum increase of settlement due to an increase of axial load of 2%, was recorded as only 9% and 5% for each pile, respectively.

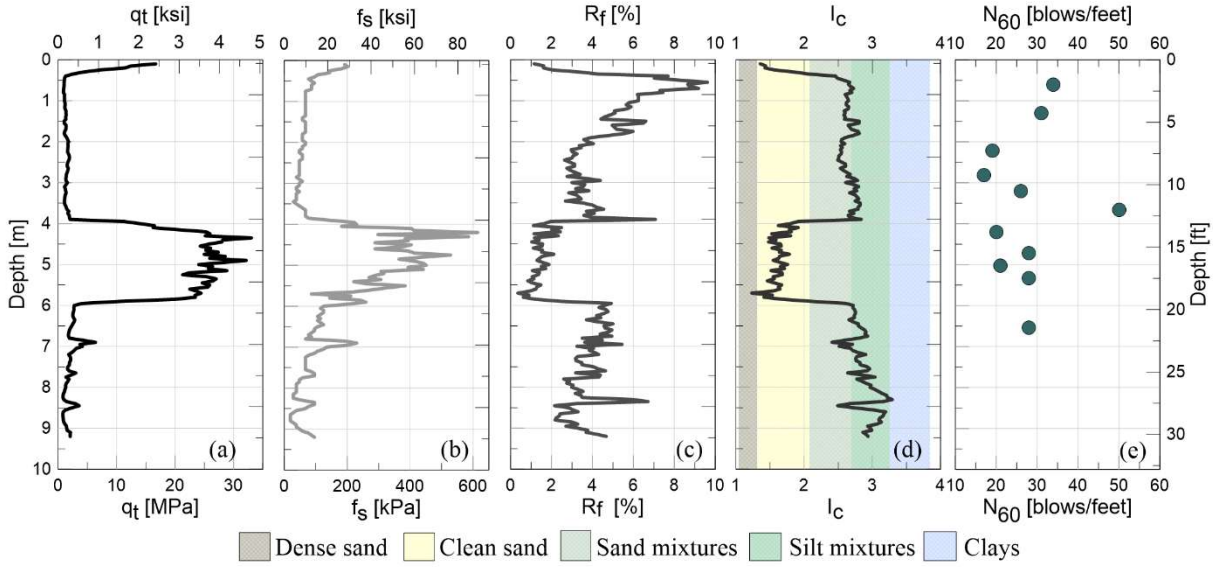

Figure 2.2. Redwood city project in-situ soil test: (a) CPT tip resistance (qt). (b) CPT side resistance (fs). (c) Friction ratio R_f in %. (d) Soil index behavior (I_c) per Robertson and Cabal (2014). (e) Energy-corrected SPT blow counts N_{60}.

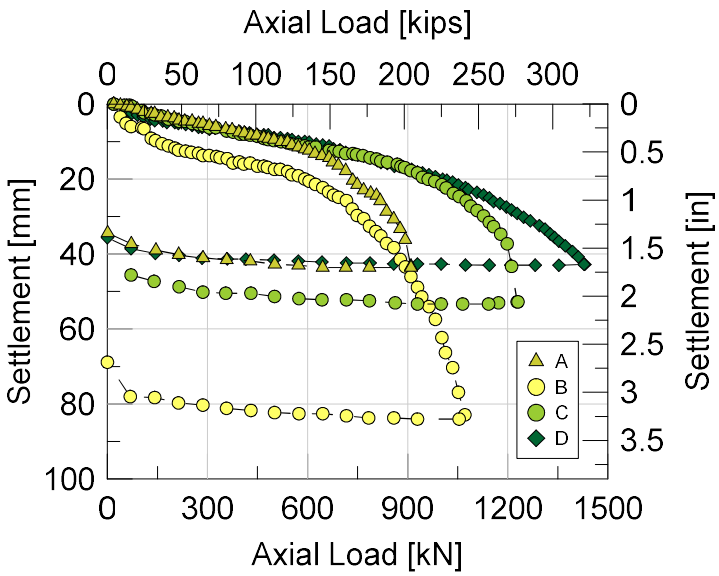

Figure 2.3. Axial load-settlement curve from test.

Table 2.1. Overall information of each project site and tested piles.

Location	D (m)	L (m)	Qdesign (kN)	In-situ test	Soil Type	SI	Piles tested
San Francisco, CA	0.45	6.4	427	SPT-CPT	*Silty clay, Clayey silt, silty sand base	3	1
Los Angeles, CA	0.40	8.2	570	SPT-CPT	*Silty clay, Clayey silt, silty sand base	3	1
San Jose, CA	0.40	6.7 - 15.2	214-390	SPT-CPT	*Silty clay, Clayey silt, silt base	3	2
Redwood, CA	0.45	7.6	355	SPT-CPT	*Silty sand, sand, silt, silt base	3	4
Los Angeles, CA	0.40	11.3	1312	CPT	*Sand, silty sand, clayey silt, sand base	3	2
Santa Clara, CA	0.45	14.6	890	SPT-CPT	Clay and silty clay, sand, sandy silt base	3	2
Stockton, CA	0.45-0.60	19.8	667-1000	CPT	Soft clay, sand, stiff clay, silty clay base	2	2
San Francisco, CA	0.40	18.3	1423	SPT	Clayey Silty sand, silty sand, silty sand base	1	1
Anaheim, CA	0.45	13.916.9	1423-2002	SPT-CPT	Silty sand, sand, silt, silt or sand base	3	3
San Francisco, CA	0.45	12.20	1112	SPT	Sand, silty sand, clay, sand base	1	1
Sacramento, CA	0.40	18.9	1112	SPT-CPT	Silty clay, silty sand, sand, silty clay base	2	1
Sacramento, CA	0.45	13.4	890	SPT	Stiff silty clay, clayey silt, sandy gravel base	3	1
San Francisco, CA	0.45	24.3	712.00	SPT	Sandy clay, clay, sand with clay base	3	1
Sacramento, CA	0.35-0.40	23.2	601	SPT-CPT	Silty sand, silty clay, clay, sand, sand base	3	2
San Francisco, CA	0.40	11.3	1120	SPT-CPT	Silty sand, silty clay, sand, sand base	3	1
Sacramento, CA	0.45	10.7-11.6	1334-1912	SPT-CPT	Sand, silty sand, clay, clay base	2	2
Sacramento, CA	0.40	8.2	534	SPT-CPT	Silty sand, silty clay, clay, sand base	3	1
McClellan, CA	0.4	20.4-21.8	569	SPT-CPT	Silty sand, sand, silt, sand base	1	2
Daly City, CA	0.40	21.3	1334	SPT-CPT	Silty sand, sand, sand base	1	1
Santa Rosa, CA	0.45	16.7	667	SPT-CPT	Silty sand, sand, sand base	1	1

Location	D (m)	L (m)	Qdesign (kN)	In-situ test	Soil Type	SI	Piles tested
Tampa, FL	0.45	7.6	-	CPT	*Sand, silty sand, silt, sand base	1	1
Caddo, LA	0.40	13.4-18.9	1470	CPT	Sand, silty sand, clay, clay base	3	7
Florence, SC	0.35	10.7-14.6	882	SPT	Sand, silty sand, clayey silt, sand base	1	8
Orlando, FL	0.40	13.1-23.2	1225	CPT	Sand, silty sand, clay, sand base	3	7
Guthrie, KY	0.35	13.2-17.8	882-980	SPT	Clay and silty clay, clay base	2	7
Miramar, FL	0.40	8.5-10.1	833	CPT	Sand, silty sand, clayey silt, sand base	1	2
Monroe, LA	0.35	7.9-9.1	980	CPT	Silty sand, silty clay, clay, sand, sand base	1	2
Westlake, LA	0.60	9.1-16.8	490-1323	CPT	Clay and silty clay, clay base	2	3
Mobile, AL	0.40	21.6-24.4	980.00	CPT	Silty clay, silty sand, sand, silty clay base	3	4
Roxana, IL	0.45	6.1-9.8	563-1225	SPT	Sand, silty sand, clayey silt, sand base	1	2
Memphis, TN	0.40-0.45	15.85	421-735	SPT	Clay and silty clay, clay base	2	2
Clayton, NC	0.35	18.3-19.8	1250	SPT	Silty clay, silty sand, sand, silty clay base	1	3
Virginia Beach, VA	0.40	9.5-12.2	735-1176	SPT	Sand, silty sand, clayey silt, sand base	1	2
Atlanta, GA	0.45	10.3-16.5	1960	SPT	Clay and sand, sand base	3	2
Memphis, TN	0.35	7.7-12.9	931	SPT	Sand, silty sand, clayey silt, clay base	1	3
Savannah, GA	0.40	14.0-17.1	1470	CPT	Sand, silty sand, clayey silt, sand base	1	3
Tuscaloosa, AL	0.35	18.6	764	SPT	Sand, silty sand, clayey silt, stiff clay base	3	1
Port Allen, LA	0.35-0.45	9.1-28.9	255-1729	CPT	Clay, silty sand base	3	4
Savannah, GA	0.35	15.9	1112	CPT	Clayey Silty sand, silty sand, silty sand base	3	1
Pensacola, FL	0.40	9.1-11.0	980	SPT	Sand, silty sand, silt, sand base	1	3
Pensacola, FL	0.40	18.29	1274	SPT	Silty sand, silty clay, sand, sand base	1	2
Mobile, AL	0.40	50.00	-	SPT-CPT	Sand, silty sand, clayey silt, sand base	1	1
Owensboro, KY	0.35	44.00	-	SPT	Silty sand, silty clay, clay, sand, sand base	1	1
Memphis, TN	0.40	50-73	-	SPT	Sandy clay, clay, sand with clay base	1	1
Fort Myers, FL	0.45	75.00	-	SPT	Sand, silty sand, silt, sand base	1	1
Memphis, TN	0.40	70.00	-	SPT-CPT	Clay and silty clay, sand base	3	3
Redwood, CA	0.40	18	711	CPT	Silty clay, sandy silt with medium sand layers	2	2
Redwood, CA	0.40-0.45	18.3	533-711	SPT	Lean and fat clay, and silty sand	2	4
Belmont, CA	0.40	18.3	-	CPT	Soft clay, stiff silty sand and silty clay	2	2
Mountain View, CA	0.40	24.4	-	CPT	Shallow stiff lean clay, and lean clay with sand	2	2
Santa Clara, CA	0.40	23	1140	CPT	High plasticity clay and stiff clay with sand layers	2	3
Kleve, DEU	0.51	9.5-10	-	DPH	Sand, silty sand, sand base	1	2
Glasgow, UK	0.51	13.5	-	CPT	Loose to medium sand, sand base	1	3
Hamburg, DEU	0.35-0.51	5.8-10.3	-	CPT	Medium sand with silt layers	1	4
Rin-Lahn, DEU	0.51	6.5	-	DPH	Sand, silty sand, silt, sand base	1	1

* Projects with Pre and Post CPT

SI: Overall Soil Interpretation. (1) sand like, (2) clay like, and (3) mixed soil

2.3. Review of analytical and empirical methods to predict axial pile capacity

Depending on the availability and quality of the in-situ geotechnical data, two primary approaches to predict pile axial load capacity have emerged in geotechnical practice: indirect methods and direct methods. As implied by the name, direct methods use in-situ soil test data "directly" within their formulation, such as the blow count (N-SPT) of the Standard penetration test (SPT), and the tip and side resistance (q_c and f_s, respectively) of the cone penetration test (CPT). In turn, indirect methods use geotechnical parameters estimated from empirical relationships, such as undrained shear strength (S_u), friction angle (ϕ), or the over-consolidation ratio (OCR). Indirect methods were not utilized for the analyses presented in this paper.

According to Eslami and Fellenius (1995), general North American geotechnical practice mostly employs the following methods for predicting axial pile capacities: Schmertmann and Nottingham (1975; 1978), DeRuiter and Beringen (1979), Bustamante and Gianeselli (1982), also known as LCPC (Laboratoire Central des Ponts et Chaussées), Bustamante and Gianeselli (1993), and the Eurocode (1993). In addition to the aforementioned methods, this study also includes methods developed by Niazi and Mayne (2016) and Brettmann and NeSmith (2000-2005). Table 2.2 provides a summary of direct methods, including a detailed description for which types of piles these methods have been originally developed, and what geotechnical parameters (or measurements) are needed to calculate the pile's side friction and toe bearing resistance. Amongst all methods listed in Table 2.2, only Bustamante and Gianeselli (1993; 1998) as well as Brettmann and NeSmith (2000; 2005) were developed specifically for DDPs. Both methods were calibrated based on axial load test results, in-situ soil tests, and geo-mechanical soil properties obtained from empirical relations. Little information was provided on the effects of soil disturbance and the axial load capacity of the piles. Therefore, these two DDP methods are similarly narrowed to particular

soil types, drilled displacement tools, and pile geometries as many of the above listed approaches. This limitation is common when empirical methodologies are developed based on proprietary information and/or technologies, predominantly led by private contractors. Brettmann and NeSmith's (2000-2005) method, developed for augered, pressure-injected drilled displacement piles, can be used with CPT and SPT data alike, and represents the only SPT-based method available in literature for DD piles. As indicated in Table 2.2, most other methods are derived for drilled or driven piles. Hence their application to DDPs is an extrapolation beyond their intended use, driven by the limited availability of DDP-specific solutions. For instance, two of the most employed SPT based methods (i.e., Decourt (1989; 1995) and Meyerhof (1976)) were derived for driven piles; and O'Neill and Reese (1988) and Brown, *et al.* (2010) are SPT-based methods recommended by the FHWA-NHI-10-016 for drilled shafts.

Table 2.2. Current SPT & CPT based methods for estimating axial pile capacity.

	Pile Type/ Installation	How to determine pile side friction	How to determine pile toe bearing
Direct Methods from CPT data			
Schmertmann and Nottingham (1975-1978)	Driven and Drilled shaft	CPT Sleeve friction (fs) and pile material	CPT Tip resistance qt and over consolidation ratio OCR
deRuiter and Beringen (1979)	Driven piles	Over consolidation ratio (OCR), undrained shear strength (S_u), CPT tip resistance (q_t).	Undrained shear strength Su (Laboratory or CPT), tip resistance qt
LCPC. Bustamante and Gianeselli (1982)	Drilled, driven, grouted, barrettes piles and piers foundations	Eslami's soil classification index, undrained shear strength (S_u), CPT tip resistance (q_t)	Tip resistance qt and pore water pressure u.
Eslami and Fellenius (1997)	Driven piles	Pile construction method and soil behavior type index (I_c)	Tip resistance qt and pile diameter D
Niazi and Mayne (2016)	Drilled piles, jacked piles and driven piles	Sleeve friction (f_s), tip resistance (q_t), soil index behavior (I_c), pile installation, loading direction, loading rate.	CPT Sleeve friction fs, CPT tip resistance, soil index behavior
Brettmann and NeSmith (2000;2005)	Auger Pressure Grouted Drilled Displacement	Soil gradation and angularity, CPT tip resistance (q_t)	Soil gradation and angularity and tip resistance

	Pile Type/ Installation	How to determine pile side friction	How to determine pile toe bearing
Bustamante and Gianeselli (1993;1998)	Drilled displacement piles	Pile installation, CPT sleeve friction (f_s), CPT tip resistance (q_t), soil index behavior (I_c)	Sleeve friction, tip resistance, index behavior
Direct Methods from SPT Data			
O'Neill and Reese (1988)	Drilled shafts	Depth below the ground and overburden effective stress Adhesion factor and undrained shear strength	N_{60} blow count, assuming good workmanship Bearing capacity factor and undrained shear strength
Brown, *et al*. (2010)	Drilled shafts	Coefficient of lateral earth pressure before and after construction, overburden effective stress	N_{60} blow count
Decourt (1989; 1995)	Driven and bored piles	Pile installation, soil type, N-index along the pile shaft	Pile installation, soil type, N-index at the pile toe
Brettmann and NeSmith (2000;2005)	Auger Pressure Grouted Drilled Displacement	Soil gradation and angularity and N_{60} blow count	Soil gradation and angularity and N_{60} blow count
Meyerhof (1976)	Bored and driven piles	Shaft coefficient based on the pile installation, N-index along the pile shaft.	Toe coefficient based on the pile installation, N-index at pile toe.

2.4. Data Analysis

2.4.1. Interpretation of axial failure based on pile load tests

The American Society for Testing and Materials (ASTM, 2020), as well as the American Association of State Highway and Transportation Officials (AASHTO, 2008) define the failure load as the load which induces a visually observable plunging behavior in the axial load versus displacement curve. The plunging behavior is referred to as a gross settlement of the tested element. In turn, Fellenius (2001) highlights the fallacy and misinterpretation of the "failure load" or "ultimate load" of a pile since the shaft resistance is the only resistance mechanism that exhibits an ultimate resistance while the axial compression of the pile and the pile toe bearing show a linear response and do not have an ultimate value besides the structural failure of the pile. As alternative, Fellenius (2001) suggests the use of the load that triggers a settlement equal to 10% of the diameter of the pile. The International Building Code (IBC), 2019, defines the allowable pile load as one

half of the ultimate axial load of the test element assessed by using Davisson Offset Limit, Brinch-Hansen 90% criterion, Butler-Hoy criterion, and other methods approved by the building official.

For piles in soft or medium clays, plunging behavior can be clearly identified in most load-settlement curves; therefore, failure loads can be easily determined through visual inspection. On the other hand, for medium soils, stiff clays, and sands, the slope of the resulting curve is stiffer and does not necessarily show the change in the slope during loading (i.e., it does not reach failure). Amongst the projects collected for this study, eight axial load tests were discarded due to the very flat load-displacement curve during the test (e.g., pile-soil system is too stiff) that no tendency towards failure can be identified within the available range of test data. Regardless of the soil conditions, geotechnical failure generally occurs well before the ultimate structural capacity of the pile is reached.

To determine the failure load for each project listed in Table 2.1, two different approaches were adapted: (i) failure was defined based on substantial strength loss (plunging) whenever clearly visible in the vertical load vs. displacement curves: this was the case for 30 piles, and (ii) failure loads were estimated using interpretation methods from literature whenever failure was not reached experimentally (which was performed for 70 piles). Additionally, a corresponding axial load for a settlement equal to 10% of the pile diameter was identified whenever possible.

2.4.2. Review of existing methods to interpret axial pile failure

Current literature offers several methods to estimate/interpret the anticipated failure load when axial failure was not reached during field testing. The most common approaches are Decourt Extrapolation (1999), the Davisson Offset Limit Load (DOL) (1972), the Hansen 80-% Criterion, the Brinch-Hansen 90% criterion, Chin-Kondner Extrapolation (1970) also known as the inverse method, the Butler & Hoy (1977) Load, also known as “double tangent method” or “L1-L2

method", De Beer's Criterion (1968) or "maximum curvature" method, and the Van der Veen's Criteria (1953). The corresponding axial load for a settlement equal to 10% of the pile diameter was defined as an alternative "failure load" for CPT methods such as the Niazi and Mayne (2016) and Bustamante and Gianeselli (1993; 1998) methods, which define the predicted failure load at a displacement equal to 10% of the pile diameter instead of the traditional definition of pile failure in literature.

The procedure to identify the failure load for each of the above-listed methods is described hereafter. Figure 2.4 summarizes these methods graphically, by depicting the required tangents and bisectors to a schematic load-displacement illustration.

2.4.2.1. Decourt Extrapolation (Decourt, 1999)

The measured values from the axial load test are assumed to be hyperbolic and required to be fitted by Equation 2.3. Once the values calculated with Equation 2.1 fit the observed data, the failure load is determined by the inverse value of the fitting constant k_2, i.e., $Q_f = 1/k_2$.

$$Q = \frac{\delta}{k_1 + k_2 \delta} \quad [2.3]$$

Where Q is the applied axial load, δ is the pile settlement, and the values k_1 and k_2, are fitting constants to the hyperbolic equation found by using ordinary square regression.

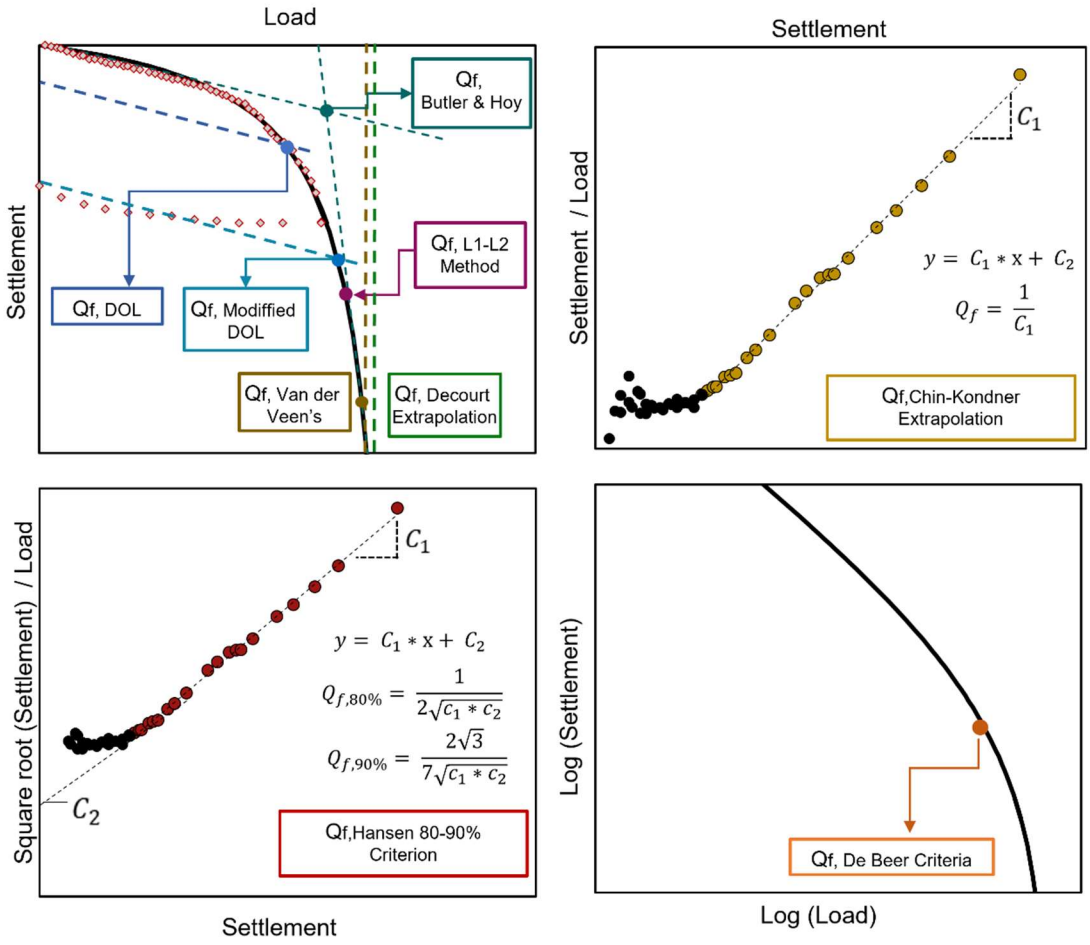

Figure 2.4. Illustration of the interpreted failure load methods for the static-axial load test.

2.4.2.2. The Davisson Offset Limit Load (DOL) (Davisson, 1972)

Widely used in North America, this method defines the ultimate failure load as the load corresponding to a settlement equal to the elastic compression of the pile (δe) (Equation 2.4) plus the sum of settlements required to mobilize the shaft and the tip resistance. The authors believe that the maximum shaft and tip resistance is achieved at a settlement equal to the sum of 3.8 mm (0.15 inches) plus a settlement equal to the pile diameter, in inches, divided by 120.

$$\delta e = QL/AE \quad [2.4]$$

$$\delta = \frac{QL}{AE} + 3.8mm + D[in]/120 \quad [2.5]$$

Hereby, Q is the test load, A is the transverse area of the pile, and E is the elastic modulus based on the compressive strength of the concrete grout utilized to construct the piles. The interpreted failure load ($Q_{f,int}$) is defined as the intersection [δ_{int} ,$Q_{f,int}$] of the offset line, δ calculated at different levels of axial load (Q), and the load-settlement curve obtained during the axial load test.

Even though the Davisson Offset Limit Load (1972) is one of the most-used failure interpretation method in practice, its accuracy is strongly dependent on the pile installation technique and is often extrapolated beyond its applicability for driven piles. Hence, its use is heavily critiqued within the deep foundation community. For instance, Stuedlein *et al.*, (2014) performed a similar study as presented in this paper, assessing a set of failure load interpretation methods to determine their suitability for augered cast in place piles (ACIP piles), and suggested the Davisson Offset Limit Load to be inappropriate for drilled foundations. This agrees with plentiful discussion in literature showing that the DOL method underestimates the failure load (NeSmith and Siegel, 2009, Baligh and Abdelrahman, 2005-2006, Stuedlein *et al.*, 2014). The difference between the interpreted failure load obtained with the DOL method and the actual failure load is attributed to two factors, namely (1) the slope of the initial straight line of the axial load test (m_I) does not always represent the slope (m_E) that the elastic axial load deformation would have per Equation (2.4); and (2.2) the soil quake deformation (third term of Equation 2.5) to mobilize the soil strength is higher for drilled foundations than the deformation needed for driven piles. To address this issue, Perlow (2020) studied the soil quake factor of the DOL method (i.e., D/120), finding that the pile width needed to calculate the soil quake deformation, should be multiplied by a factor ranging from 2 to 6 depending on the drilled foundation type (i.e., drilled shafts, cased micropiles, drilled displacement piles, among others). This adjustment enables a better estimate for drilled shaft failure loads when using the Davisson Offset Limit Load method.

From the DDP data collected in this study, 30 axial load tests showed a clear plunging behavior, and were used to evaluate the limitations of the DOL method with respect to drilled displacement piles. Since the uncertainty of the DOL method is associated with the discrepancy between the slope of the first line of the test results (m_1) and the elastic slope (m_E), the ratio between these two lines (k) was obtained for each test using Equation (2.6). As shown in Figure 2.5, when mE/m1 is less than one, the pile settlement is higher than the elastic deformation for small loads (Equation 2.4), on the other hand, when the ratio is higher than one, the initial axial deformations are lower than the amount of elastic deformation expected. Figure 2.6 shows the ratio k versus the piles' slenderness ratio L/D. For slender piles, L/D higher than 20, the initial settlement of the pile is not shown at early stages (shaft is effectively resisting the dragging forces). On the other hand, m_E/m_1 lower than one demonstrates how the pile settlement starts developing at earlier stages.

$$k = \frac{m_E}{m_1} \qquad [6]$$

where m_E is the elastic slope, and m_1 is the slope of the first line from the axial load test.

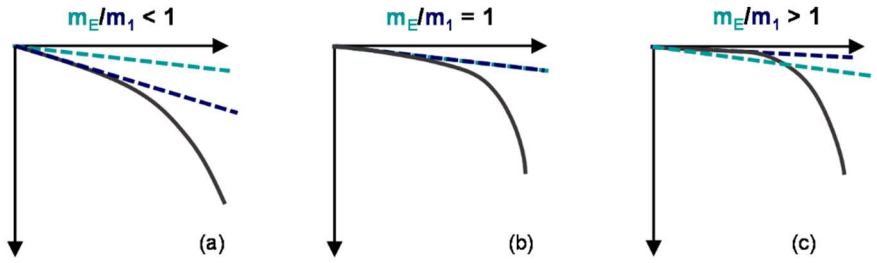

Figure 2.5. m_E/m_1 diagram

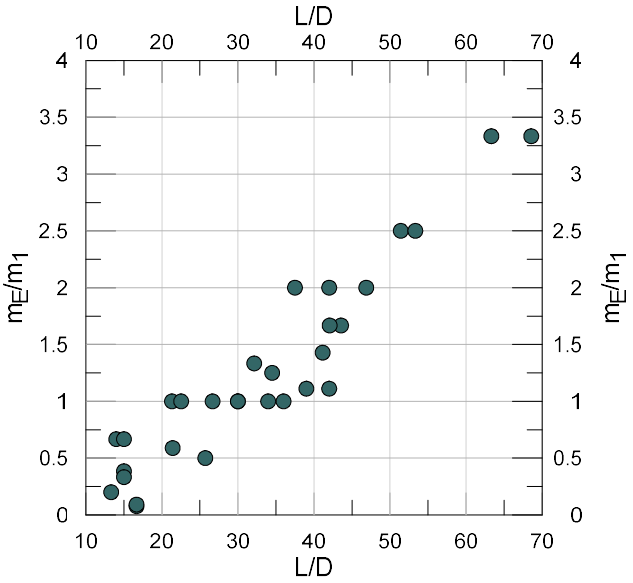

Figure 2.6. m_E/m_1 values vs. pile slenderness.

Following Perlow (2020), the DOL method was modified by applying an amplification factor of 4 to the soil quake deformation (third term of the DOL equation – Eq. 2.5). Figure 2.7 shows the comparison between the measured failure load vs. the interpreted failure load estimated with Davisson Offset Limit Method (DOL) and Modified Davisson Offset Limit (MDOL). The MDOL data points align better to the 45-degree line which represents the perfect agreement between the measured and the interpreted failure load. The ratio between experimental and the interpreted axial failure load was obtained for the piles that reached the geotechnical failure while testing. The μ value represents the average ratio for all piles and σ represents the standard deviation. The MDOL method shows a 12% increase in accuracy compared to the original DOL method. The standard deviation of the ratio between the interpreted failure load $Q_{f,interpr}$ using the modified DOL and the measured failure load $Q_{f,measured}$ in the field, as introduced later in this paper, reduced by 30%, showing less scatter amongst results when comparing interpreted failure with the actual failure load obtained during the test.

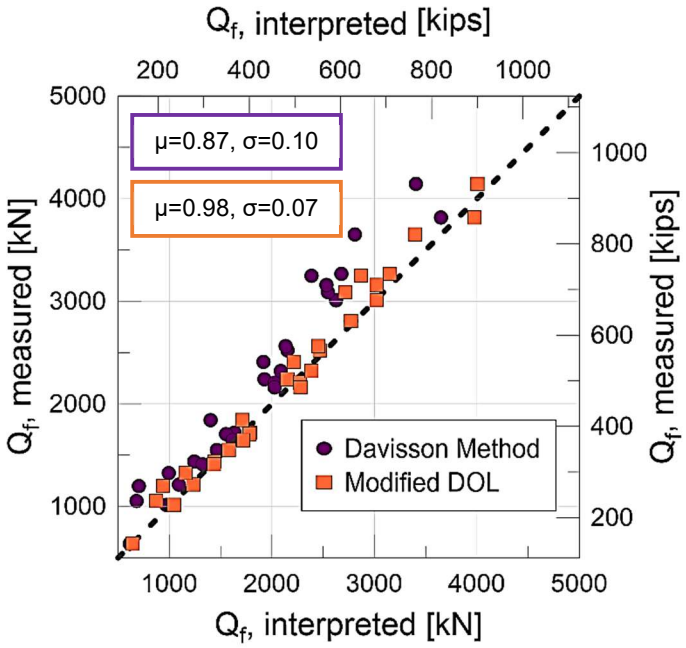

Figure 2.7. Comparison of the measured (geotechnical failure) and predicted failure load with the DOL and the MDOF methods.

2.4.2.3. Brinch Hansen 80% Failure Criterion (Hansen, 1963)

The Brinch-Hansen 80% criterion suggests the failure load to be reached at the level of compressive stress (Q/A) at which the axial strain in the pile is equal to four times the strain at a 20% smaller stress. This concept was translated by Dotson (2013) into a direct solution that requires plotting the square root of each pile displacement value normalized by its corresponding load plotted against the respective pile settlement. Hereafter, a trendline with slope C_1 and intercept C_2 is fitted to the plotted data. The Hansen 80% criterion defines the failure load as the inverse value of two times the square root of C_1 times C_2 as shown in Equation (2.7).

$$Q_u = \frac{1}{2\sqrt{c_1 c_2}} \qquad [2.7]$$

2.4.2.4. Brinch-Hansen 90% criterion (Hansen -1963)

The Brinch Hansen 90% criterion interprets pile failure as the load for which strain is equal to two times the strain at a 10% smaller stress. Similarly, to the 80% criterion, Dotson (2013) proposed a direct solution of the failure load obtained with the 90% criterion as shown in Equation (2.8),

$$Q_u = \frac{2\sqrt{3}}{7\sqrt{c_1 c_2}} \quad [2.8]$$

where Q_u represents the interpreted failure load, and C_1 and C_2 are the slope and the intercept of the linear tendency defined for the Hansen-80% criterion.

2.4.2.5. Chin-Kondner Extrapolation (Chin, 1970)

To apply the Chin-Kondner Extrapolation method, a plot of the pile settlement measured during the axial load test (x-Axis) vs. settlement divided by its corresponding load (y- axis) needs to be constructed (Figure 2.4). A trendline is fitted to the data above ($y = C_1x + C_2$), its slope is defined as C_1 and its y-intercept as C_2. The failure load is calculated as the inverse of the trendline's slope, i.e., $Q_f = 1/C_1$.

2.4.2.6. Butler-Hoy Criterion (Butler and Hoy, 1977)

The interpreted ultimate failure load is defined as the point of intersection between a line fitted to the initial straight part of the load-settlement plot, and a second line with a pre-defined slope of 0.13 mm/kN (0.05 in/ton). This second line is to be placed at the point of minimum curvature in the pile's load-settlement curve.

2.4.2.7. L_1-L_2 method (Hirany and Kulhawy, 1989)

The interpreted failure load is defined based on the points L_1 and L_2, where L_1 represents the "end point" of the initial straight-line portion of the pile load-settlement curve, and L_2 represents the first point of the final linear region. L_2 simultaneously defines a failure threshold, as any

incrementally small load beyond point L2 produces a significant increase in pile displacement. Q_{L1} and Q_{L2} are the loads corresponding to points L_1 and L_2, respectively.

2.4.2.8. De Beer Yield Load (De Beer, 1968)

The pile load test data is plotted on a log scale of the measure load (Q), and a log scale of the settlement (δ) (Figure 2.4). If the plunging behavior was reached during testing, two consecutive lines approximations will show. The point where the lines change their direction, or the maximum curvature of the plot is interpreted as failure load or yield load as defined by the authors.

2.4.2.9. Van der Veen's Criteria (Van der Veen, 1953)

The measured values from the axial load test are assumed to fit an exponential relationship shown by Equation 2.9, where Q_u is the interpreted failure load, δ is the in-situ settlement, and β represents a curve fitting parameter. Q_u and β can be found by using ordinary square regression. Q represents the axial load at any point along the exponential curve.

$$Q = Q_u(1 - e^{\frac{-\delta}{\beta}}) \quad [2.9]$$

To date, there is no established best practice in selecting the appropriate interpretation method. Stuedlein *et al.* (2014) found pile failure of Auger Cast Piles to be best interpreted with the Butler & Hoy (1977) and L_1-L_2 methods. The Davisson method is widely known for its application and validity for small-diameter driven piles, and although the criteria was originally developed for tip bearing driven piles, it has been proven that it can also be utilized for driven friction piles (NeSmith and Siegel, 2009). However, similarly to the earlier-described predictive equations for axial pile capacity, extrapolation of formulations beyond their original empirical development is generally recommended against. For drilled displacement piles, no such relationship has been established yet. Hence, a preliminary assessment of the interpretive failure

load methods was carried out to identify the methods that best describe the failure load of DDPs included in this study. First, all failure interpretation methods listed above were applied to 30 DDP tests during which experimental failure was reached and the corresponding failure load is known. Similarly, all tests for which a settlement equal to 10%D was obtained, were included. Hereafter, the ratio of interpreted failure load ($Q_{f,int}$) and actual, measured failure ($Q_{f,meas}$) was calculated. The best-performing interpretation method was defined as the one with an average ratio closest to one (1.0) and minimal standard deviation for all tests considered. A normal distribution was calculated to assess the accuracy and precision of the methods. Figure 2.8 shows the Probability Density Function (PDF) of the normal distribution calculated for each method and suggests the Van der Veen's Criteria (1953) to provide the closest match and most accurate estimate of the actual failure load, followed by Butler and Hoy (1977), and the L_1-L_2 method. De Beer's Criterion (1968) and the DOL Method underestimates the failure load of the piles, and the Decourt Method and Chin-Kondner Extrapolation overestimate the failure load. Even though the L_1-L_2 method shows good predictive performance of the failure load, a significant number of assumptions are needed when load test data don't reach the magnitude of settlements needed to establish the second "linear" portion of the load-settlement curve. Finally, the interpreted failure load at settlement equal to 10% of the pile diameter (i.e., 0.1D) was estimated based on the axial load – settlement data. Even though the 10%D approach closely approximates the measured failure, this criterion had to be discarded since not enough load tests reached this level of settlement, which is common particularly for piles with large diameters. Figure 2.9 summarizes the load ratios obtained through all methods in a single graph. Based on this summary, the Van der Veen's method (1953) method was found to be most suitable and consequently applied to all tests that did not reach failure in order to interpret and estimate the anticipated pile failure load, hereafter referred to as $Q_{f,interpreted}$.

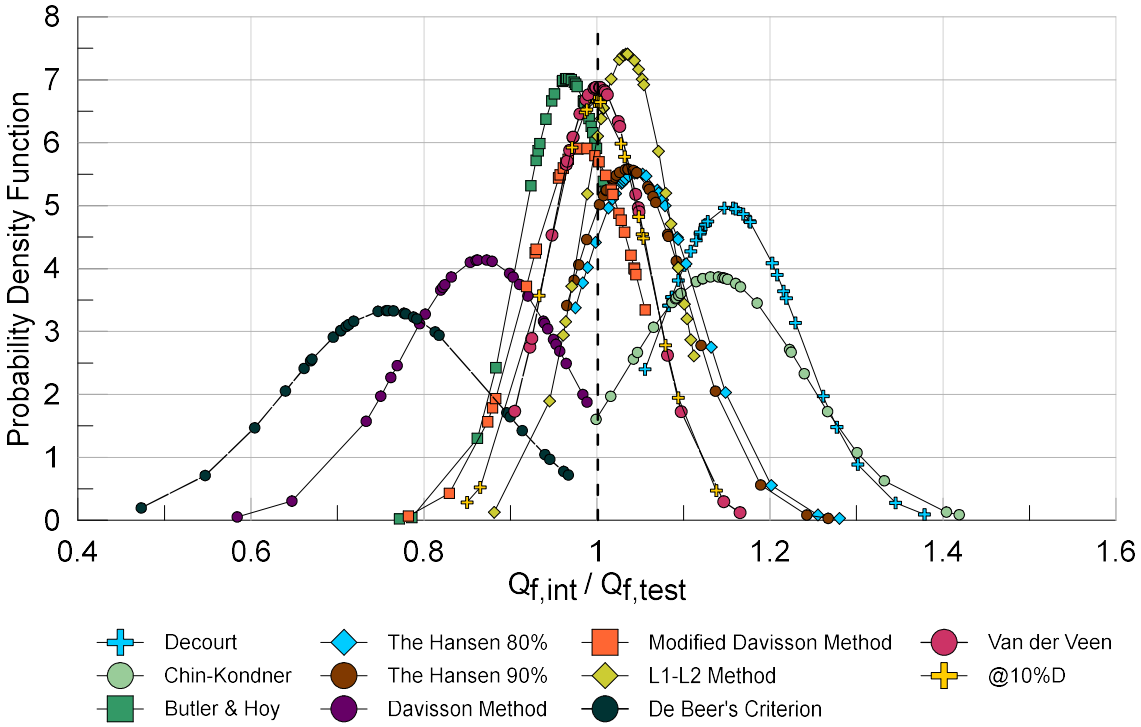

Figure 2.8. Probability density function for the $Q_{f,int}/Qf_{,test}$ ratio of each interpretation method.

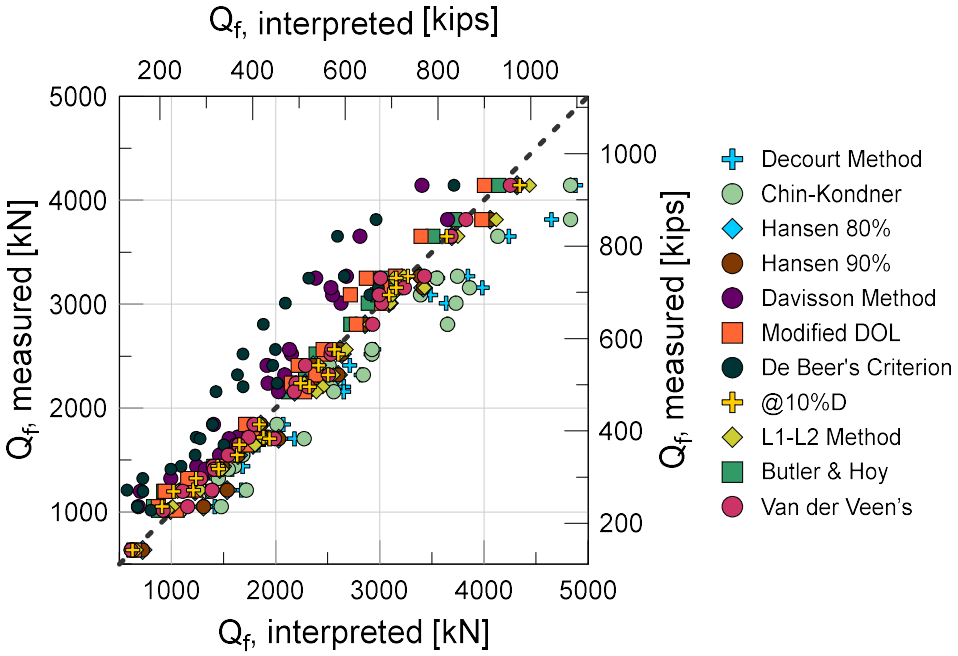

Figure 2.9. Comparison of the measured (plunging failure) and predicted failure load.

2.5. Data Evaluation and Results

The accuracy of each available direct method in predicting pile axial capacity was assessed by calculating the ratio between the measured experimental axial failure load (Q_f) and the analytically predicted (i.e., calculated) axial capacity (Q_c) for each pile specimen listed above. The axial failure load was either taken as the measured load at failure ($Q_{f.measured}$) or the interpreted load ($Q_{f.interpreted}$) per Van der Veen's (1953) criteria when plunging behavior was not observed experimentally. 100% predictive accuracy is reached when the ratio of failure load divided by the predicted load is one (1.0). The arithmetic mean (μ) and the standard deviation (σ) were calculated according to Equation 2.10 and Equation 2.11. The confidence limit (CL) was also calculated for the ratio Q_f/Q_c based on Equation 2.12, where Z is equal to 1.96 for a 95% confidence limit according to Hogg and Craig (1995). The Confidence Interval (CI) (Equation 2.13) represents the range in which 95% of the mean of the samples will fall. The results for Q_f/Q_c are presented in Figure 2.10 for sand, in Figure 2.11 for clay and in Figure 2.12 for mixed type of soils. An optimum result is defined by a mean value (μ) near unity and a minimal standard deviation to assure the trend (ratio of under or over prediction) with a higher precision. The CPT direct methods are shown with round symbols, and the SPT results with square symbols.

$$\mu = \frac{\sum_{i=1}^{n}(\frac{Q_{f,i}}{Q_{c,i}})}{n} \quad [2.10]$$

$$\sigma = \frac{\sum_{i-1}^{n}(\frac{Q_{f,i}}{Q_{c,i}}-\mu)^2}{n-1} \quad [2.11]$$

$$CL = \mu \pm Z * \frac{\sigma}{\sqrt{n}} \quad [2.12]$$

$$CI: \left[\mu - Z * \frac{\sigma}{\sqrt{n}}, \mu + Z * \frac{\sigma}{\sqrt{n}}\right] \quad [2.13]$$

Figure 2.10 suggests that measured and analytically predicted capacities (i.e., Q_f/Q_c) in sandy soils reach closest agreement when using Brettmann and NeSmith (2000; 2005) and Schmertmann and Nottingham (1975;1978) to calculate the pile axial capacity. De Ruiter and Beringen (1979), LCPC (1982), and Niazzi and Maine (2016) were found to almost exclusively underpredict the in-situ pile capacity in sands, implying a strong conservatism when applied for drilled displacement piles. On the other hand, Eslami and Fellenius (1997) and Bustamante and Gianeselli (1993; 1998) were found to yield to axial load capacities 1.25 times higher than what the measured or interpreted results shown. By comparing SPT-based methods with the measured or interpreted failure load, the O'Neill and Reese (1988) method showed slightly better alignment with the 45 degrees line than other methods, even though a high dispersity is visible. Figure 2.10 suggests that the Brown *et al.* (2010), and Meyerhof (1976) methods tend to generally underestimate the in-situ capacity of the piles. Decourt (1989; 1995) show uniform datapoints on both side of the spectrum (under and overpredicting), with larger variability. Brettman and Nesmith (2000; 2005) appears to overpredict the capacity when N_{60} values are used to calculate the axial load capacity.

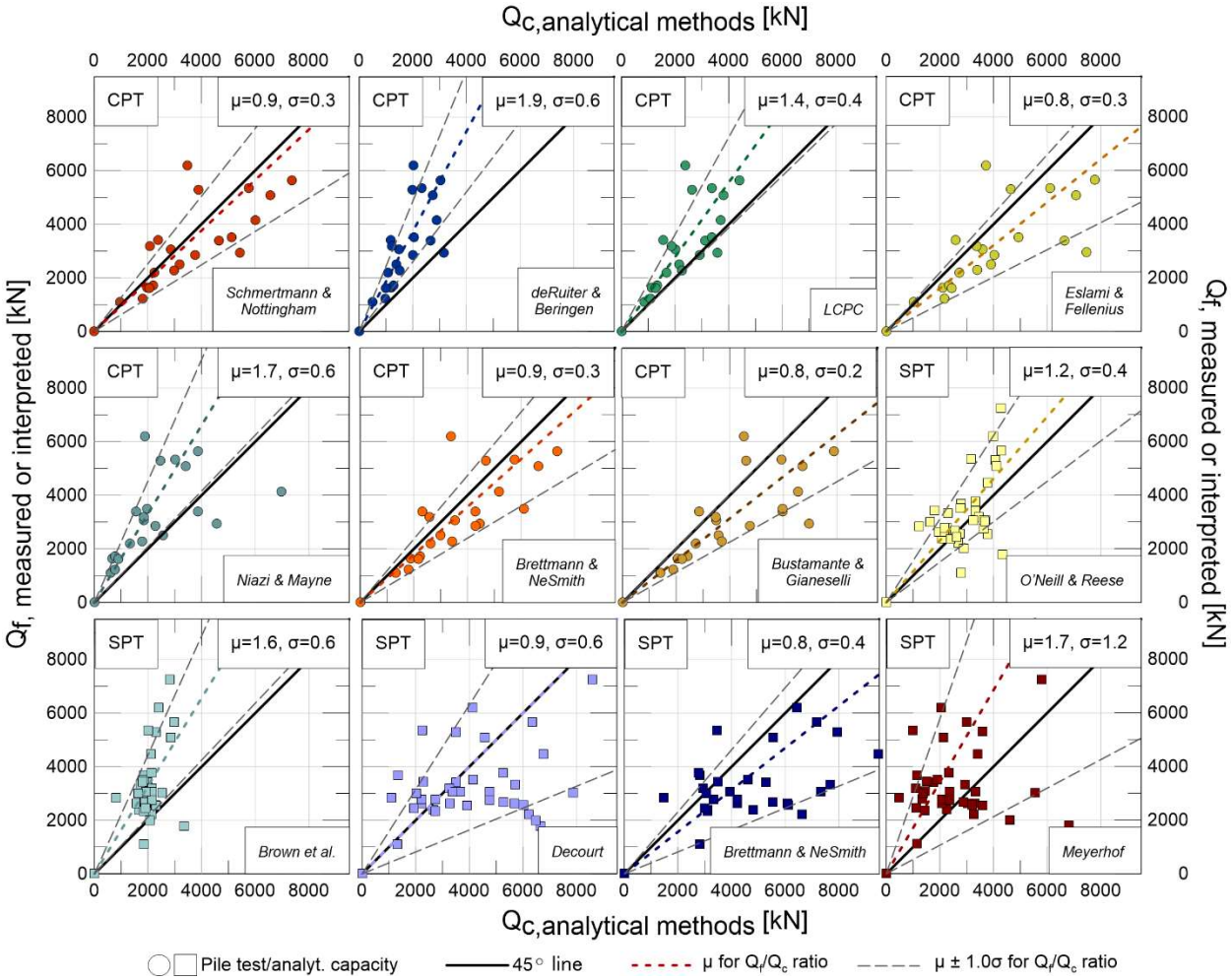

Figure 2.10. Measured or interpreted failure load versus the axial load capacity estimated analytically from the CPT (point symbol) and SPT (square symbol) direct methods for sandy soils.

Figure 2.11 presents the comparison of Q_f/Q_c in clayey soils. For axial loading below 2000kN (450 kip), all methods align well with the CPT-based predictions. Above this load threshold, all methods tend to significantly underestimate the actual capacity of the elements except for Eslami and Fellenius (1997) which methos seems to overestimate the real capacity of some piles. The Eslami and Fellenius method appears to provide the best statistical fit regardless of the axial failure load, however, this is primarily due to an even scatter above and below the 45degree line. Due to the absence of SPT field data for load tests in clayey soils, the analytical SPT methods could not be assessed.

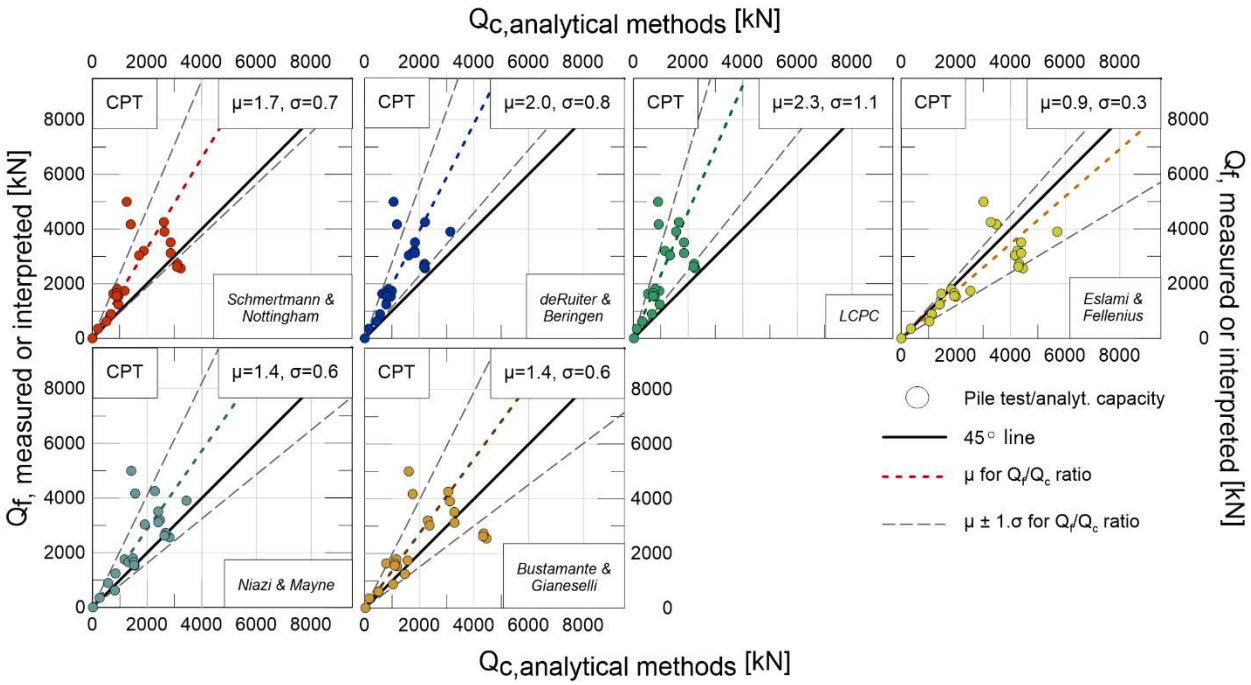

Figure 2.11. Measured or interpreted failure load versus the axial load capacity estimated analytically from the CPT (point symbol) for clayey soils.

Figure 2.12 shows measured vs. analytically predicted pile capacities for mixed soil profiles. Data points for most CPT methods suggest very consistent predictions (very small scatter for most methods). Within the CPT-based methods, Bustamante and Gianeselli (1993; 1998) provide the best approximation of the pile failure load in mixed soils, followed by Eslami and Fellenius (1997). De Ruiter (1979), LCPC (1982), Niazi and Mayne (2016), as well as Brettman and NeSmith (2000; 2005) conservatively underpredicted the field capacity. The O'Neill and Reese (1988) method provides the closest predictions when SPT data is utilized.

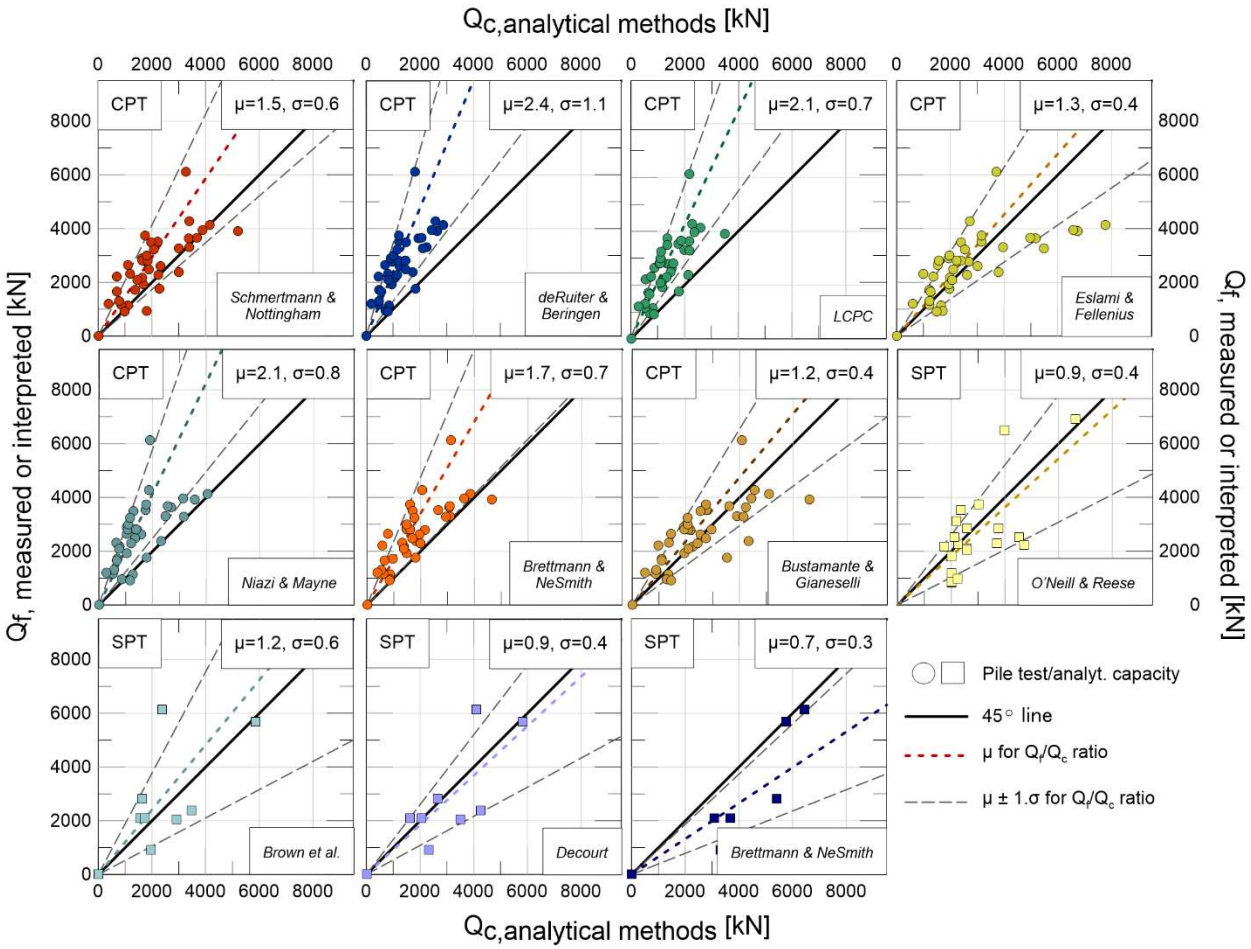

Figure 2.12. Measured or interpreted failure load versus the axial load capacity estimated analytically from the CPT (point symbol) and SPT (square symbol) direct methods for mixed type of soils.

Figure 2.13 shows the mean values and confidence interval for the ratio Q_f/Q_c for the different soil types and analytical methods. The more accurate the method is, the closer is the mean value (circular mark) to one, accompanied by a small confidence interval (shorter vertical line). As it can be seen in

Figure 2.13, the ratio Q_f/Q_c exhibits the highest variability and largest confidence intervals for clayey soils.

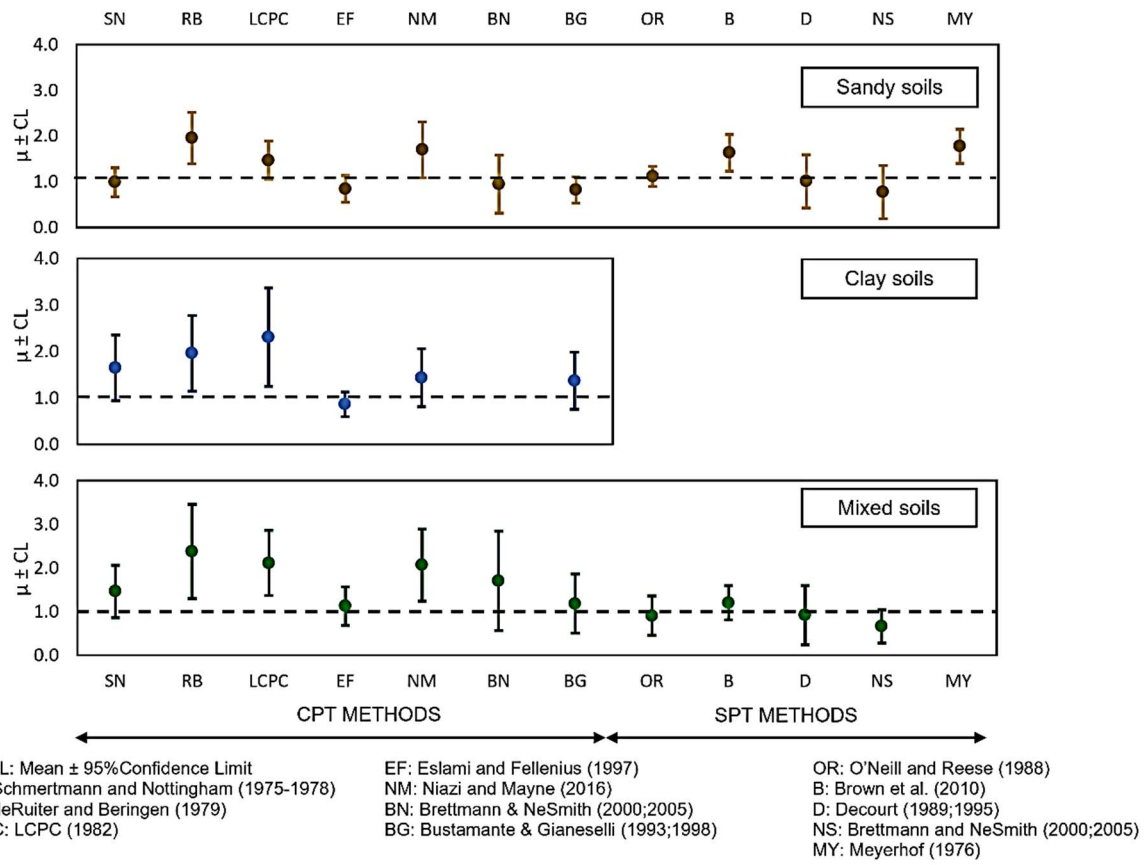

Figure 2.13. Arithmetic mean (dot mark), and upper and lower confidence bounds (vertical line) for the ratio "Measured or interpreted failure load" over the axial load capacity estimated analytically from the CPT and SPT direct methods.

Figure 2.14 and Figure 2.15 display a comprehensive comparison between all experimental failure loads (measured and interpreted) (y-axis), and their respective, analytical predictions using all methods (x-axis) combined into one single graph. The three symbol types (e.g., square, circle, and triangle) categorize the results into sandy soils (square), clayey soils (circle), and the mixed soils (triangle) from CPT (Figure 2.14) and SPT (Figure 2.15), respectively. A global comparison of all CPT-based methods suggests a general underestimation of the pile failure loads, SPT based methods tend to underestimate the axial load capacity often.

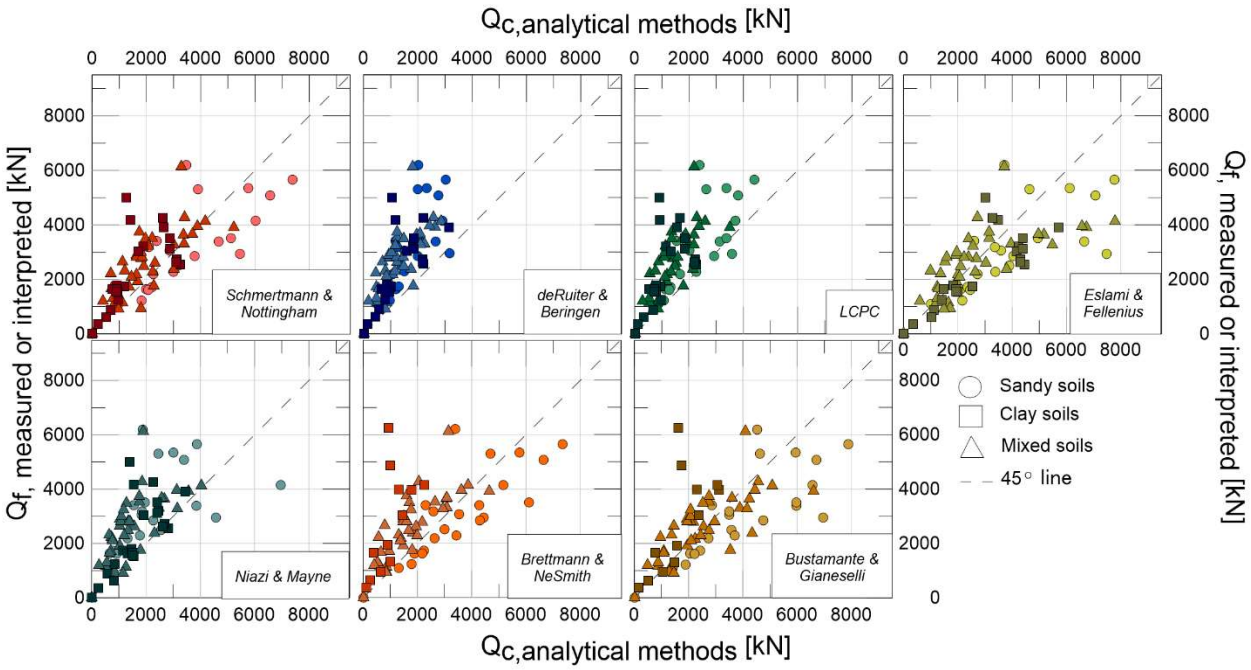

Figure 2.14. Interpreted failure load versus the axial load capacity estimated analytically from the CPT methods. (Data from all soil types plotted in one graph)

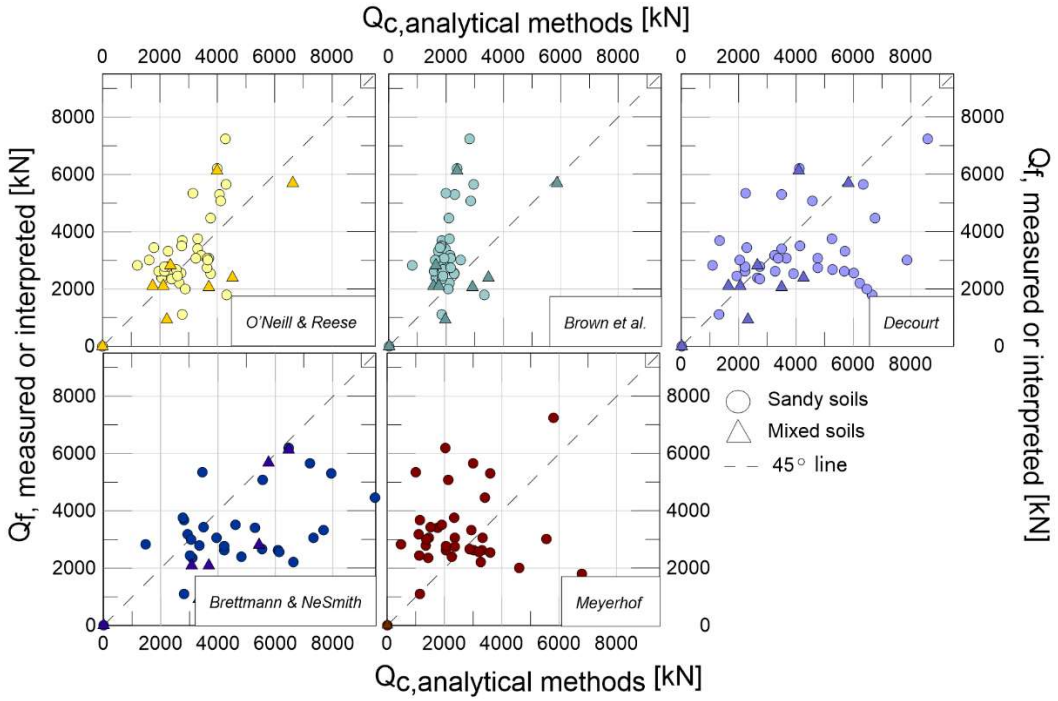

Figure 2.15. Interpreted failure load versus the axial load capacity estimated analytically from the SPT methods.

To study the influence of pile geometry on the Q_f/Q_c ratio, the pile slenderness ratio, defined as L/D was computed for each pile (*where* L represents the total pile length and D defines the pile diameter). The L/D ratio was plotted versus Q_f/Q_c ratio in Figure 2.16. It can be observed that regardless of the pile slenderness, a general trend of capacity underestimation using CPT-based methods is observed for all pile geometries, ranging from small to large slenderness ratios (i.e., more data plot above the 1.0 line).

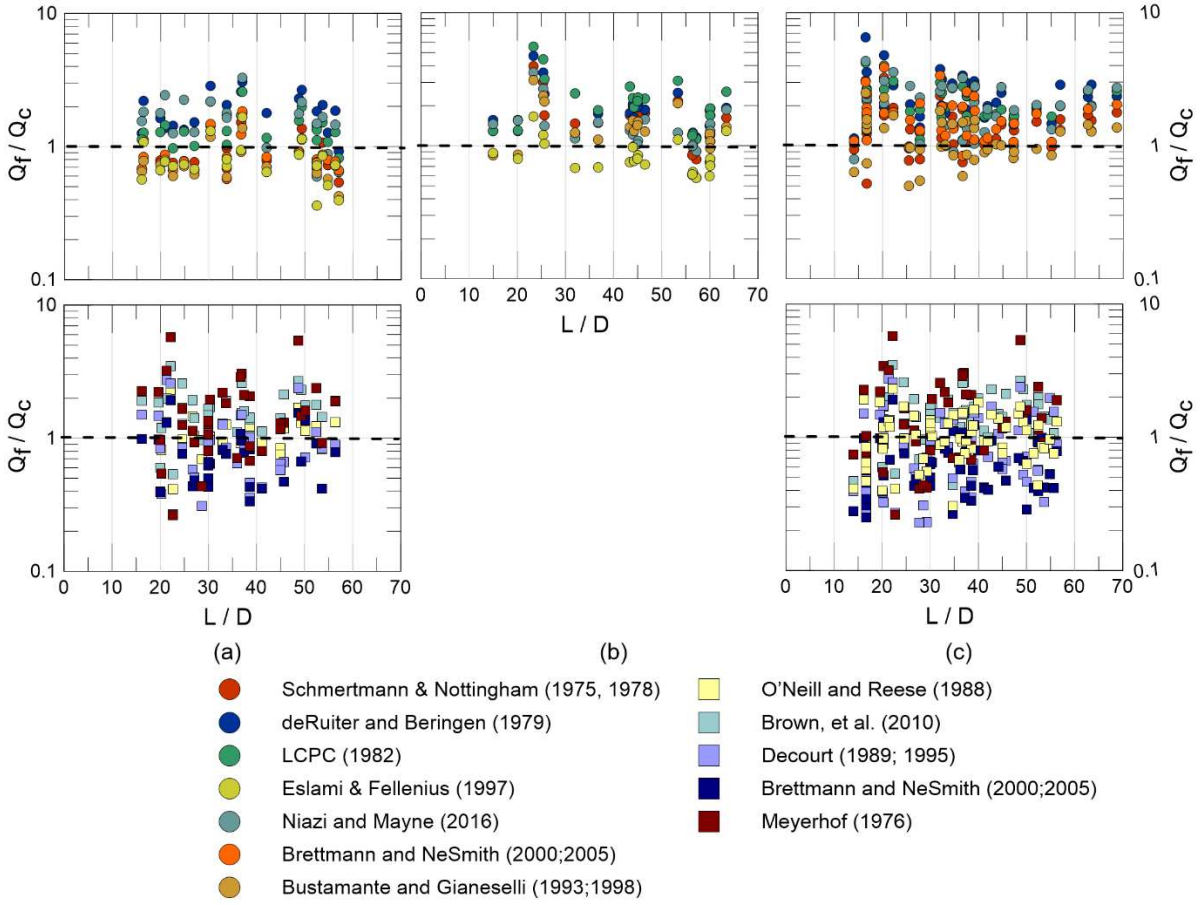

Figure 2.16. L/D ratio versus the Q_f/Q_c ratio. Columns: (a) Mostly sandy soils. (b) Mostly clay soils, (c) Mixed soils.

Figure 2.17 compares the axial load at failure (measured or interpreted) with the axial capacity predicted by the different analytical methods by separating the methods based on their empirical derivation: the upper row corresponds to the methods developed specifically for drilled

displacement piles (i.e., Brettmann and NeSmith (2000; 2005) for SPT and CPT data, and Bustamante and Gianeselli (1993; 1998)). The second row depicts all remaining methods. Similary, the three columns categorize the results into sandy soils (left column), clayey soils (center), and the mixed soils (right column). Unfortunately, the desired imrpoved accurancy (when using methods developed for DDPs specifically) is not recognizable in Figure 17. The DDP methods and the "other" methods shows similar data scatter.

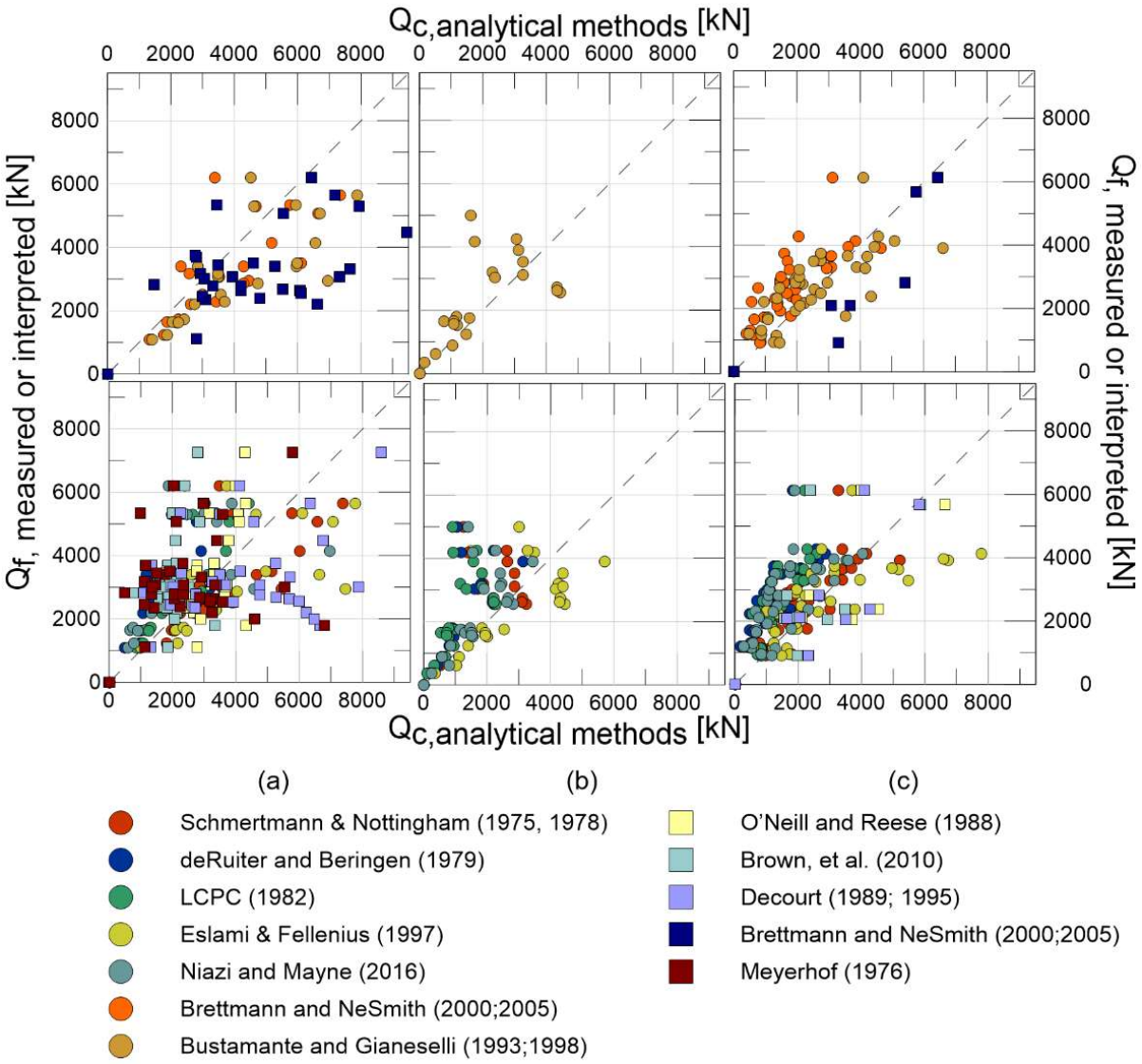

Figure 2.17. Measured or interpreted failure load versus the axial load capacity estimated analytically, comparison according to the installation method for which the analytical methods were developed. Columns: a) Mostly sandy soils. (b) Mostly clay soils, (c) Mixed soils

According to Siegel et al. (2007), the installation of drilled displacement piles in sandy sites results in densification of the soil surrounding the pile and the increase in lateral stresses. In this study, an increase in CPT tip resistance (qt) was encountered following several pile installations. Even though data were limited, the available average CPT tip resistance (q_t) and the SPT-based N_{60} resistance measured before the pile installation was compared with the Q_f/Q_c ratio for each sandy and mixed soil site. The average tip resistance (q_t) was computed as the arithmetic mean of the q_t values at different depths for sandy and clayey soils. For mixed type of soils, the average tip resistance was computed for soils with a soil index behavior (I_c) higher and lower than 2.6, clay-like and sand-like behavior, respectively; with those two values, and the percentage of each type of soil within the soil profile, a weighted average was calculated. Figure 2.18 shows the Q_f/Q_c ratio against the average pre-pile installation cone tip resistance (q_t) (top row) and the SPT N_{60} values (bottom row) for sandy (a), clayey (b) and mixed soils (c). For soils with initially low strength (e.g., q_t = 5-10 kPa, or N60<15) Figure 2.18 suggests an inverse relationship between the soil resistance, (i.e., q_t or N_{60}). The ratio between failure load and the estimated capacity seems to follow a slight downward trend. Even though the soil improvement during pile construction is a complex topic with high variability, different authors have proven that the higher the initial soil resistance (i.e., high initial soil strength), the less improvement the soil experiences due to DDP installation. Consequently, a higher accuracy, and a Q_f/Q_c ratio closer to one is obtained for dense sands and stiffer silt mixtures since the soil does not experience great changes. On the other hand, for looser soils, the implementation of the analytical methods without soil improvement considerations can lead to the underestimation (or conservatism) of the pile's capacity Q_f/Q_c >1. For clayey soils no relationship between the ratio Q_f/Q_c and q_t was found, this is due to the unique degree of "improvement" or "relaxation" this type of soil can experience.

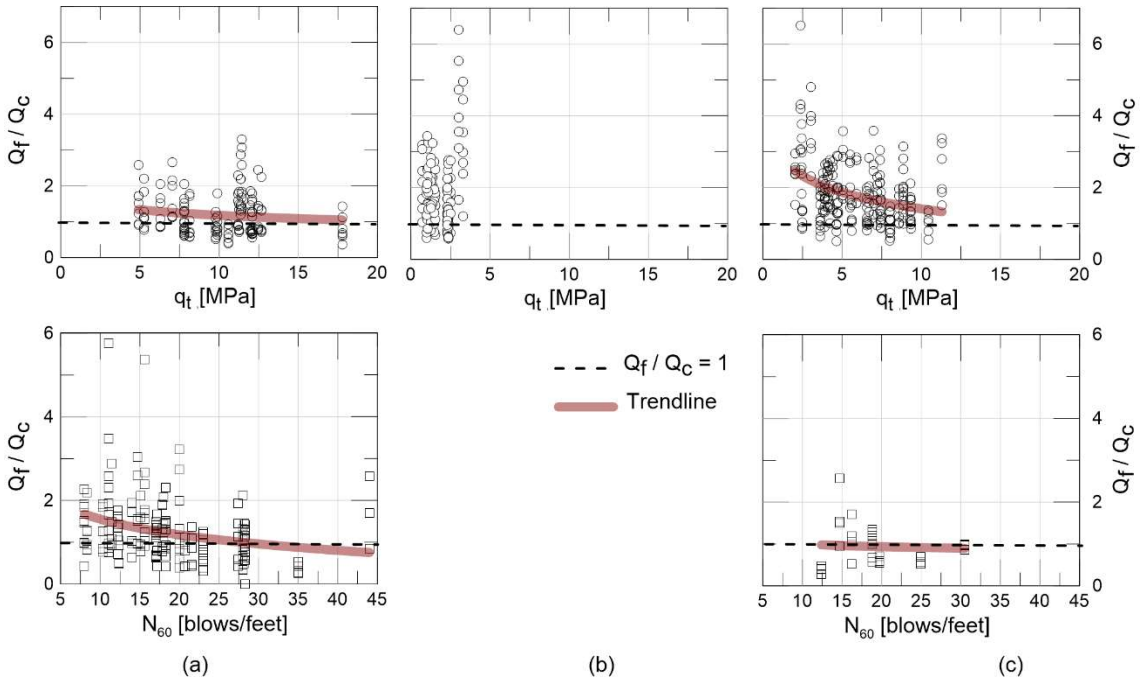

Figure 2.18. Average cone tip resistance (q_t) in MPa, and N_{60} versus the Q_f/Q_c ratio. (a) Mostly sandy soils, (b) Clay soils, and (c) Mixed soils.

Chapter 3
Evaluation of soil improvement surrounding drilled displacement piles

3.1. Summary of DDP project database with pre- and post-installation CPTs

Within the DDP database, 10 construction projects conducted pre-and post-pile installation soil measurements, and 6 projects conducted pre-and post-measurements and axial load tests at the same pile. All data was collected from— and generously provided by the members of the Deep Foundation Institute's AC&DD technical committee. The authors performed a comprehensive review of all project data to ensure uniform site information and consistent data quality across all project sites. The authors documented the type of field testing performed, the availability of groundwater table locations; the comprehensiveness of before and after in-situ tests (i.e., CPT_{PRE} and CPT_{POST}) and their spatial distribution around the DDP. The authors also ensured the availability of DDP design and construction data, including the pile diameter, pile length, pile arrangement, as well as the availability of axial load test data that contain a significant level of displacement to estimate pile failure loads.

The project data summarized in Table 3.1 shows the site location, Ground Water Table (*GWT*) depth, pile diameter (*D*), pile length (*L*), and DDP pattern and spacing (if applicable). Figure 3.1 shows the two different patterns utilized during DDP construction, namely, a rectangular pattern (Figure 3.1a) with piles spaced at distance "x" times the pile diameter *D*, or a triangular pattern (Figure 3.1b). Furthermore, Table 3.1 provides the number of pre- and post-CPT tests at each site along with the distance between CPT_{POST} locations and piles in terms of the pile diameter (*D*). Finally, the number of days between pile construction and post-construction CPT testing (CPT_{POST}) is also shown in Table 3.1. The sites consisted of either sandy soils, or mixed soils with strongly stratified sand, silt, and clay layers. The nominal shaft diameters varied from

40 cm to 45 cm (16 to 18 in). The embedment length of the piles ranged from 6 m to 15 m (19.7 ft to 49.2 ft). The various types of displacement drilling tools are not included in Table 3.1, as this information was not consistently available for all projects and restricted through non-disclosure/proprietary agreements for several projects.

Table 3.1. Overall information of each project site and tested piles.

Location		GWT Depth (m)	D (m)	L (m)	Arrangement -Spacing	# PRE-CPT	# POST-CPT	Distance pile-CPTpost	# Days
P1	Tampa, FL	3.7	0.45	7.6	Square – 4D	1	4	1-3D	1
P2	Los Angeles, CA	9.0	0.40	10.3	Triangle – 8.5D	1	1	4D	6
P3	San Jose, CA	2.1	0.40	7.2	Square – 7.5D	3	16	1.5-3.8D	2
P4A	San Francisco, CA	10.5	0.45	5.8	Single	4	4	1-1.5D	27
P4B				6.4	Square – 2.7D				39
P5	Milipitas, CA	2.1	0.40	8	Square – 3D	3	6	1-1.3D	7
P6	Los Angeles, CA	-	0.40	8.2	Square – 3D	3	7	1.5-2.0D	11
P7	Myrtle Beach, SC	2.4	0.40	8	Square – 4D	4	11	1-2D	7
P8	Orlando, FL	4.6	0.40	12	Square – 3D	2	3	0.5-2D	7
P9	Redwood, CA	2.4	0.45	4	Triangle – 4D	8	36	1.2-3.2D	6
P10	Washington DC	8.0	0.40	8	Square – 3D	1	2	0.5-3D	7

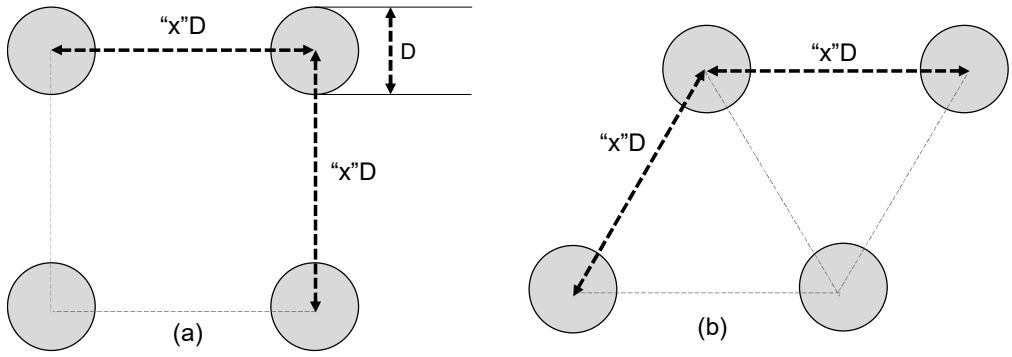

Figure 3.1. Pile arrangement patterns and spacing. (a) Square pattern, (b) Triangle pattern.

3.2. Geotechnical data review

In 1990, Robertson (1990) established a convenient way to describe commonly observed soil behavior by defining different soil behavior "zones" based on field tests of young, un-cemented, insensitive, normally consolidated soils. Later, Robertson (2010) presented an updated version of

the Normalized CPT Soil Behavior Type (SBT) chart in which Zone 1 describes sensitive, fine-grained soils, Zones 2 describes organic soils and soft clays, Zone 3 suggests clay-like behavior, Zone 4 has transitional behavior, and Zones 5 to 7 represent sand-like soil behavior. Zones 8 and 9 describe very stiff sands and heavily-consolidates or cemented fine-grained soils. A graphical illustration of this concept is included and described later in the paper (Figure 3.10). Additionally, Robertson (2010) formulates the soil behavior type index, I_c (Eq. 3.1), as function of CPT tip- and side resistances, where Q_t is the normalized cone penetration resistance (Eq. 3.2), and F_r is the normalized friction ratio, in % (Eq. 3.3).

$$I_c = ((3.47 - log\ log\ (Q_t)\ )^2 + (log\ log\ (F_r)\ + 1.22)^2)^{0.5} \quad [3.1]$$

$$Q_t = (\frac{q_t - \sigma_{vo}}{\sigma'_{vo}}) \quad [3.2]$$

$$F_r = \left(\frac{f_s}{q_t - \sigma_{vo}}\right) * 100\% \quad [3.3]$$

An I_c value higher than 2.6 implies the soil to behave silt-like, clayey-silt like to silty clay like, or clay-like; an I_c value lower than 2.6 suggests sand-like behavior, including silty sands to sandy silts and sands. The 2.6 value serves as threshold and has historically been used to separate liquefiable soils (cohesionless, sandy materials) from non-liquefiable materials (mostly cohesive materials). Table 3.2 shows the various soil behavior types and their corresponding indices (I_c), and zones per Robertson (2010). Figure 3.2 shows the percentage of each "zone" within each soil profile of the 10 project sites included in this study. Except for P1 and P8, all projects exhibit a noticeable heterogeneity of representative soil types.

Table 3.2. Soil behavior type index (I_c) based on Eq. (3.1) by Robertson (1990).

Soil Behavior Type	I_c	Zone
Organic soils – clay	> 3.6	2
Clays – silty clay to clay	2.95 - 3.6	3
Silt mixtures – clayey silt to silty clay	2.60 - 2.95	4
Sand mixtures – silty sand to sandy silt	2.05 - 2.60	4 - 5
Sands – clean sand to silty sand	1.31 - 2.05	6
Gravelly sand to dense sand	<1.31	7

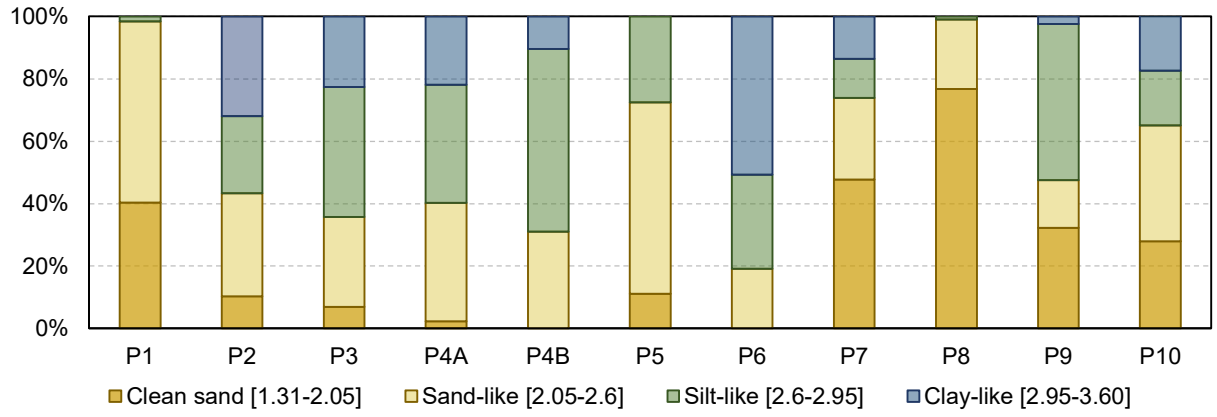

Figure 3.2. Analysis of soil profiles at each project site.

Figure 3.3, 3.4, and 3.5 present the raw CPT data of each project, along with axial load predictions and test results (to be discussed later in this paper). Columns (a), (b), and (c) display the raw CPT tip resistance (q_t), the CPT side friction (f_s), and the pore water pressure (u) vs. depth measured before (dashed line) and after (solid line) pile installation, as well as the GWT elevation for each site. For some of the projects (P1, P4B, P5, P7, P8, P10), the improvement in tip resistance and side friction can be easily noticed by visually comparing CPT pre and post profiles; for most of these projects the improvement in tip resistance and side friction go "hand-in-hand". However, for the remaining projects (P2, P3, P4A, P6, P9) the change in CPT measurements is smaller and cannot be easily quantified visually. Please also note that the side friction recorded on project P10 might be showing an incorrect reading, as data suggest constant CPT readings below three meters of depth. This discrepancy was considered when analyzing pre and post CPT data later in the paper.

Another interesting observation within the data arises from a noticeable difference in data from P4A and P4B (Figure 3.3, 3.4), both piles being tested at the same site and belonging to the same project. The noticeable difference in soil improvement can likely be attributed to the pile arrangement and time of post-CPT testing; P4A studies the improvement of a single pile installed at the site and P4B represents the change in the soil within a square arrangement of DDPs. In addition, the number of days between the construction of the single and group of DDP and the CPT_{POST} execution varies between P4A and P4B. Post installation testing was generally performed within 2 weeks of installation for all projects; however, post-installation testing for both P4 projects were performed substantially later (≥4 weeks). It is worth noting that for projects P2, P3, P9, i.e., soil profiles with more than 50% silt-like or clay-like soil behavior type index, the change in the tip resistance (q_t) and side friction (f_s) cannot be observed visually. This could be attributed to two potential reasons: (1) the soil improvement was minimal/nonexistent, or (2) the number of days between the DDP construction and the CPT_{POST} testing (2 to 6 days) was too short to observe any noticeable difference for these projects. Particularly for cohesive soils, the time dependency plays a critical role. For P6, a soil profile with more than 80% silt-like or clay-like soil behavior type index, post installation CPTs were performed after 10 days, and some improvement of tip resistance (q_t) can be noticed at around 4 to 6 meters of depth. As explained by Meng *et al.* (2015), the pore water pressure dissipation, and subsequent radial consolidation for cohesive soils could take several days until it reaches it residual resistance. Columns (d) and (e) in Figure 3.3, 3.4, and 3.5 will be discussed later in the manuscript.

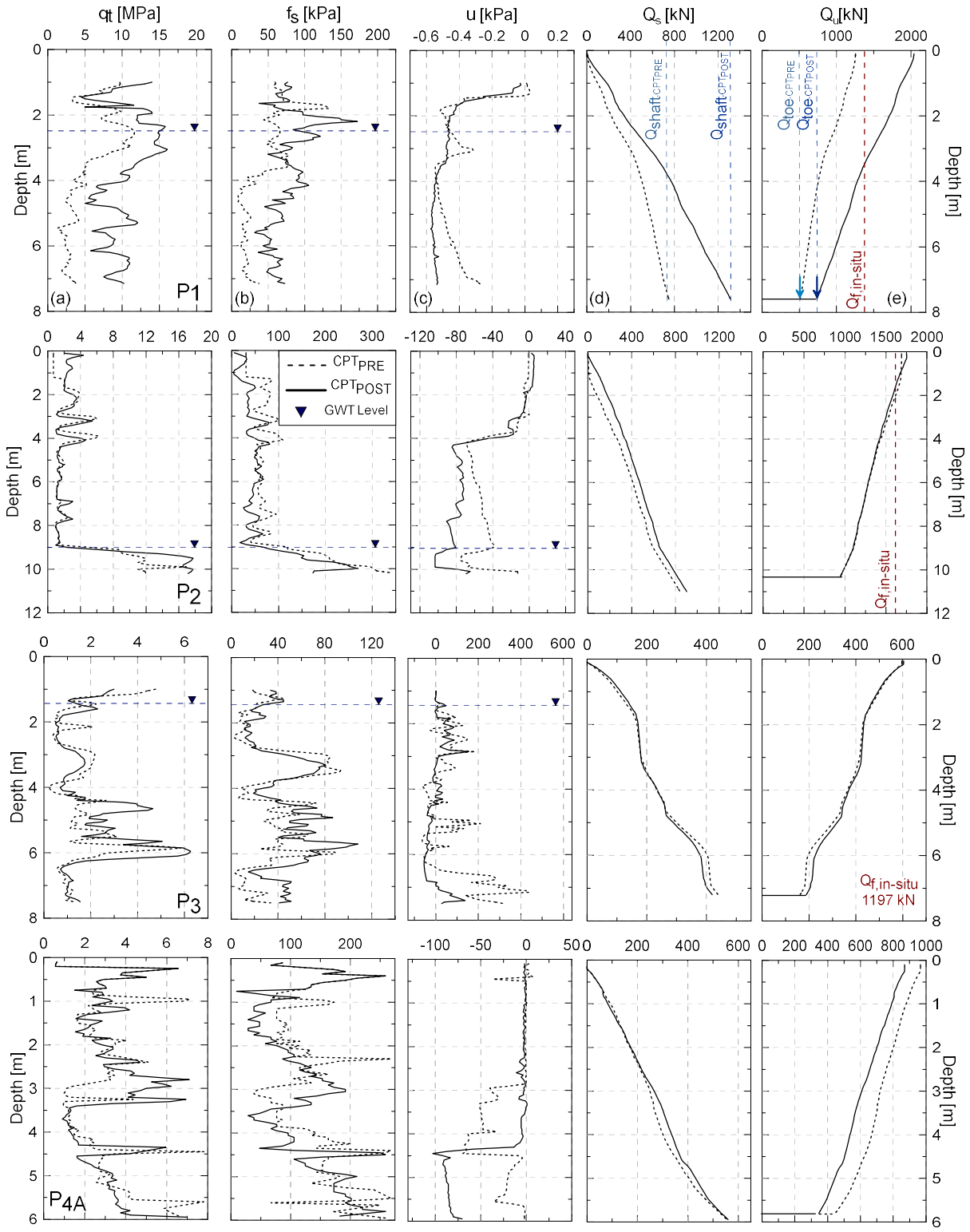

Figure 3.3. Change in CPT raw data and analytical axial load capacity of the DDP vs. depth for projects P1 to P4A. (a) tip resistance (q_t), (b) side friction (f_s), (c) pore water pressure (u), (d) analytical, cumulative shaft resistance (Q_s), and (e) ultimate axial load capacity (Q_u): analytical and experimental.

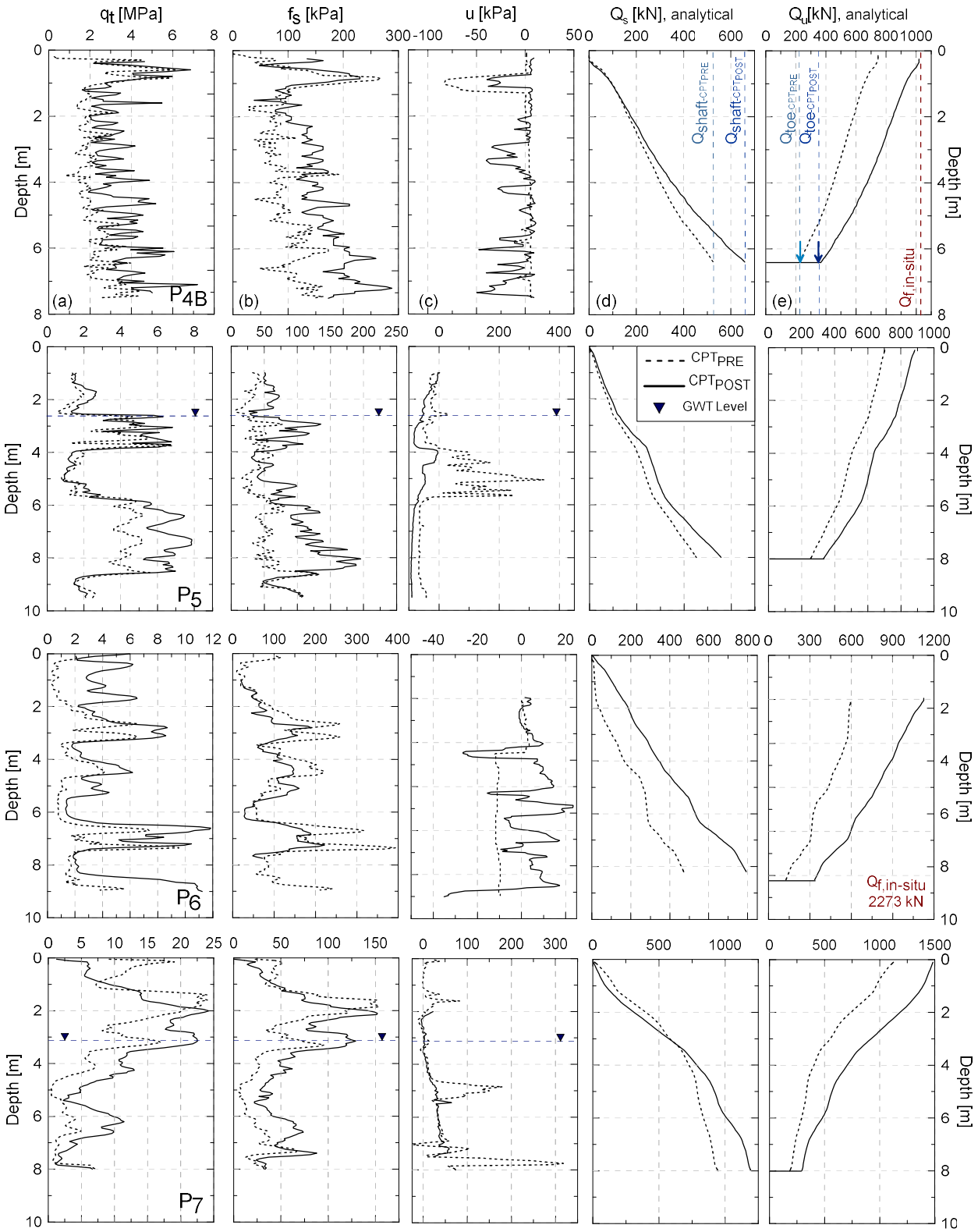

Figure 3.4. Change in CPT raw data and analytical axial load capacity of the DDP vs. depth for projects P4B to P7. (a) tip resistance (q_t), (b) side friction (f_s), (c) pore water pressure (u), (d) analytical cumulative shaft resistance (Q_s), and (e) ultimate axial load capacity (Q_u): analytical and experimental.

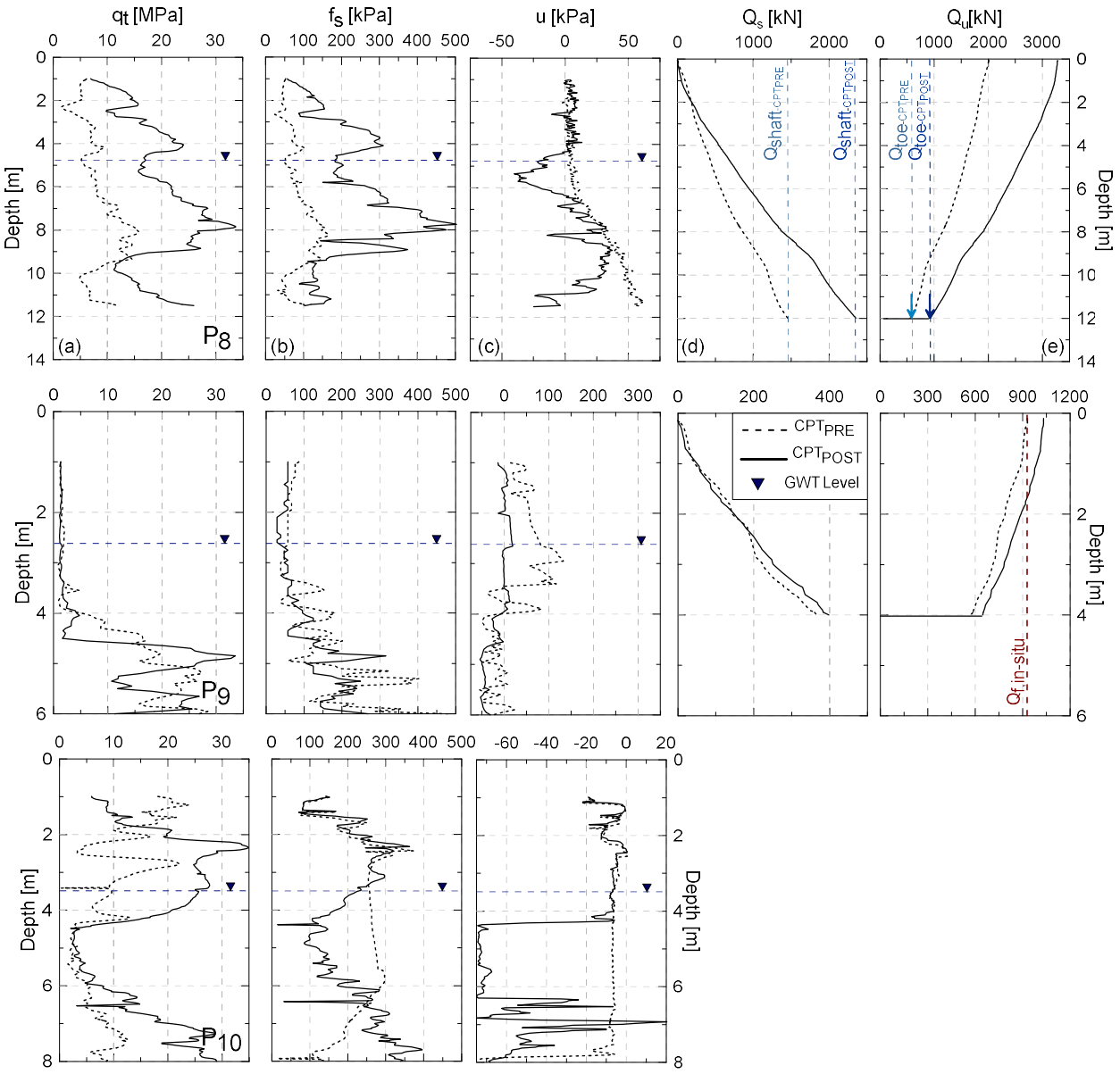

Figure 3.5. Change in CPT raw data and analytical axial load capacity of the DDP vs. depth for projects P8 to P10. (a) tip resistance (q_t), (b) side friction (f_s), (c) pore water pressure (u), (d) analytical cumulative shaft resistance (Q_s), and (e) ultimate axial load capacity (Q_u): analytical and experimental.

3.3. Data Analysis

3.3.1. Quantitative assessment of potential improvement

The CPT_{PRE} and CPT_{POST} data was first normalized by the in-situ vertical stresses. This correction accounts for depth effects and allows for comparison of data with similar soil behavior regardless of depth. The data was then used to calculate the soil behavior type index (I_c) based on Robertson,

2010 (Eq. 3.1). Hereafter, a code was set up to determine the difference in post and pre-CPT measurements along the pile depth. The ratio of post- vs. pre pile-installation soil-data was calculated for CPT side friction, friction ratio, normalized cone resistance, and normalized friction ratio; i.e., $f_{s.post}/f_{s.pre}$, $R_{f.post}/R_{f.pre}$, $Q_{t.post}/Q_{t.pre}$, and $F_{r.post}/F_{R.pre}$, respectively. The normalized cone resistance, and normalized friction ratio (Q_t and F_r) were obtained per Eq. (3.2) and Eq. (3.3). The friction ratio was obtained with Eq. (3.4).

$$R_f = \left(\frac{f_s}{q_t}\right) * 100\% \quad [4]$$

Figure 3.6 to Figure 3.9 show the improvement ratios for Q_t, f_s, R_f, and F_r respectively; all ratios were plotted against their respective field data points obtained prior to pile installation (i.e., $f_{s.pre}$, $R_{f.pre}$, $Q_{t.pre}$, and $F_{r.pre}$). Hereby, all datapoints were evaluated regardless of whether they showed "positive" or "negative" improvement. All results shown in Figure 3.6 to Figure 3.9 were obtained from CPT_{POST} testing performed inside a pile group arrangement or within a maximum distance of 1D from the DDP. The graphical presentation of improvement ratio is separated by soil-behavior type to better visualize the potential improvement of each soil type. The separation of Figure 3.6 to Figure 3.9 follows the criteria and nomenclature suggested by Robertson (2010):

- Sands – clean sand to silty sand - I_c [1.31 - 2.05]
- Sand mixtures, silty sand to sandy silt – I_c [2.06-2.60]
- Silt mixtures, clayey silt to silty clay – I_c [2.60-2.95]
- Clays – silty clay to clay – I_c [2.95-3.60].

Figure 3.6 shows the ratio of overburden-pressure-normalized post-pile-installation tip resistance versus pre-pile installation tip resistance for all soil behavior types (i.e., $Q_{t.post}/Q_{t.pre}$ vs. $Q_{t.pre}$). All soil behavior types suggest some level of improvement (data points above 1.0 line), with

improvement ratios reaching up to 3 for clean sands, ~4 for selected sand-like layers, and an average of ~2 for silt-like and clayey soils (with large data scatter). While a trendline has been added to the data points, the large scatter of data points in the cohesive soils (Figure 3.6c and 3.6d) misleads the reliability of the improvement ratio obtained for predominantly silty and clayey soils and should be used with caution. An (expected) inverse trend between the improvement ratio and the pre-installation tip resistance can be identified for most soils, i.e., the higher the initial resistance (i.e., initial density of the soil), the lower the improvement achieved during pile installation. Figure 3.6 furthermore includes the data points for which no improvement was obtained. These data points plot below the 1.0 ratio line. Within the clean sand and clay-like soils, the post-pile-installation "decrease" in tip resistance was limited, only few data points have a ratio less than one. The sand-like and silt-like soil layers (Figure 3.6b and 3.6c) contain the most data points with "negative q_t improvement".

Simultaneously, as visible in Figure 3.6d, clay-like soils, traditionally expected to generate limited improvement, showed selected data points with very high improvements ratios. The authors investigated those points closely to see whether these data points are outliers based on the mathematical approach used to evaluate pre-and post CPT data, or whether these improvements are "real". The highest improvement data points ($Q_{tpost}/Qt_{pre} > 5$) plotted in Figure 3.6d originate primarily from Projects P4B and P5 and were either achieved in very thick clayey or silt soil layers (h≥2m for P5) and/or after a very long time of waiting ($CPT_{POST} > 4$ weeks for P4A and P4B). Points with lower improvement ratios in clayey materials were found to stem from thinner layers of clay or silty soils embedded in between cohesionless soils. However, these lower improvements in the interbedded layers could also be associated with the "thin layer effect", which suggests the

thickness of the cohesive soil layer not being long enough to capture the real improvement by the CPT cone (explained later).

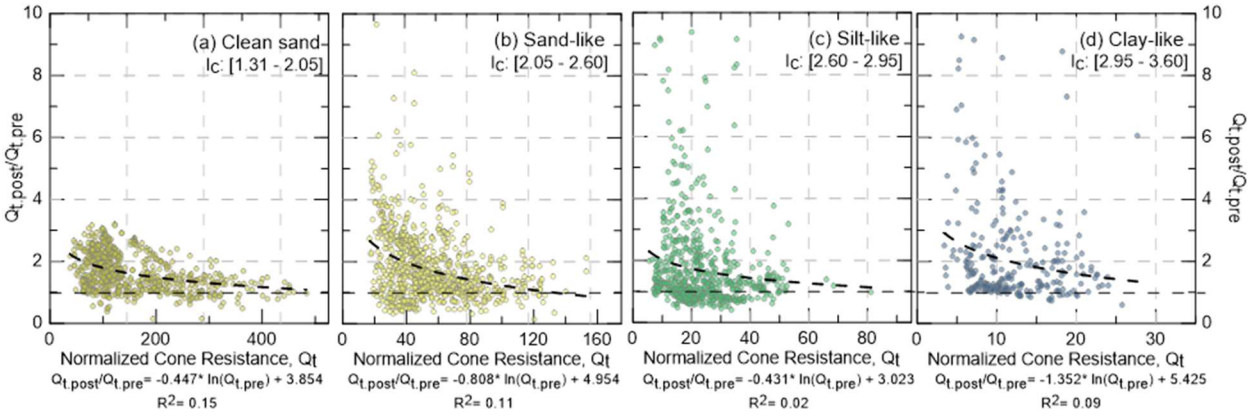

Figure 3.6. $Q_{t.post}/Q_{t.pre}$ ratio vs $Q_{t.pre}$ for all projects arranged based on the soil behavior type index. (a) Sands – clean sand, (b) Sand mixtures, (c) Silt mixtures, (d) Clay-silty clay.

Figure 3.7 presents the ratio of pre-and post-installation side friction (f_s) obtained during the DDP installation (i.e., $f_{s.post}/f_{s.pre}$ ratio vs $f_{s.pre}$.) Figure 3.7 suggests the majority of soil data points to see some level of improvement (i.e., ratio >1.0). A trendline was also added to capture the general data trend. Selected layers show an increase in side friction of up to >6times, however, the general improvement in side friction for soil with initial side frictions $f_{s.pr}$ of 0-100kPa ranges between 1-3 for all soil types. It is also noticeable that the side friction shows very consistent behavior and much less scatter than observed for the CPT tip resistance (Figure 3.6).

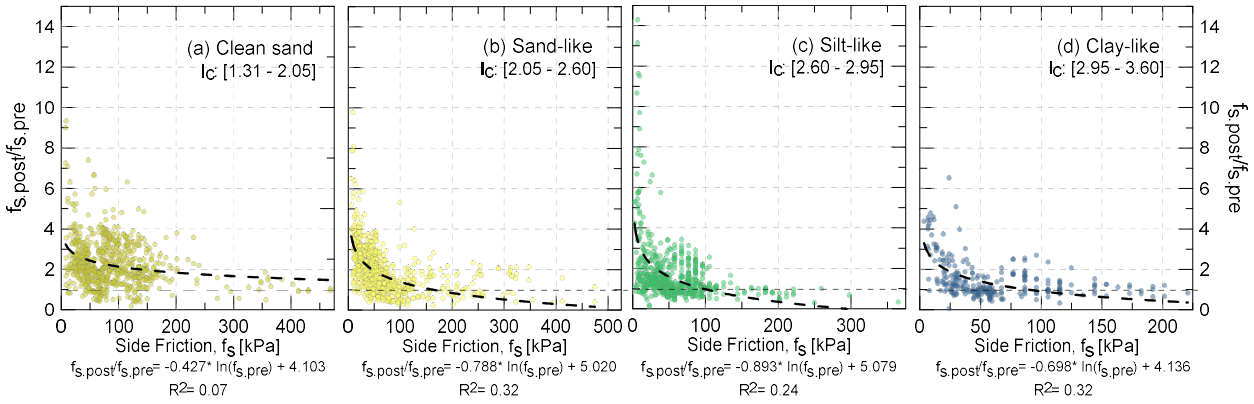

Figure 3.7. $f_{s.post}/f_{s.pre}$ ratio vs $f_{s.pre}$ for all projects classified based on the soil index behavior. (a) Sands – clean sand, (b) Sand mixtures, (c) Silt mixtures, (d) Clay-silty clay.

The change in normalized friction ratio (F_r) and friction ratio (R_f) and (Eqs. 3.3 and 3.4) is shown in Figure 3.8 and Figure 3.9. Both graphs indicate substantial scatter for clean sands and sand-like soils. The normalized friction ratio is a relationship frequently employed to locate soils within the soil-behavior type chart and used to identify behavioral trends of soil (e.g., contractive/dilative behavior, liquefiable and non-liquefiable potential). Figure 3.8 and Figure 3.9 show a similar data trend in the normalized friction ratio as identified in Figure 3.7. For initial resistances of F_r lower than 1.0, an increase in friction ratio can be >3.0 times higher than its pre-installation ratio. However, this data should be used with care and is primarily needed for the SBT chart later in this paper.

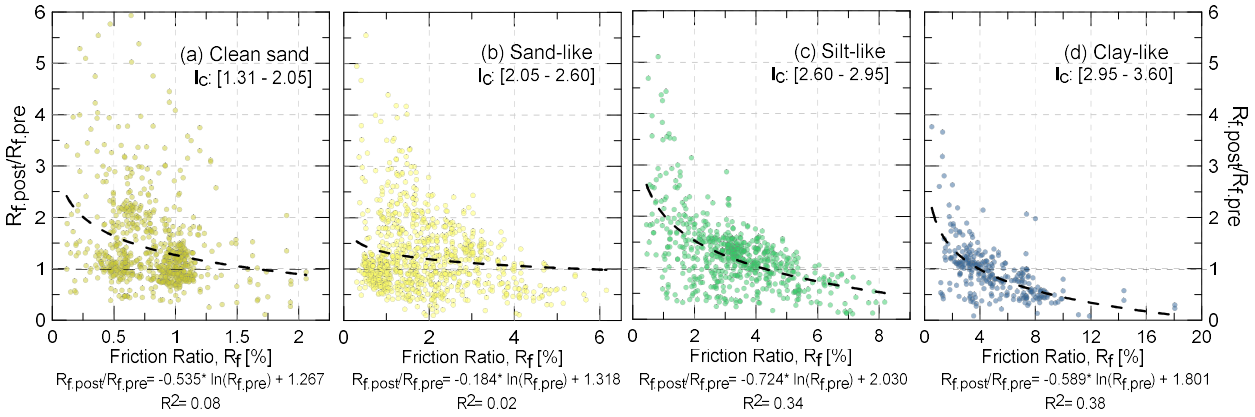

Figure 3.8. $R_{f.post}/R_{f.pre}$ ratio vs $R_{f.pre}$ for all projects classified based on the soil index behavior. (a) Sands – clean sand, (b) Sand mixtures, (c) Silt mixtures, (d) Clay-silty clay.

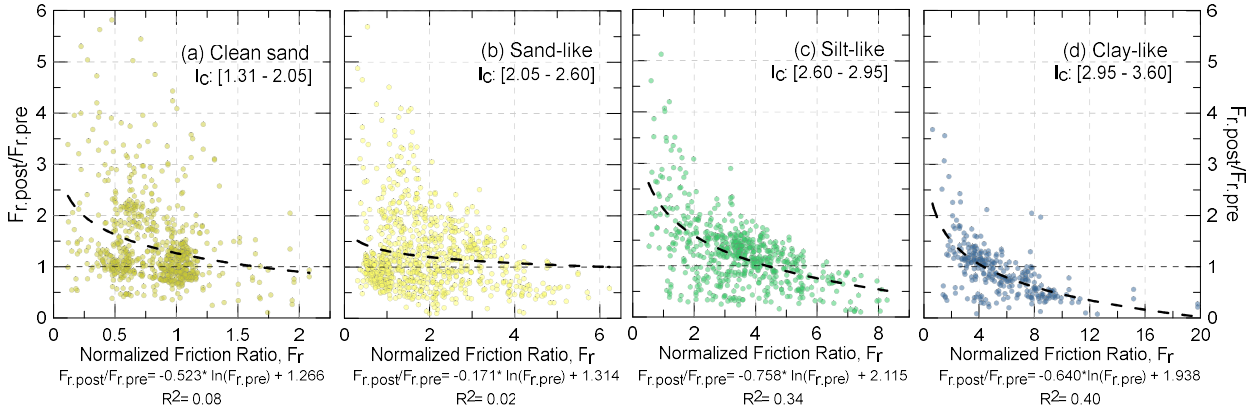

Figure 3.9. Normalized friction ratio $F_{r.post}/F_{r.pre}$ ratio vs $F_{r.pre}$ for all projects classified based on the soil index behavior. (a) Sands – clean sand, (b) Sand mixtures, (c) Silt mixtures, (d) Clay-silty clay.

Traditionally, cohesionless soils represent the most preferred site condition for DDP installation, and successful soil improvement has generally been attributed to sandy soils (NeSmith, 2002). A comparison of before-after CPT tip resistance and side friction (Figure 3.6 and Figure 3.7) supports this argument; however, suggests that some amount of fines content can be beneficial to increase the level of improvement achieved, evidenced by the magnitudes of post installation side friction and tip resistance reached in sand-like soils vs. clean sands. This concept (leaning on general principles of optimum fines content as used in compaction analyses) is further investigated by visualizing the shift of data points within the soil-behavior type charts. The Normalized CPT Soil Behavior Type (SBTn) charts by Robertson (2010) correlates the change in soil behavior type index based on CPT parameters $Q_{tn.pre}$ and $F_{r.pre}$. The Q_{tn} values were obtained based on Eq. (3.5).

$$Q_{tn} = \left(\frac{q_t - \sigma_{vo}}{P_{a2}}\right)\left(\frac{P_a}{\sigma'_{vo}}\right)^n \quad [3.5]$$

Where P_{a2} represented the atmospheric pressure (0.1MPa) and the exponent n varies based on the soil classification and stress level. The n factor was calculated based on a flow chart to evaluate the cyclic resistance ratio from CPT after Robertson, 2009 (Figure 46 of the Guide to Cone Penetration Testing for Geotechnical Engineering by Robertson & Cabal, 2014).

Figure 3.10 illustrates the normalized soil behavior type chart (SBTn) by Robertson (2010), which includes information about expected soil behavior depending on the location of soil data within the chart. These attributes include the soil's sensitivity, the increase of over-consolidation ratio (OCR) for cohesive soils, the increase of density, age, and cementation for cohesionless soils. The gray-shaded area suggests the region with normally consolidated soil behavior. The thick black line starting at around F_r=0.1, and Q_t=75 is the contractive-dilative (CD) boundary proposed by Robertson (2016) based on the normalized cone resistance and normalized friction ratio

(Q_{tn}, F_r). Based on the location of soil data relative to the CD line, soils can be identified as "contractive" or "dilative" at large shear strains. CD values higher than 70 (above the black line) indicate dilative behavior, CD values lower than 70 (below the black line) suggest contractive soil behavior.

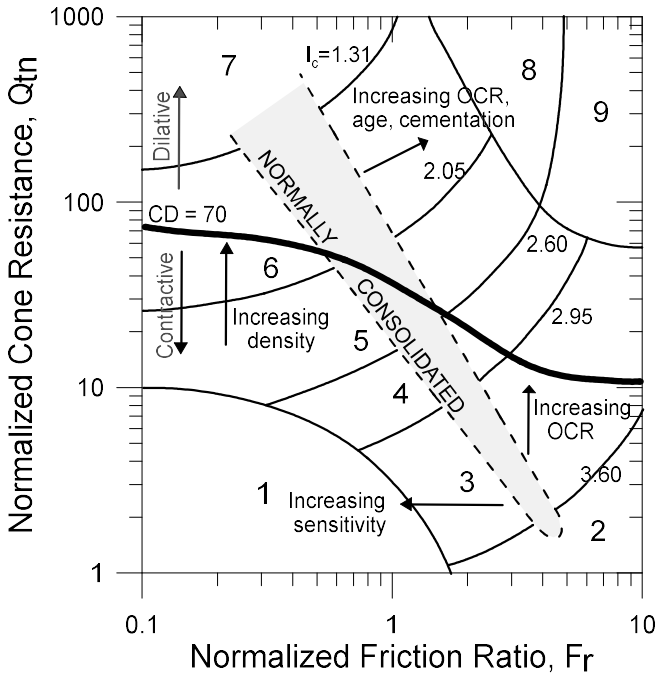

Figure 3.10. Normalized CPT Soil Behavior Type (SBTn) chart by Robertson, 2010 (Redrawn after Guide to Cone Penetration Testing for Geotechnical Engineering by Robertson & Cabal, 2014 and Robertson, 2016)

Figure 3.11 shows the location of all clean sand data points (i.e., I_c: 1.31 – 2.05) before (Figure 3.11a (CPT_{PRE})) and after (Figure 3.11b (CPT_{POST})) pile installation. A shift in data points towards more dilative soil behavior is evident. In addition, the soils identified as normally consolidated shifted out of the grey area towards a region within soil behavior similar to over-consolidated soils. The data points are further distinguished by color to trace the movement of datapoints within the chart and to investigate a possible correlation of soil improvement ratio and location within the SBTn chart. For clean sands, most soil data stayed within their initial I_c range within the chart but moved significantly away from the CD line (indicating more dilative soil behavior upon soil

improvement); selected data points moved away and downward (into a new region with Ic > 2.05). Amongst these selected data points are the soil data with the lowest or below 1.0 “improvement” ratio.

Figure 3.11 shows the location of all clean sand data points (i.e., I_c: 1.31 – 2.05) before (Figure 3.11a (CPT_{PRE})) and after (Figure 3.11b (CPT_{POST})) pile installation within the SBTn chart. A shift in data points towards more dilative soil behavior is evident. In addition, the soils identified as normally consolidated shifted out of the grey area towards a region with soil behavior similar to over-consolidated soils. The data points are further distinguished by color to trace the movement of datapoints within the chart and to investigate a possible correlation of soil improvement ratio and location within the SBTn chart. For clean sands, most soil data stayed within their initial I_c range within the chart but moved significantly away from the CD line (indicating more dilative soil behavior upon soil improvement); selected data points moved away and downward (into a new region with I_c > 2.05). Amongst these selected data points are the soil data with the lowest or below 1.0 “improvement” ratio. Figure 3.11c and 3.11d depict the same data set as Figure 3.11a and 3.11b but color-code each data point by its respective Fines Content (*FC*). The fines content is defined as the % soil particles passing the N. 200 sieve. Figure 3.11d suggests the soils with the lowest fines content (0-15%; dark blue) to disperse the most within the chart. Hereby, the large amount of these low *FC* data points experience a decrease of the F_r values while maintaining the same Q_t (i.e., moving from Zone 6 to Zone 5). Soils with a higher *FC* between 30% to 40%, originally located in the normally consolidated zone, tend to improve the $Q_{tn.pre}$ value, and shift towards more dilative behavior (i.e., to a higher density), the $Q_{t.post}/Q_{t.pre}$ ratio for this type of soils appears to be between 1.5 and 3.

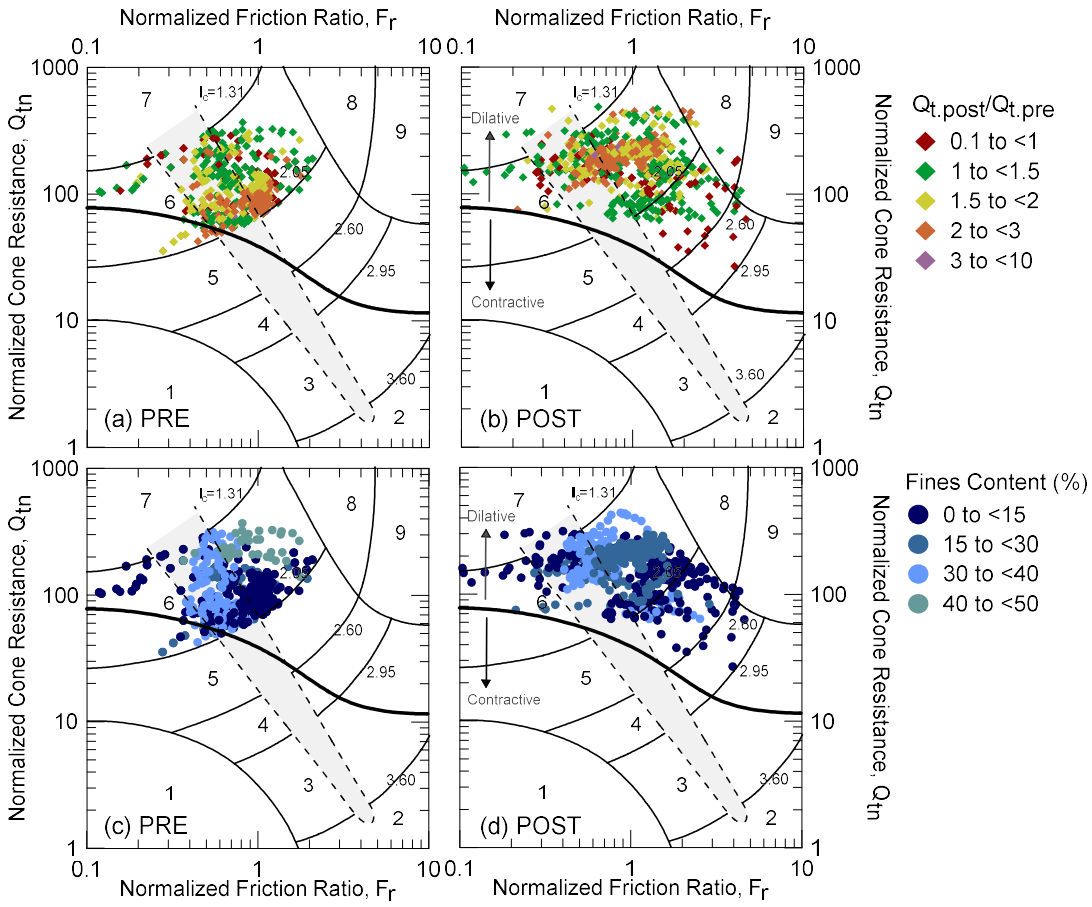

Figure 3.11. Soil Behavior Type (SBTn) chart with pre and post Q_{tn} and F_r values and soil index behavior evolution for clean sands, Ic: [1.31 – 2.05]. (a) $Q_{tn.pre}$ and $F_{r.pre}$ values with $Q_{t.post}/Q_{t.pre}$ markers, (b) $Q_{tn.post}$ and $F_{r.post}$ values with $Q_{t.post}/Q_{t.pre}$ markers, (c) $Q_{tn.pre}$ and $F_{r.pre}$ values with *FC* markers, (d) $Q_{tn.post}$ and $F_{r.post}$ values with *FC* markers.

The same analysis was performed for sand-like soils (I_c: 2.05 – 2.60), with results shown in Figure 3.12. From Figure 3.12a (CPT_{PRE}) and Figure 3.12b (CPT_{POST}) a shift in the soil type behavior can be noticed, when $Q_{t.post}/Q_{t.pre}$ is higher than 2. The sand-like soils behavior changes to a clean sand behavior (Zone 6). On the other hand, when the Q_t "improvement" ratio is lower than 1.0, the soil tends to simulate a silty-like type of behavior. Moreover, almost all soil data points located on the contractive side, displace to a dilative behavior. Figure 3.12c and 3.12d highlight the change of soil data in terms of fines content. The majority of data points that switch from sand-like behavior to clean sand behavior, has a *FC* between 15% to 40%. Soil data with very low fines content (*FC*<15%) tend to shift downwards towards more cohesive soil behavior (from Zone 5 towards Zone 4) and away from the CD line towards more dilative behavior.

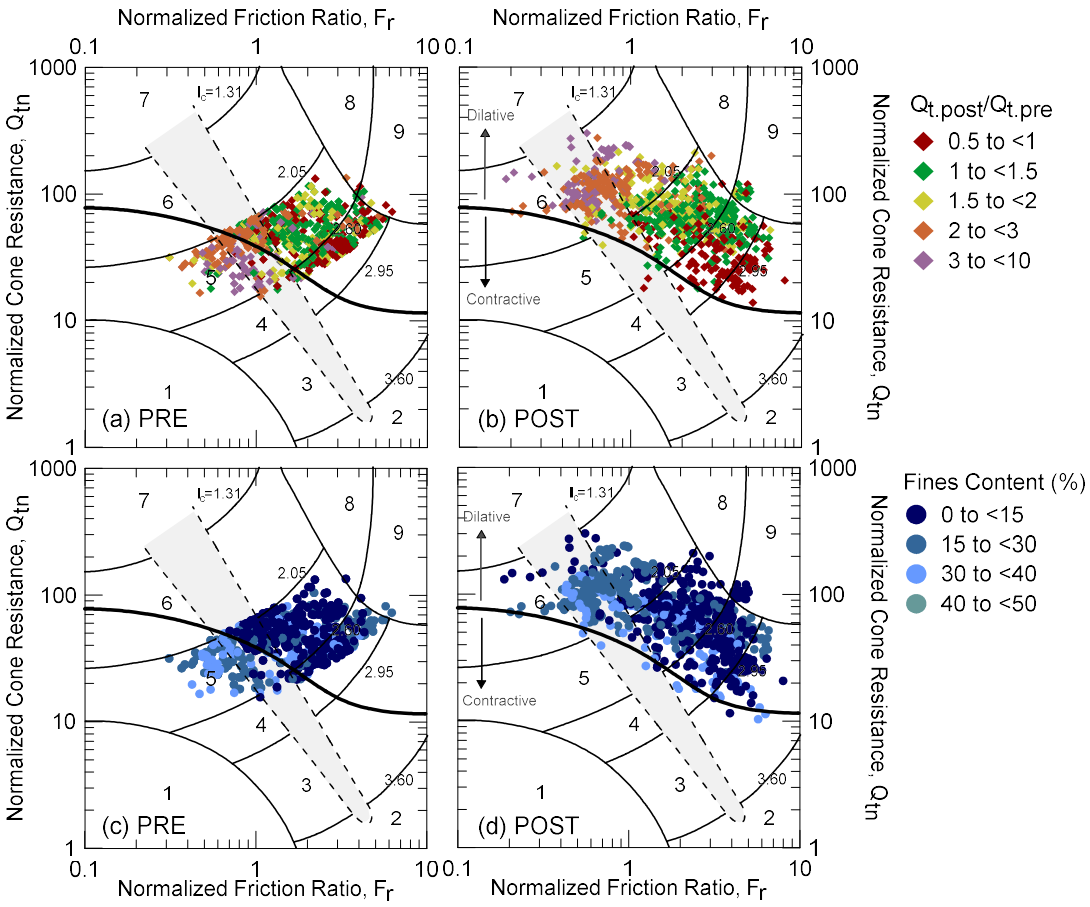

Figure 3.12. Soil Behavior Type (SBTn) chart with pre and post Q_{tn} and F_r values and soil index behavior evolution for sand-like, I_c: [2.05 – 2.60]. (a) $Q_{tn.pre}$ and $F_{r.pre}$ values with $Q_{t.post}/Q_{t.pre}$ markers, (b) $Q_{tn.post}$ and $F_{r.post}$ values with $Q_{t.post}/Q_{t.pre}$ markers, (c) $Q_{tn.pre}$ and $F_{r.pre}$ values with *FC* markers, (d) $Q_{tn.post}$ and $F_{r.post}$ values with *FC* markers.

To better correlate the effect of fines with the soil improvement obtained following DDP construction, the $Q_{t.post}/Q_{t.pre}$ ratio was plotted against $Q_{t.pre}$ for different FC ranges in Figure 3.13 and Figure 3.14 for clean sands and sand-like soils, respectively. For clean sands with pre-installation tip resistance $Q_{t.pre}$ lower than ~150, Figure 3.13 suggests the highest improvement ratio to be achieved for soils with fines contents between 15% to 30%. Similar behavior is observed for soils with higher fines content (*FC* 30%-40%), even though fewer data points are available for this chart. The lowest improvement within sandy soils was reached when fines were less than 15%, suggesting that some amount of fines content positively affects the level of densification achieved

around the pile. For sand-like soils, Figure 3.14b and Figure 3.14c show a higher improvement for soils with *FC* ranging from 15% to 40%.

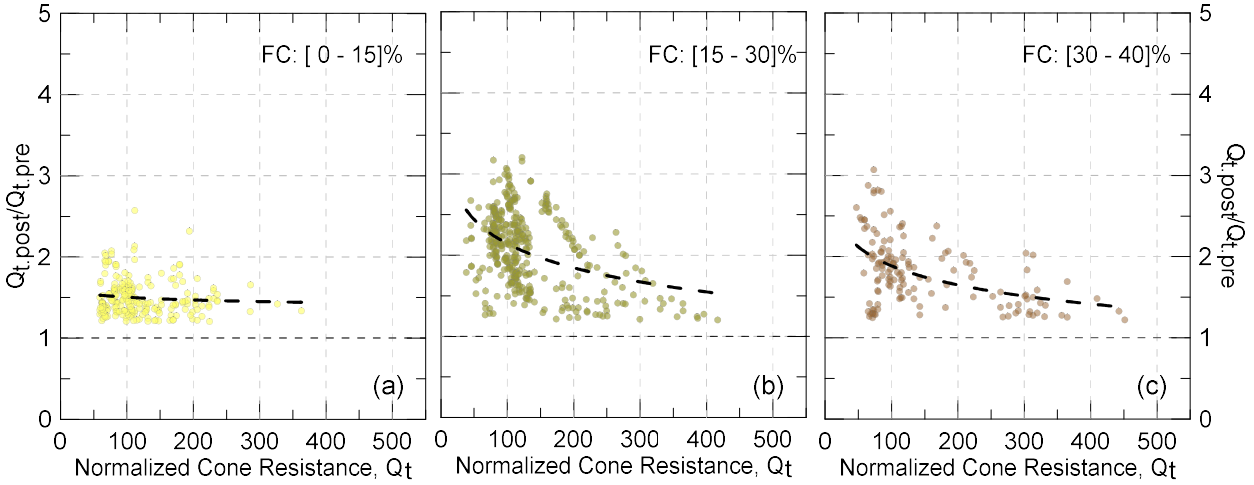

Figure 3.13. $Q_{t.post}/Q_{t.pre}$ ratio vs $Q_{t.pre}$ for "clean sands (Ic: [1.31 – 2.05])" type of soils. (a) Fines content lower than 15%, (b) *FC* between 15% to 30%, (c) *FC* between 30% to 40%.

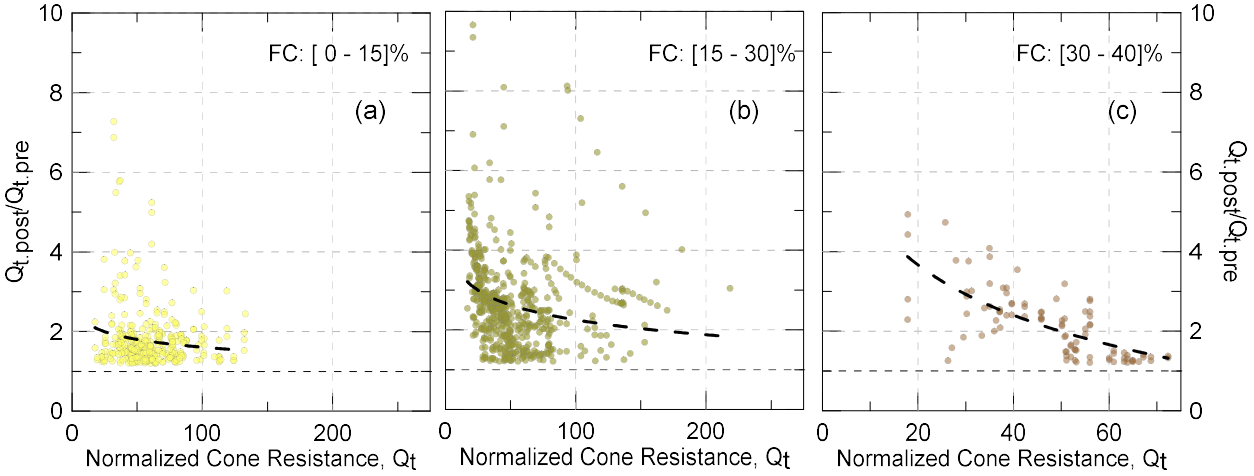

Figure 3.14. $Q_{t.post}/Q_{t.pre}$ ratio vs $Q_{t.pre}$ for "sand-like (Ic: [2.05 – 2.60])" type of soils. (a) *FC* lower than 15%, (b) *FC* between 15% to 30%, (c) *FC* between 30% to 40%.

The results presented in Figures 3.5 to 3.13 show a strong correlation between the initial tip resistance, the fines content of the soil, and the level of improvement achieved during the construction of the DDP. Table 3.3 visualizes the improvement observed from the case studies included in this manuscript (i.e., the $Q_{t.post}/Q_{t.pre}$ ratio) based on the soils *FC* and pre-installation

Q_t value. Table 3.3 is limited to sandy soils, showing (1) clean sands (I_c 1.31 - 2.05) in Table 3.3 (a), and (2) sand-like soils (I_c 2.05 – 2.60) in Table 3.3 (b). These improvement ratios are only applicable for soils located inside a DDP arrangement (rectangular or triangular) with < 4D pile spacing, and for soils outside a pile arrangement but within a maximum distance of 1D from the pile.

Table 3.3. Improvement ratio based on the soils index behavior (I_c) and fines content (FC) for different values of the normalized cone resistance Q_t obtained from CPT$_{PRE}$ results. (a) Sands – clean sand, (b) Sand mixtures.

I_c	Q_t	FINES CONTENT [%]		
		<15	15-30	30-40
[1.31 - 2.05]	50	1.5	2.4	2.1
	100	1.5	2.1	1.9
	150	1.5	2.0	1.7
	200	1.5	1.8	1.7
	250	1.5	1.7	1.6
	300	1.5	1.7	1.5
	350	1.4	1.6	1.5
	400		1.5	1.4
	450			1.4

(a)

I_c	Q_t	FINES CONTENT [%]		
		<15	15-30	30-40
[2.05 - 2.60]	25	2.0	3.0	3.3
	50	1.8	2.6	2.0
	75	1.7	2.4	1.3
	100	1.6	2.2	
	125	1.5	2.1	
	150	1.5	2.0	
	175		1.9	
	200		1.9	
	225		1.8	

(b)

Similarly to Figure 3.11 and Figure 3.12 for sandy soils, the pre-and post-installation soil data was placed within the SBTn chart for silt-like and clay-like soils (Figure 3.15 and Figure 3.16), but no clear relationship with fines content was identified. Figure 3.15 and Figure 3.16 show the shift in Q_{tn} and F_r values. For silt-like and clay-like soils, similar to what was observed for the cohesionless soils, some of the data points originally located in the contractive behavior zone shift to a more dilative behavior, but this shift does not apply to the majority of the data point. Soil data points with an improvement ratio of 1.5 and higher tend to relocate from the silty soil behavior zone towards cohesionless soil behavior (from Zone 4 towards Zone 5 and 6). For silt-like soils, (I_c: 2.60 – 2.95) without improvement or noticeable decrease in post-installation parameters, i.e., $Q_{t.post}/Q_{t.pre} \leq 1$, the datapoints moved downward towards a clay-like behavior (Zone 3).

Figure 3.16 depicts clay-like soils, (I_c: 2.95 – 3.60) and suggests several observations. Clay-like soils with low initial tip resistance located on the contractive side shift upward and into dilative post-installation behavior (purple and orange data points). Data points with minimal or limited improvement (1.0 – 2.0) largely maintain their tip resistance and increase in friction ratio, shifting their location in the chart toward the right side, but do not necessarily across the CD line towards dilative behavior.

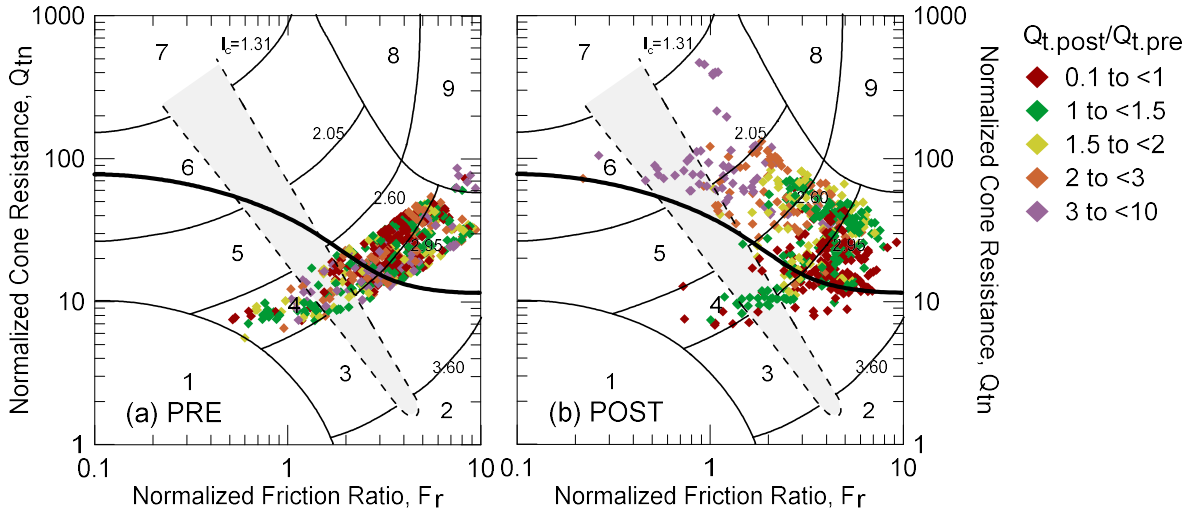

Figure 3.15. Soil Behavior Type (SBTn) chart with pre and post Q_{tn} and F_r values and soil index behavior evolution for silty-like, Ic: [2.60 – 2.95]. (a) $Q_{tn.pre}$ and $F_{r.pre}$ values with $Q_{t.post}/Q_{t.pre}$ markers, (b) $Q_{tn.post}$ and $F_{r.post}$ values with $Q_{t.post}/Q_{t.pre}$ markers.

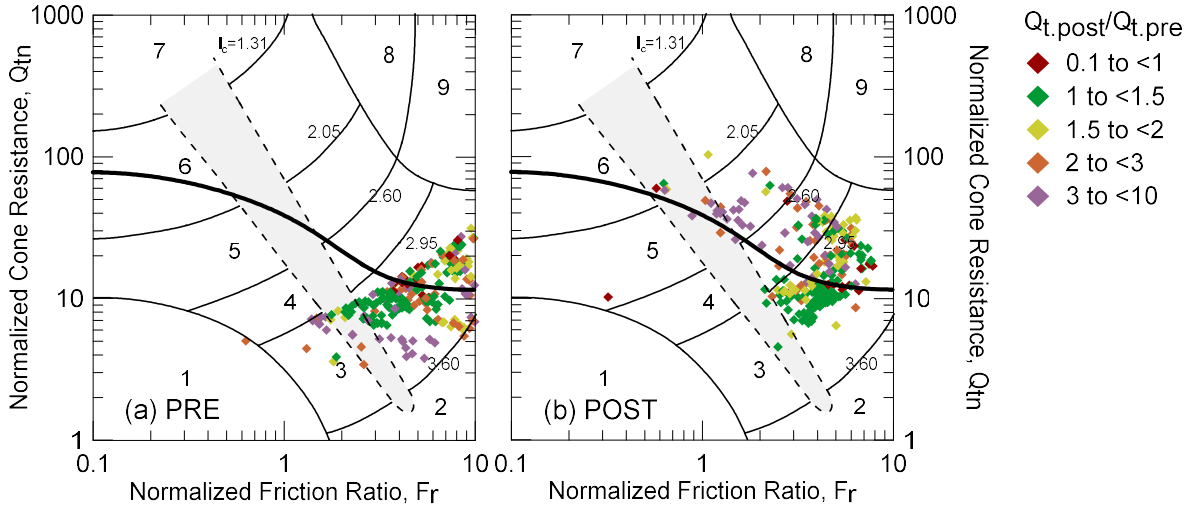

Figure 3.16. Soil Behavior Type (SBTn) chart with pre and post Q_{tn} and F_r values and soil index behavior evolution for clay-like, Ic: [2.95 –3.60]. (a) $Q_{tn.pre}$ and $F_{r.pre}$ values with $Q_{t.post}/Q_{t.pre}$ markers, (b) $Q_{tn.post}$ and $F_{r.post}$ values with $Q_{t.post}/Q_{t.pre}$ markers.

As suggested by fundamentals of soil mechanics and supported experimentally by Meng *et al*. (2015), the level of improvement in cohesive soils is dependent on the excess pore water pressure dissipation. For instance, Karlsrud *et al.*, (2014) tested axially 400 mm to 600mm diameter driven steel pipe piles in sandy soils and clayey deposits to evaluate pile setup and aging effects. The shaft resistance for piles installed in sand deposits doubled in a period of 12 months and remained constant afterwards. For piles installed in clayey deposits, Karlsrud *et al*. observed the following: the gain in shaft resistance is due to the initial pile set-up, but also due to the dissipation of the excess pore water pressure. Clays with low plasticity and low over consolidation ratio (OCR) showed a higher increase of axial load resistance compared to clays with high plasticity and high OCR; the increase in axial load capacity ranged from 1.1 for clays with high plasticity and to 2.0 for clays with low plasticity after 2 years and full re-consolidation. The authors believe that for some of the projects presented herein (P2, P3, P9), the number of days between the DDP construction and the CPT_{POST} performance was too short [2-6 days] to show the maximum possible soil improvement, therefore, the analysis and definition of an improvement ratio in cohesive soils cannot be broadly determined in a precise manner and more time dependent testing is suggested for future research and testing efforts. The data points with very high improvement ratios (3-10, purple data points) are almost always associated with project sites that have large clay layers and very long wait times between pile installation and post-CPT testing (as discussed before). These data points clearly jump from the SBTn Zone 3 to Zone 5 and across the CD line (Figure 3.16b).

3.3.2. Spatial Improvement

To further assess the spatial improvement around the DDPs, the normalized cone resistance Q_t was compared at distances of 1*D*, 2*D*, and 3*D* away from the pile (Figure 3.17). All data presented in Figures 3.3 through 3.16 was obtained from CPT_{POST} tests performed inside a pile arrangement, or

within a distance of 1D away from the DDP. Rows in Figure 3.17 correspond to the different distances (1D, 2D, and 3D), and the columns correspond to the different soil types based on the soil behavior type index I_c. The highest improvement was consistently recorded (for all soil types) within one pile diameter away from the pile, hereafter, a substantial drop in achievable improvement is notable. For instance, clean sands (Figure 3.17, left column) experienced a maximum $Q_{t.post}/Q_{t.pre}$ ratio of up to 3.0 within 1D from the pile, while at a distance of 2D or 3D, the improvement ratio reduces by at least 50%. Across all soil types, no soil improvement was recorded (i.e., $Q_{t.post}/Q_{t.pre} \cong 1$) at distances larger than 3D.

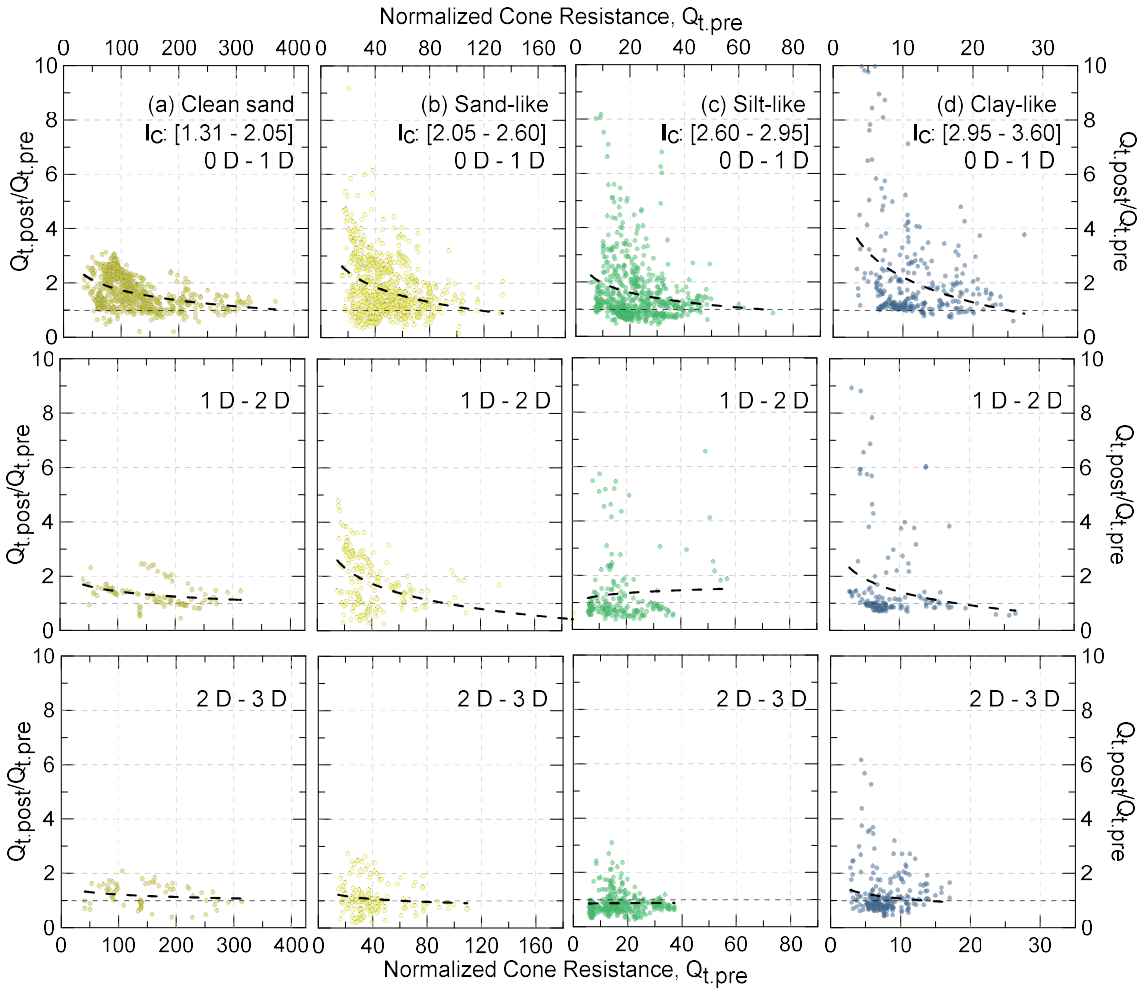

Figure 3.17. $Q_{tn.post}/Q_{tn.pre}$ ratio vs $Q_{tn.pre}$ for the main four soil index behavior at different distances measured from the DDP to the CPT$_{POST}$ location (Rows). (a) Sands – clean sand, (b) Sand mixtures, (c) Silt mixtures, (d) Clay-silty clay (Columns).

3.3.3. Lack of improvement

The comparison of before-after CPT data presented in Figures 3.3 and 3.5 suggests the ratio of "improvement" to be less than 1.0 for several stretches of the soil profile; indicating a "reduction" of soil resistance to occur. The majority of unimproved soil stretches are found in projects P2, P3, PA4, and P9, often characterized by very low initial tip resistances close to-, or less than 2 MPa. Simultaneously, all these above-mentioned sites, have very stratified soil profiles, alternating quickly between cohesive and cohesionless soils, hence the CPT "thin-layer effect" (Robertson and Fear, 1995) could highly affect the "improvement" measurements for this type of soil profiles. The authors investigated whether common parameters can be identified that reveal which combination of site conditions make a soil profile less- or non-improvable (e.g., GWT, very high or low shear strength, soil composition, soil type). However, no clear and generalizable relationship between the improvement or the reduction of soil resistance and the elevation of the ground water table or other parameters could be derived. For instance, P2 (GWT at 9 m depth), and P3 (GWT at only 2.1 m depth) show a decrease in both, q_t and f_s, but the location of the GWT for both sites vary significantly for both. Likewise, for P8 (GWT at 4.7 m) the improvement of the tip resistance appears to be the same across the entire the soil profile, above and below the GWT.

3.3.4. Comparison of axial load capacities estimated with CPT_{PRE} and CPT_{POST} data

Soil parameters used to estimate the axial pile capacity (design capacity) are often determined using a combination of pre-pile-installation in-situ and laboratory soil testing programs. Frequently, the pile design capacity is validated and updated based on field testing prior to the installation of production piles. An improvement in soil parameters surrounding the DDP as observed in the case studies presented herein could suggest a potential increase in axial pile capacity as benefit of the unique installation technique. An initial study by Siegel *et al*. (2019)

conducted in cohesive soils, showed that the tip resistance of Continuous Flight Auger (CFA) piles compared with the tip resistance of DDPs showed no difference, implying that installation effects did not translate into different pile tip capacities. This observation is somewhat expected as (1) a large amount of soil (i.e., the soil below the pile tip) remained unimproved and only limited soil thicknesses above and below the pile tip is included in the traditional analysis of pile tip resistance, and (2) the change of soil properties in clays is limited (Siegel *et al.* only studied cohesive soils). This study will analyze the change in shaft and pile toe capacity for all case histories presented herein, and then present the total capacity for comparison. The results of axial load tests are presented when available and compared to the analytically estimated pile capacities using the before-after in-situ CPT data.

All 9 projects sites were classified into two categories: “sandy sites” and “mixed sites”. When more than 65% of the soil profile constituded of clean sands and sand-like type of soils, the site was treated as ¨sandy site¨; all remaining sites were considered “mixed sites”. Accordingly, P1, P5, P7, and P8, were classified as “sandy sites”, while P2, P3, P4, P6, and P9, were classified as “mixed sites”. The analysis carried out on Chapter 2 showed that two of the most suitable methods to estimate axial load capacities of drilled displacement piles via CPT data were proposed by Brettmann and NeSmith (2000; 2005) for sandy soils; and by Bustamante and Gianeselli (1993; 1998) for mixed soils. A major drawback within Bustamante and Gianeselli (1993; 1998) is the required load that triggers a pile settlement equal to 10% of the pile diameter (D). Not all axial load tests, and especially piles with larger pile diameters, do not reach this level of deformation, hence, the method by Eslami and Fellenius (1997) was applied when the Bustamante and Gianeselli 10%D requirement could not be met. These three methods are subsequently employed

for all 9 projects (as applicable), and pile side friction and toe capacity were estimated using CPT_{PRE} and CPT_{POST} data. A brief description of each of the methods is given below.

3.3.4.1. Brettmann and NeSmith (2000; 2005) Method

The method was developed based on 28 axial load tests (22 compression test, and 6 tension tests) executed on augered, pressure-injected displacement piles (APID) with lost toe, installed in granular materials. The method can be used with SPT and CPT data in different types of granular soils (loose to medium sands). The pile diameters ranged from 0.36 m to 0.46 m (14 inch to 18 inch), and the pile lengths varied between 6 m and 21 m. For both, shaft and toe resistance, the authors observed a higher unit resistance when the sand had a low *FC*, was well-graded, and had an angular grain shape. The unit shaft resistance ($r_{s.CPT}$ – force/area) can be estimated by Eq. 3.6, where q_c is the uncorrected cone resistance along the pile in MPa, (with a limit value for q_c of 19 MPa), and the shaft resistance modifier (w_s) is a component of the unit shaft resistance (i.e., side friction) based on the fines content (FC), material uniformity, and shape of the soil grains. The resistance w_s value can vary between 0 MPa for rounded, uniform sands with a FC lower than 40%, to 0.05 MPa for well-graded, angular materials with a FC lower than 10%. For soils with granulometry properties between these to limit values, the w_s resistance can be interpolated. The limit unit shaft resistance ($r_{s.CPT}$) defined by Brettman and NeSmith is 0.21MPa.

$$r_{s.CPT} = 0.01 q_c + w_s \quad [3.6]$$

The unit toe resistance ($r_{t.CPT}$ – force/area) can be calculated using Eq. 3.7. Herein, the q_{cm} value is the average uncorrected cone resistance calculated from four pile diameters above and below the pile toe in MPa but limited to a maximum value of 19 MPa. The toe resistance modifier (w_t) ranges from 0 MPa for rounded, uniform sands with *FC* lower than 40%, to 1.34 MPa for well-graded, angular materials with FC lower than 10%. The limit unit toe resistance for both types of

sands was set to 7.2 MPa and 8.62 MPa, respectively. Interpolation can be made for granular soils with different properties.

$$r_{t.CPT} = 0.4q_{cm} + w_t \quad [3.7]$$

3.3.4.2. Bustamante and Gianeselli (1993; 1998)

Based on 24 axial load tests performed on Atlas piles, the authors developed an analytical capacity method to estimate the axial load resistance of DDPs in clayey, sandy, and silty materials. The ultimate pile capacity was defined as the load that triggers a settlement equal to 10% of the pile diameter. The unit shaft resistance ($r_{s.CPT}$) can be obtained as function of the soil type, CPT tip resistance, pile configuration, and construction type: cast-in-DDPs or DDP with casing. Based on these parameters, a design curve is utilized to estimate the unit shaft resistance. While this method does not provide limiting values for $r_{s.CPT}$, the maximum values of each design curve were used as limiting resistance. The unit toe resistance ($r_{t.CPT}$) can be estimated by Eq. 3.8, where K depends on soil type and varies from 0.55 for clayey soils, to 0.75 for sandy soils. α represents the arithmetic mean of the CPT tip resistance q_c, taken over a distance of $1.5D$ above and below the elevation of the pile toe.

$$r_{t.CPT} = K * \alpha \quad [3.8]$$

3.3.4.3. Eslami and Fellenius (1997) Method

The method was developed based on 102 case histories where CPTu data and static axial load test data were available, for piles with a variety of shapes, materials, and different installation techniques (i.e., the method was not specifically developed for drilled displacement piles). The case histories sites vary from soft to stiff clay, medium to dense sand, and mixtures of clay, silt, and sand. The authors defined an effective cone resistance (q_E) by subtracting the measured pore water pressure (u) from the measured cone tip resistance (q_t) the for the calculation of the pile toe

and shaft resistance. The unit shaft resistance ($r_{s.CPT}$) can be estimated by Eq. 3.9, where the shaft correlation coefficient (C_s) is selected based on q_E and the CPT sleeve friction (f_s). The unit toe resistance ($r_{t.CPT}$) is determined by Eq. 3.10, and the toe correlation coefficient (C_t) in most cases is equal to one. If the pile diameter (D) is larger than 0.4 m, C_t can be obtained by Eq. 3.11. The tip resistance, q_{Eg}, is the geometric average of the effective cone resistance (q_E) over an influence zone which length is controlled by the soil layering above and below the pile toe.

$$r_{s.CPT} = C_s * q_E \quad [3.9]$$

$$r_{t.CPT} = C_t * q_{Eg} \quad [3.10]$$

$$C_t = \frac{1}{3D};\ D[m] \quad [3.11]$$

Based on the unit shaft resistance, and unit toe resistance defined by each method, and the corresponding site classification, the total axial load resistance was determined via Eqs. 3.12 to 3.14.

$$Q_u = Q_{shaft} + Q_{toe} \quad [3.12]$$

Where:

$$Q_{shaft} = r_{s.CPT} * A_{shaft} \quad [3.13]$$

$$Q_{toe} = r_{t.CPT} * A_{toe} \quad [3.14]$$

A_{shaft}: shaft area – perimeter times the pile length

A_{toe}: Toe area – transversal area of the pile using the nominal diameter.

3.3.5. Analytical pile capacities before and after soil improvement

Projects P1, P5, P7, and P8 consist of mostly sands and were analyzed using Brettman and NeSmith's method. All remaining projects, characterized by more heterogeneous soil composition were analyzed using Bustamente and Gianeselli's (P3, P6) or Eslami and Fellenius' approach (P2,

P4A, P4B, P9). Columns (d) and (e) in Figures 3.3-3.5 present the analytically obtained pile capacities using CPT_{PRE} and CPT_{POST} data as input parameters into the methods described above. This theoretical exercise helps visualize how installation effects, i.e., the change in raw soil resistance data (columns (a) through (c), could translate into potential changes of overall pile capacity. All (d) columns depict the analytical change in shaft friction (Q_{shaft}) along the profile depth. All (e) columns present the cumulative analytical shaft friction (Q_{shaft}), toe resistance (Q_{toe}), and the total pile capacity (Q_u) using unimproved soil parameters (dashed line) and improved soil parameters (solid line). For "sandy sites" (P1, P5, P7, and P8), the improvement of the axial load capacity can be easily visualized; the total pile axial load capacity analytically increased by a factor of 1.3 to 1.7 when using CPT_{POST} vs. CPT_{PRE} data. It is worth noticing that, for P8, the pile toe capacity reached the limit resistance following soil improvement. Almost all mixed soil type projects (P2, P3, P4A, and P9) showed ratios of post vs. pre ultimate pile capacities near 1.0. An exception to this generalization was observed for projects P4B and P6. P4B consists of a homogeneous clayey site with CPT_{POST} testing executed after 39 days; the theoretical improvement reached 1.4. For P6 the total shaft resistance increased by a factor of 1.7; CPT_{POST} tests were performed more than 10 days after DDP construction. Similarly, the toe resistance of P6 increased by 2.7 times when using post-installation soil properties.

The bar chart of Figure 3.18 separates the axial pile resistance into the analytically estimated toe resistance (Q_{toe}, Figure 3.18a), side friction (Q_{side}, Figure 3.18b), and the total, ultimate load (Q_u, Figure 3.18c) based on before and after soil data. For the sandy sites projects, where the Brettmann and NeSmith (2000; 2005) method was applied to estimate the analytical capacities of the piles, Figure 3.18 display the upper and lower bound capacity since the sieve analysis and particle shape information was not available for these sites. Except for P4A, all sites

maintain or improve their analytical tip resistance and indicate similar or higher toe capacity. Similar observations can be made for the cumulative shaft resistance (side friction) shown in Figure 3.18b. Except for P3, which is mostly composed by silt-like and clay-like soils, all piles maintained or increased their side friction due to the installation technique. The CPT_{POST} for P3 was performed 2 days after the pile construction, hence potential improvements are likely not captured.

More importantly however, is the comparison of analytically predicted axial load capacities with experimentally observed failure loads. The in-situ axial load that triggered plunging behavior ($Q_{f,in-situ}$) was either obtained directly from the load test or estimated using Van der Veen's Criteria (1953) when the plunging behavior was not reached experimentally. In addition to identifying these failure loads, the axial load that triggers a settlement equal or higher than 10% of the pile diameter ($Q_{\Delta=10\%D}$) was also identified (whenever pile settlements reached that level of deformation). The maximum load ($Q_{max.test}$) and corresponding settlement (Δ_{max}) during the test are also presented to assess the pile behavior more completely (Figure 3.18 and Table 3.4). Projects P4A, P5, P7, and P9 do not have axial load test data, therefore the comparison between the analytical capacity and experimental failure load was not possible for these sites. Figure 3.18c displays the axial load test results, such as $Q_{failure}$, $Q_{\Delta=10\%D}$, and $Q_{max.applied}$. When the red and blue dashed lines are next to each other, the axial load test reached plunging failure and the failure load equals the max applied load accordingly. This was the case for P2, P4B, and P9. The representative loads are also compiled in Table 3.4 along with the "before-after pile capacity ratio".

Results presented in Figure 3.18c, suggest the data and methods to be assessed more closely, making it difficult to draw general conclusions given the limited availability of data. Projects P4B and P9 show very good agreement between the in-situ pile load failure, and the

capacity analytically estimated with the CPT_{POST} data. Both projects were analyzed using Eslami and Fellenius. The analytical predictions for P1(Δ_{max}=2.0 cm) and P2 (Δ_{max}=2.4 cm) notably overestimate the actual pile load capacity. P1 consists of clean sand and sand-like materials, and the use of CPT_{Post} data unconservatively overestimates the expected pile capacity. Project P2, a highly mixed site, analyzed with Eslami and Fellenius shows similar trends, the analytically estimated capacity (using both, CPT_{Pre} and CPT_{Post}) being unconservative.

For P3 (Δ_{max}=6.1 cm) and P6 (Δ_{max}=5.8 cm) the pile capacity was conservatively underestimated by Bustamante and Gianeselli (1993; 1998). This method estimates the load corresponding to the settlement of 10%*D* as ultimate capacity. However, both tests reached a much higher "10%*D* (4 cm) load" in the field, and also stopped prior to reaching the plunging behavior (i.e., $Q_{max,applied}$ < experimental failure), implying much higher in-situ capacity than analytically suggested. These results might be inherent to the method and its definition of max pile capacity. For piles with small diameters, the 10% *D* limit might generally yield conservative predictions while large diameter piles, or piles in stiff soils, might not reach the 10%*D* settlement threshold. Given the broad spectrum of comparative results, a generalized conclusion is nearly impossible and warrants the plead for future testing or sharing of existing results that encompass a wide range of axial load tests in various soil types with before-after testing.

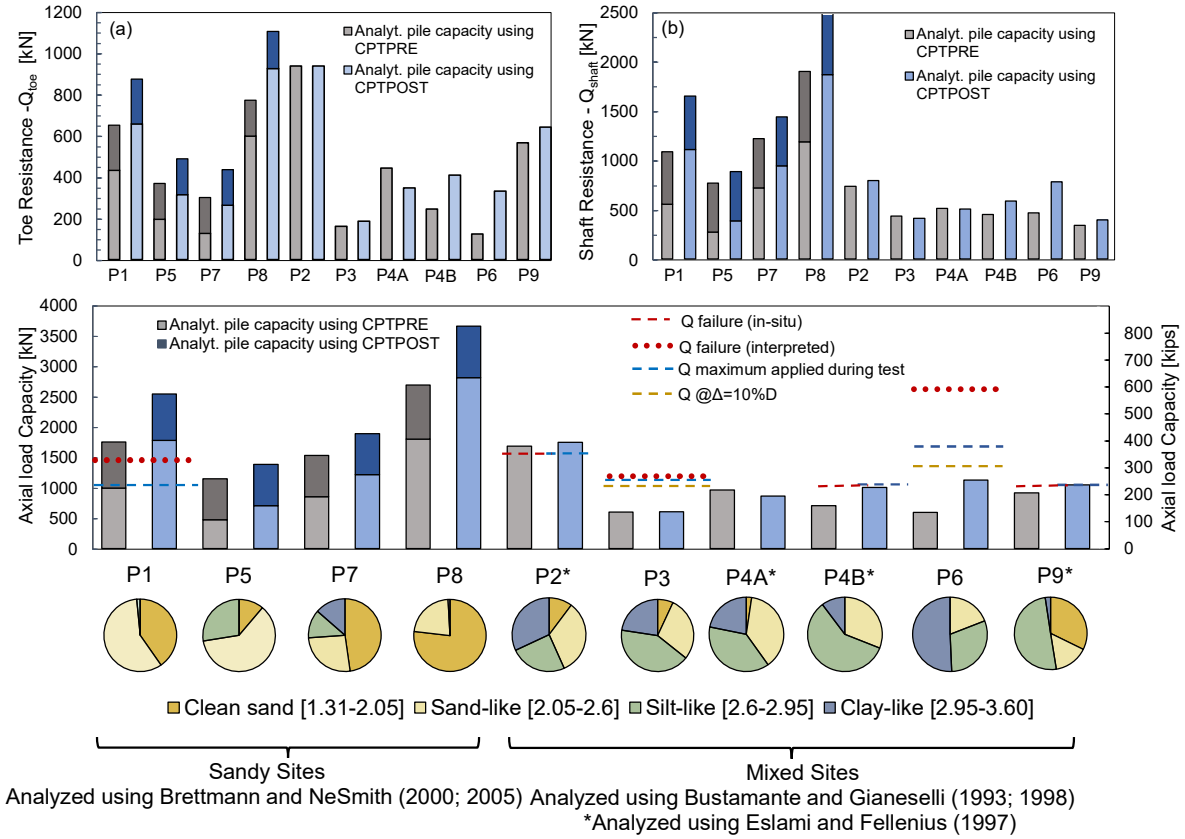

Figure 3.18. Analysis of the axial load capacity of the DDP using the CPT_{PRE} and CPT_{POST} data. (a) Analytical Q_{toe} capacity, (b) Analytical Q_{shaft} capacity, (c) Total capacity Q_u showed in bars, $Q_{failure}$, $Q_{max.test}$, and $Q_{\Delta=10\%D}$ showed with dashed lines. Pie charts: Soil profile composition – sites classification.

Table 3.4. Pile axial load summary. Design, test, and analytical methods results.

Project			D (m)	L (m)	Piles tested	Q_{design} (kN)	$Q_{max.\ test}$ (kN)	$\Delta_{max.test}$ (cm)	$Q_{@\Delta=10\%D}$ (kN)	$Q_{failure}$ (kN)	Analyt. Qu CPT_{PRE}(kN)	Analyt. Qu CPT_{POST}(kN)
P1	Tampa, FL	Sandy Sites	0.45	7.6	1	-	1078	2.0	-	1416	1277	2014
P5	Milipitas, CA		0.40	8.0	-	-	-	-	-	-	706	949
P7	Myrtle Beach, SC		0.40	8.0	-	-	-	-	-	-	1130	1487
P8	Orlando, FL		0.40	12.0	-	-	-	-	-	-	2014	3283
P2	Los Angeles, CA	Mixed Sites	0.40	10.3	1	-	1657	2.4	-	1657*	1691	1751
P3	San Jose, CA		0.40	7.2	1	214	1141	6.1	983	1197	602	608
P4A	San Francisco, CA		0.45	5.8	1	427	-	-	-	-	967	865
P4B				6.4			1019	1.8	-	1019*	708	1010
P6	Los Angeles, CA		0.40	8.2	1	570	1700	5.8	1289	2273	598	1129
P9	Redwood, CA		0.45	4	1	355	912	4.3	-	912*	917	1049

* In-situ pile failure loads

3.4. Limitations of the analysis

Despite the huge advantage associated with CPT testing (e.g., continuous and high-quality soil profiling), some challenges present itself when comparing before and after CPT data from the same site. Extrinsic factors affecting a 1:1 comparison of CPT_{PRE} and CPT_{POST} measurements include the use of different CPT companies (with potentially different CPT performance unique to each company and operator), the use of predrilling, the variation in push velocities, or the use of different CPT rod diameters (10cm vs 15cm diameter). While these effects are considered minimal, they do represent a potential source of error that is known to the geotechnical community.

A more intrinsic issue with the comparison of CPT data can be the "thin-layer effect" on the CPT measurements when testing in highly stratified soils. Different authors such as Lunne *et al.* (1997), Ahmadi and Robertson (2005), and Van den Berg *et al.* (1996) have studied the effects of subsequent soil layers on the CPT readings of preceding layers through experimental and numerical modeling. Their findings suggest the distance at which the CPT load cell begins sensing the next soil layer to be strongly dependent on the respective layer thickness and stiffness. For example, when penetrating into soft materials, the length of the influence zone can be as small as two times the cone diameter, while entering stiffer materials can cause this influence zone to be as large as 10 to 20 times the cone diameter (Lunne *et al.,* 1997). Moreover, depending on the layer thickness, the real resistance of thin layers can be reduced by the subsequent layers, leading to inaccurate measurements. Among the soil profiles collected for the studies, different projects, such as, P2, P3, P4A, and P5, present stratified soil profiles, therefore, the measurements obtained by the CPT_{POST} (higher resistance due to the improvement) and the comparison with the CPT_{PRE} data may be selectively affected by this phenomenon.

Simultaneously, the analytical methods are limited by their empirical derivation. While the Brettmann and NeSmith (2000; 2005) method was developed for DDP, the DDPs consisted of Augered Pressure-injected Drilled Displacement Piles (APID). The difference between the concrete cast technique, i.e., tremie or pressure-grouted technique, could alter the pile behavior due to a distinct pile stiffness. Moreover, the method requires information about the granulometry, gradation uniformity, and grain shape of the sand. When only CPT data is available, the assumption of the abovementioned physical properties can introduce errors in the axial load capacity estimation. Finally, the calculation of the pile shaft resistance does not take into consideration the CPT sleeve friction resistance (f_s) but uses CPT tip resistance (q_t) for both, toe, and shaft pile resistance. Similarly, Bustamante and Gianeselli (1993; 1998) method was developed based on Franki-Atlas, De Waal, Omega, and Spire DDP installed in 5 different sides, 3 of which contained chalk and marl materials. Although the two remaining sites were sandy clay with sand, and clayey fill with sandy gravel, the values proposed by the method can be influenced by the unique type of soils leading to overly conservative estimations. Additionally, the method suggest that the pile ultimate load is reached when a settlement of 10%D is triggered; but as observed in Table 3.4, plunging behavior was observed in the field and settlement reached only to 6% and 4% of the pile diameter, respectively (P3 and P6).

Chapter 4

Summary

A database of 55 construction sites, in which more than 120 DDPs were installed and tested, was utilized to (1) evaluate the predictive accuracy of CPT and SPT based direct methods in estimating axial pile load capacity for DDPs in sand like, clay like, and mixed soil sites and (2) to assess the soil improvement associated with the DDP installation technique. Prior to comparing predicted and measured axial capacities of drilled displacement piles, this study first investigated a variety of literature-based methods to interpret/estimate pile failure in the absence of experimentally reached failure. A comparison of eleven different methods, including the "Load at 10% of the pile diameter" method suggested that the Van der Veen's method (1953) provided the best match between estimated and measured failure. This method was closely followed by Butler & Hoy (1977), which slightly underpredicted the in-situ failure and L1-L2 method by Hirany and Kulhawy (1989) which slightly overpredicted the in-situ failure load of the 100+ piles investigated. The Decourt Method and Chin-Kondner Extrapolation methods overestimate the DDP failure loads across a large spectrum, while the De Beer's Criterion (1968) and the DOL Method generally underestimate the failure load of the drilled displacement piles. A modification factor to Davisson method for DDP interpretation was iterated following suggestions from Perlow (2020). With a modification factor of 4 to the last term of Davisson's failure interpretation equation, the failure load of DDPs can be much more accurately estimated and extrapolated from its original application to driven piles.

When comparing experimental failure to analytically predicted failure, almost all examined methods underpredict the capacity of the piles. Among all CPT-based methods, Brettmann and NeSmith (2000; 2005) showed a better agreement between the measured and analytically failure load for sandy soils, the Bustamante and Gianeselli (1993;1998) method showed the most

favorable approximation of the pile failure loads for mixed type of soils, and Eslami and Fellenius (1997) provided a more accurate estimation for clayey soils. The performance of the SPT direct methods was also evaluated, the most acceptable Q_f and Q_c agreement was achieved with the O'Neill and Reese (1988) method for sandy and mixed type of soils. However, overall, the authors recommend against the use of SPT-based prediction given the large scatter in analytically determined axial pile capacities.

The maximum axial load achieved during the pile tests was 200% to 300% of the design load; at this level of force, the settlement of the piles was considerably far from the plunging behavior. The higher pile capacity could be partially attributed to the higher resistance achieved due the installation effects. The effect of soil improvement obtained through DDP installation was evaluated based on pre- and post-installation CPT data. Favorable ground improvement effects such as the densification of soil surrounding the DDP can translate favorably into more accurate predictions of the actual pile failure load and represent an added factor of safety during the design phase, as pile design often relies on pre-pile installation based in-situ data. For piles with pre-and post-test CPT testing small improvements were documented in soil layers with low initial strength.

The estimation of axial load pile failure remains a function of high quality in-situ data and methods specifically developed for a certain pile type, inherently accounting for pile installation and construction effects. The current data reduces (but does not eliminate this gap) by providing recommendations for more accurately estimating pile failure from load test data and predicting pile capacities using existing methods.

Within the DDP database, nine case histories provided the opportunity to explore and quantify potential soil improvement following the installation of Drilled Displacement Piles in sandy and mixed-soil sites by assessing the change in CPT measurements such as the side friction,

friction ratio, normalized cone resistance, and normalized friction ratio (f_s, R_f, Q_t and F_r). The piles were constructed with diameters ranging from 0.40 m to 0.45 m (16 to 18 inches) and a length of up to 12 m. The installation pattern followed a single, square or triangular layout, with minimun and maximum pile distances of 3 to 8.5 times the pile diameter (D). Most CPT_{POST} tests were executed inside the pile's arrangement and within a radius of 3D; a limited number of additional CPT_{POST} tests were performed up 3.8D away from the pile.

An initial assessment of raw CPT data showed clear (and nearly immediate) improvement for soil profiles with mostly clean sands and sand-like soil types. For stratified soil profiles, or sites with mostly cohesive soils, the change in the CPT tip and side friction, q_t, and f_s, respectively was not visually quantifiable as limited improvement, or in some cases lower resistances, within the soil column was observed. The number of days between the DDP construction and CPT_{POST} execution suggested a strong dependency of the improvement recorded with the range of time between the DDP construction and the CPT_{POST} execution for cohesive soils. Cohesive soils were found to improve substantially when the soil profile consisted of thick and homogeneous layers, and a long time between pile installation and post CPT testing can be guaranteed.

By employing the soil behavior type index (I_c) proposed by Robertson, 2010, an improvement ratio was defined as the soil resistance measured after the pile installation divided by the soil resistance measured before the construction of the piles, i.e., $Q_{t.post}/Q_{t.pre}$. Improvement ratios were plotted against the pre-pile installation CPT resistances. An inverse relationship between the improvement ratio and the initial resistance was identified for all soil types (e.g., the higher the initial density of the "before" soil, the lower its potential to improve after pile installation), and the ratio of the $Q_{t.post}/Q_{t.pre}$ improvement shows a higher variability compared to the change in the side friction.

To trace the change in soil behavior due to the modification in soil resistance, before and after soil data were plotted on the Normalized CPT Soil Behavior Type (SBTn) chart by Robertson (2010). Results showed the soil behavior to change from a contractive behavior to a more dilative state for the majority of improved soil data points regardless the soil classification. A strong correlation between the level of improvement and the fines content (*FC*) was also found. While sand-like soils with a FC between 15 to 30% improved slightly more than soils with a FC between 30 and 40%, clean sands with a FC lower than 15% improve the least amongst all granular soils.

The spatial improvement of the surrounding soils was studied by plotting the improvement ratio vs CPT_{POST}-DDP distance (0-1D, 1-2D, 2-3D). The magnitude of achievable improvement decreased with increasing distance, for CPT_{POST}-DDP distance higher than 2D, the construction of the DDP has not effect on the normalized tip resistance (Q_t) of the surrounding soil.

The change in the axial pile capacity was assessed with CPT_{PRE} and CPT_{POST} data using the following three methods as applicable: Brettmann and NeSmith (2000; 2005), Bustamante and Gianeselli (1993; 1998), and Eslami and Fellenius (1997). For sandy soils the analytical failure load obtained with the CPT_{POST} data was approximately 1.3 to 1.6 times higher than the pile capacity obtained with the CPT_{PRE} data. On the other hand, several projects in cohesive soils revealed a ratio of $Q_{u.post}/Q_{u.pre}$ close to 1.0, showing no improvement on the overall pile capacity. This lack of improvement is likely associated with excess pore water pressure not being dissipated at the time when the CPT_{POST} testing was executed; as well as the "thin layer effect" on the tip resistance (q_t) measured during the CPT_{POST} execution in highly stratified soils.

When available, axial load test results were compared to analytical predictions. Best agreement between analytically predicted pile capacity obtained with the CPT_{POST} data and in-situ failure loads was achieved for primarily homogeneous soil profiles. For projects with the pile toe

resting in a strong sand layer, the analytical methods appear to overestimate the in-situ pile capacity of the elements, while for projects with thin sand layers between clayey soils, the analytical pile capacity underestimated the axial load pile capacity in the field. While important trends could be identified with the data sets available to the authors, the need for future field testing became critically apparent. Particularly well-designed field programs that include spatial, time, and geometric aspects of DDPs as well as more diversified field instrumentation is recommended to gain additional insight into the soil improvement due to the installation technique and pile load-behavior. Similarly the assessment of short term vs. long term improvement aspects of the installation technique remain unexplored to date.

REFERENCES

AASHTO (American Association of State Highway and Transportation Officials) (2008). *Load and* Resistance *Factor Design Bridge Design Specifications*. Washington, D.C.:

ASTM (American Society for Testing and Materials) (2020). *Standard Test Methods for Deep Foundation Elements* Under *Static Axial Compressive Load*. ASTM International, Standard D1143M. West Conshohocken, PA. doi: 10.1520/D1143_D1143M-20.

Baligh, F. A., & Abdelrahman G. E. (2005-2006). Modification of Davisson's method. Proceedings of the 16th International Conference on Soil Mechanics and Geotechnical Engineering. *International Society for Soil Mechanics and Geotechnical Engineering, 2079-2082*. doi:10.3233/978-1-61499-656-9-2079

Basu, P., & Prezzi M. (2009). Design and Applications of Drilled Displacement (Screw) Piles. Publication FHWA/IN/JTRP-2009/28. *Joint Transportation Research Program, Indiana Department of Transportation and Purdue University.* doi.org/10.5703/1288284314278

Baxter, D. J., Dixon, N., Fleming, P. R. & Dadley, S.P. (2006). The design and formation of bored displacement piles - a United Kingdom perspective. Proc. of the 10th Inter. Confer. on Piling and Deep Foundations, 2006, pp. 9-18.

Brettmann, T., & NeSmith W. (2005). *Advances in auger pressure grouted piles: design, construction, and testing*. Advances in Designing and Testing Deep Foundations. Austin, Texas, United States: Geotechnical Special *Publication* No. 129ASCE, 262–274. doi:10.1061/40772(170)5

Brown, D.A., Turner, J.P., & Castelli, R.J. (2010). *Drilled shafts: construction procedures and LRFD design methods*. National Highway Institute, U.S. Department of Transportation, Federal Highway Administration. Publication No. FHWA-NHI-10-016, Washington, D.C.

Bustamante, M., & Gianeselli, L. (1982*).* Pile bearing capacity predictions by means of static penetrometer CPT. *Proc*., *2nd European Symposium on Penetration Testing (ESOPT-II)*, 2, 493–500.

Bustamante, M., & Gianeselli., L. (1993). Design of auger displacement piles from in-situ tests. *Deep Foundations on Bored and Auger Piles*, BAP II, Balkema: Rotterdam, 21–34.

Bustamante, M., & Gianeselli., L. (1998). Installation parameters and capacity of screwed piles. *Deep Foundations on Bored and Auger Piles*, BAP III, Balkema: Rotterdam, 95–108.

Butler, H.D. & Hoy, H.E. (1977). *User's manual for the Texas quick load method for foundation load testing.* Department of Transportation Federal Highway Administration Office of Development. Publication No. *FHWA*-IP-77-8, Washington, D.C.

Caltrans (California Department of Transportation) (2015). *Foundation Manual Chapter 8, Static Pile Load Testing and Pile dynamic Analysis.* Revision No. 2, California. Retrieved from https://dot.ca.gov.

Chin, F.K. (1970). Estimation of the Ultimate Load of Piles Not Carried to Failure. *Proceedings of Second Southeast Asian Conference on Soil Engineering*, 81-92.

Davisson, M. T. (1972). High-capacity piles. *Proceedings of Lecture Series on Innovations in Foundation Construction,* American Society of Civil Engineers (ASCE), Illinois Section, Chicago, 81 - 112.

DeBeer, E. E. (1968). Proefondervindlijke bijdrage tot de studie van het grensdraag vermogen van zand onder funderingen op staal. (Experimental contribution to the study of the limit bearing capacity of sand under *foundations* on steel*)." Tijdshift der oOpenbar Verken van Belgie,* No. 6.

De Ruiter, J., & Beringen, F. L. (1979). Pile foundations for large North Sea structures. *Marine Georesources & Geotechnology*, 3, 267–314.

Decourt, L. (1995). Prediction of load-settlement relationships for foundations on the basis of the SPT. Ciclo de Conferencias Internationale, Leonardo Zeevaert, UNAM, Mexico, 85-104.

Decourt, L. (1999). Behavior of foundations under working load conditions. Proceedings of the 11th Pan-American Conference on Soil Mechanics and Geotechnical Engineering, Brazil, 4, 453 - 488.

Dotson D. W. (2013). Direct solution of the Brinch-Hansen 90% Pile Ultimate Failure Load. Deep Foundation Institute (DFI)- Journal of Deep Foundation Institute, 7(1), 18-21.

Eslami, A., & Fellenius, B.H. (1995). Toe bearing capacity of piles from cone penetration test (CPT) data. Procedure of the International Symposium on Cone Penetration Testing. Linköping, Sweden, Swedish Geotechnical Institute, SGI, 2.

Eslami, A., & Fellenius, B. H. (1997). Pile capacity by direct CPT and CPTU methods applied to 102 case histories. Canadian Geotechnical Journal, 34, 886–904.

Fellenius B. H. (2001). What capacity value to choose from the results of a static loading test. We have determined the capacity, then what?. Deep Foundation Institute, Fulcrum, Winter, 19 – 22 and Fall 2001, 23 - 26.

FHWA (Federal Highway Administration) (1992). Static Testing of Deep Foundations. U.S. Department of Transportation. Washington, D.C. 20590. Publication No. FHWA-SA-91-042, Washington, D.C.

Hansen, J.B., (1963). Discussion on hyperbolic stress-strain response. Cohesive soils. *American Society of Civil Engineers, ASCE, Journal for Soil Mechanics and Foundation Engineering*, 89, 241 - 242.

Hara, A., Ohta, T., Niwa, M., Tanaka, S., & Banno, T. (1974). Shear modulus and shear strength of cohesive soils. *Soils and Foundations*, 14, 1-12. doi.org/10.3208/sandf1972.14.3_1

Hansen, J.B. (1961). A general formula for bearing capacity. *Ingeniøren International Edition*, Copenhagen, 5, 38-46.

Hogg, R. V., & Craig, A. T. (1995). *Introduction to mathematical statistics*. Ed. 5. Upper Saddle River, New Jersey, Prentice Hall.

IBC (International Building Code) (2018*). Chapter 8 - Soils and Foundations.* International Code Council.

Lunne, T., Robertson, P.K., and Powell, J.M. (1997). Cone penetration testing in geotechnical practice. Blackie Academic & Professional, London, UK.

Meng Z., Chen J., Zhang L., Wang J., and Yao J. (2015). Field Tests to Investigate the Installation Effects of Drilled Displacement Piles with Screw-Shaped Shaft in Clay. Journal of Geotechnical and Geoenvironmental Engineering – – DOI: 10.1061/(ASCE)GT.1943-5606.0001371.

Meyerhof, G. G. (1976). Bearing Capacity and Settlement of Pile Foundations. *Journal of the Geotechnical* Engineering *Division*, 102(3), 195–228. doi: 10.1061/AJGEB6.0000243

Moshfeghi, S., & Eslami, A. (2018). Failure analysis of CPT-based direct methods for axial capacity of driven piles in sand. *Georisk: Assessment and Management of Risk for Engineered Systems and Geohazards.* 13, 1-19.

Nesmith, W.M. (2002). Static capacity analysis of augered, pressure-injected displacement piles. *Proceedings, International Deep Foundations Congress, M. O'Neill and F. Townsend.* Publication No.116, 1174-1186.

NeSmith W. M. & Siegel, T. C. (2009). Shortcomings of the Davisson Offset Limit applied to axial load *compressive* load test on cast-in-place piles. *American Society of Civil Engineers. International Foundation Congress and Equipment Expo*. doi:10.1061/41021(335)71

NeSmith, W. M., (2002). "Design and Installation of Pressure-Grouted, Drilled Displacement Piles," Proceedings of the Ninth International Conference on Piling and Deep Foundations, Nice, France, June 2002, pp. 561-567.

Niazi, F., and Mayne, P., 2016. CPTu-based enhanced UniCone method for pile capacity. Engineering Geology. 212. 10.1016/j.enggeo.2016.07.010.

O'Neill, M. W., & Reese, L. C. (1988). Drilled Shafts: Construction Procedures and Design Methods. *ADSC (The International Association of Foundation Drilling)*. Publication No. ADSC-TL4, 471

Paniagua, W.I. (2005). Construction of Drilled Displacement and Auger Cast In Place Piles.

Peck, R. B., Hanson, W. E., & Thornburn, T. H. (2nd Edition) (1974). *Foundation engineering*. New York: Wiley.

Perlow M. (2020). A soil quake Davisson Offset Method for Drilled Foundations. *Deep Foundation Institute 45th Annual Conference*, USA, Red Hook, NY, 183

Prezzi, M. & Basu D. (2010). Drilled displacement piles– current practice and design. *Journal of the Deep Foundations Institute,* 4(1), 3–20.

Pucker, T. & Grabe, Jürgen. (2012). Numerical Simulation of the Installation Process of Full Displacement Piles. Computers and Geotechnics. 45. 93-106. 10.1016/j.compgeo.2012.05.006.

Rad S. H., Ghareh S., Eslami A., and Ganjian N. (2021). Experimental and field studies on the behavior of drilled displacement piles. Innovative Infrastructure Solutions, 6, 188.

Robertson, P.K., (1990). Soil classification using the cone penetration test. Canadian Geotechnical Journal,27(1): 151-158.

Robertson, P.K., and Fear, C.E. (1995). Liquefaction of sands and its evaluation. In IS-Tokyo '95, Proceedings of the 1st International Conference on Earthquake Geotechnical Engineering, Tokyo. Edited by K. Ishihara. A.A. Balkema, Rotterdam, The Netherlands. Vol. 3, pp. 1253–1289

Robertson, P.K. (2009). Interpretation of cone penetration tests – a unified approach. Canadian Geotechnical Journal,46:1337-1355.

Robertson, P.K. (2010). Soil behavior type from the CPT: an update.2nd International Symposium on Cone Penetration Testing, CPT'10, Huntington Beach, CA, USA.

Robertson, P. K., Cabal K. L. (2014). Guide to Cone Penetration Testing for Geotechnical Engineering. Gregg Drilling & Testing, Inc.

Robertson, P.K. (2016). Cone penetration test (CPT)-based soil behavior type (SBT)classification system—an update. Canadian Geotechnical Journal. 53(12): 1910-1927. https://doi.org/10.1139/cgj-2016-0044

Schmertmann, J. H. (1978). Guidelines for Cone Penetration Test, Performance and Design. *Rep. No. FHWA-TS-78-209, U.S. Department of Transportation*, Washington, D.C., 145.

Shah, F.R. & Deng, L. (2016). Comparing Axial Behavior of Non-Displacement and Displacement Piles using Field Load Tests. *69th CGS Conference Vancouver*, B.C. Canada.

Siegel, T. C., NeSmith W. M., & Cargill, P. E. (2007). Ground Improvement resulting from Installation of Drilled Displacement Piles. *Deep Foundation Institute 32nd Annual Conference*, Colorado Springs, CO, October 11-13, 2007.

Siegel, T.C., Day, T.J., Turner, B., and Faust, P. (2019). Measured end resistance of CFA and drilled displacement piles in San Francisco Area alluvial clay. DFI Journal - The Journal of the Deep Foundations Institute, 12 (3), 186-189

Stacho, Jakub & Ladicsova, E. (2014). Numerical analysis of drilled displacement system piles. International Multidisciplinary Scientific GeoConference Surveying Geology and Mining Ecology Management, SGEM. 2. 665-671

Stuedlein, A. W., Reddy, S. C., & Evans, T. M. (2014). Interpretation of augered cast in place using static load tests. *Deep Foundation Institute- Journal of Deep Foundation Institute*, 8(1), 39-47.

Van den Berg, P., de Borst, R., and Huetink, H. (1996). An Eulerean finite element model for penetration in layered soil. International Journal for Numerical and Analytical Methods in Geomechanics, 20: 865–886

Van der Veen, C. (1953). The bearing capacity of a pile proceedings. *3rd International Conference on Soil Mechanics and Foundation Engineering*, 2, 84-90.

Van Impe, W.F. and Peiffer, H. (1997). "Influence of screw pile installation on the stress state in the soil," Proceedings of the ERTC3 Seminar, Design of Axially Loaded Piles European Practice, Brussels, Belgium, pp. 3 – 19.